Electrolyte-gated organic field-effect transistors integrated into a microfluidic platform: Towards point of care testing

A thesis submitted to The University of Manchester for the degree of Doctor of Philosophy in the Faculty of Science and Engineering

Amadou Doumbia

2019

Organic Materials Innovation Centre (OMIC)

School of Chemistry

The University of Manchester

List of contents

Abstract

Discoveries in immunology are correlating the levels of some biomolecules present in bodily fluids with the type, subtype, and sub-state of illnesses. Monitoring these biomarkers can facilitate early diagnosis of diseases and the assessment of potential risk for each patient. Thus, empowering the administration of individualised treatments. The deployment of such medicine requires the availability of high throughput, reliable portable molecular detection systems. This thesis aimed to address to this demand for point of care devices, by focusing on the development and study of a printed electronic microfluidic molecular detection platform. The building block is an array of Organic Field-Effect Transistors (OFETs) gated through an electrolyte called Electrolyte-Gated OFET (EGOFET). It is designed for multiplex detection of biomarkers in parallel. Initially, OFETs gated with a droplet of water were investigated to benchmark three organic semiconductors, namely 2,5-bis(3-hexadecylthiophen-2-yl)thieno[3,2-b]thiophene, indacenodithiophene-co-benzothiadiazole and diketopyrrolopyrrole-dithienylthieno[3,2-b]thiophene (DPPDTT) based polymers. The purpose is to study the electronic behaviour of these semiconductors and to choose the best performing material for the development of a reliable microfluidic integrated EGOFET. Devices based on DPPDTT displayed the highest mobility (~0.18 $cm^2.V^{-1}.s^{-1}$) and good on-off current ratio (~3×10^3), comparable to the state-of-the-art performance reported to date in EGOFET. Hence, DPPDTT was selected for further investigation. Microfabrication and fast prototyping technologies were combined to engineer arrays of microfluidic integrated DPPDTT based EGOFETs. The device has a network of 4 fluidic channels in each of which there are 4 EGOFET. By functionalisation of individual gates in the array with self-assembled-monolayer of capturing deoxyribonucleic acid (DNA), *in operando* and specific detection of the hybridization of DNA in ~30 s with errors on the measured figures below 15% was demonstrated. This is faster that related DNA Enzyme-linked Immunosorbent assay (ELISA) kits (~1h) with similar reproducibility. Finally, the transfer of the technology to printable electronics was assessed by developing an EGOFET with a printed DPPDTT. Reproducible average mobility and on-to-off current ratio were respectively ~0.13 $cm^2.V^{-1}.s^{-1}$ and ~10^2 in printed devices. This EGOFET operated with minimal change in performance for up to 40 minutes under flowing electrolyte with 11%, 8% and 18% changes in transconductance, on-state drain current and threshold voltage. Overall these results suggest that reliable and reproducible technologies based on EGOFET can be developed for high throughput point of need testing and at low cost with *en masse* facile fabrication techniques.

Declaration

No portion of the work referred to in the thesis has been submitted in support of an application for another degree or qualification of this or any other university or other institute of learning.

Copyright statement

i. The author of this thesis (including any appendices and/or schedules to this thesis) owns certain copyright or related rights in it (the "Copyright") and s/he has given The University of Manchester certain rights to use such Copyright, including for administrative purposes.

ii. Copies of this thesis, either in full or in extracts and whether in hard or electronic copy, may be made only in accordance with the Copyright, Designs and Patents Act 1988 (as amended) and regulations issued under it or, where appropriate, in accordance with licensing agreements which the University has from time to time. This page must form part of any such copies made.

iii. The ownership of certain Copyright, patents, designs, trademarks and other intellectual property (the "Intellectual Property") and any reproductions of copyright works in the thesis, for example graphs and tables ("Reproductions"), which may be described in this thesis, may not be owned by the author and may be owned by third parties. Such Intellectual Property and Reproductions cannot and must not be made available for use without the prior written permission of the owner(s) of the relevant Intellectual Property and/or Reproductions.

iv. Further information on the conditions under which disclosure, publication and commercialisation of this thesis, the Copyright and any Intellectual Property and/or Reproductions described in it may take place is available in the University IP Policy (see http://documents.manchester.ac.uk/DocuInfo.aspx?DocID=24420), in any relevant Thesis restriction declarations deposited in the University Library, The University Library's regulations (see http://www.library.manchester.ac.uk/about/regulations/) and in The University's policy on Presentation of Theses

Acknowledgement

"This was another yet very interesting experience during which I again learn so much from family, friends, mentors, supervisors, sponsors, colleagues and examiners. So many thanks, for your time"!

AD

Main supervisor: Professor Michael Lewis Turner

Co-supervisor: Doctor Michelle Webb

Collaborators at Cambridge Display Technology Ltd.:

- Doctor Richard Wilson
- Doctor Jonathan Maximilian Behrendt

External Examiner: Professor David Martin Taylor

Internal Examiner: Professor Stephen George Yeates

Internal independent Assessor: Professor Krishna Persaud

Sponsors:

- Cambridge Display Technology Limited (CDT Ltd.)
- The Engineering and Physical Sciences Research Council (EPSRC)

Dédié à la famille Alfred Kabnè et Oumou Doumbia.

Dedicated to Alfred Kabnè and Oumou Doumbia family.

Blank page

Chapter 1

1.1. Introduction

In traditional healthcare systems, medical drugs are dispensed based on symptomatic diagnosis of diseases. Patients displaying similar illness symptoms receive the same medicine. It is well recognised that this may lead to prescriptions of inappropriate drug therapy[1]. In fact, different diseases manifest similar symptoms; and patients with the same illness respond differently to a given treatment in part due to the heterogeneity in both patient and disease biology[2].

In these days, progress in scientific and technical fields, including immunology, pharmacology, and micro/nanotechnology are inducing a gradual shift from the traditional health care to an improved system, so-called precision and personalised medicine[1]. Instead of grouped symptoms, diagnostics will be based on the cause and effect of the diseases via the identification and quantification of biological markers[3 and 4]. Diseases will be stratified and detectable before onset. Necessary information can be gathered to identify individual predisposition for future diseases, occasioning prescription of specific treatment based on a personalised assessment of clinical effectiveness and adverse drug effects[5].

Nowadays, such medicine is becoming a reality for some cancer patients[6, 7 and 8]. For its effective application, numerous obstacles including the identification of robust disease markers, need to be addressed. Its expansion can be facilitated via the development and improvement of analytical tools capable of detecting biomarkers in the clinically relevant range at the point of need. Among others, an OFET gated with an electrolyte, the so-called EGOFET, is attracting a great degree of attention as a building block of cutting-edge bioelectronics systems[9, 10, 11, 12 and 13]. A miniaturised array of EGOFET biosensor needs to be facilitated including a microfluidic cell. This will enable the integration of EGOFET with other electronic systems to deliver a point of need device. Such a technology can have a tremendous impact on the patient outcome as vital and immediate intelligent treatment can be advised.

The aim of this research was to help step further towards the development of such a universal low power consumption point of need system for precision medicine. It focused on the development and evaluation of an Electrolyte-Gated Organic Field-Effect Transistor integrated into a microfluidic device (M-EGOFET) for detection of

biomolecules *in operando*. Initially, the dissertation in **Chapter 2** provides the reader with the necessary knowledge background to understand the field of organic biosensors and bioelectronics. After highlighting what a biosensor is, it introduces the basic properties of organic semiconductor. Particular attention is given to the unique characteristics these materials offers for interfacing electronic devices with biological medium. This is followed by a brief introduction to the fundamentals of Electrolyte gated organic field-effect transistors. Its operation mechanism including the underlying physics as well as the materials explored, and their performance were covered. Equally, some of the biochemical sensors based on EGOFET reported in the literature are highlighted.

The 3rd, 4th, and 5th chapters present the outcome of the scientific investigations. Each chapter contains a brief explanation of the importance of the study, a description of the experiments, and a discussion of the results obtained. In **Chapter 3**, EGOFET technology is assessed. Three polymeric semiconductors, namely poly[2,5-bis(3-hexadecylthiophen-2-yl)thieno[3,2-b]thiophene] (PBTTT), indacenodithiophene-co-benzothiadiazole (IDT-BT) and diketopyrrolopyrrole-dithienylthieno[3,2-b]thiophene (DPPDTT)), are employed as conducting channels. DPPDTT and IDT-BT were chosen because they are high performance unexplored organic semiconductors in EGOFET. And PBTTT was used as reference as it is well established materials in the development of EGOFET. In this chapter, the devices are in droplet gated configuration with a gold wire acting as the gate terminal and purified water as the electrolyte. By comparing the obtained electrical figures of merit, particularly due to its higher field effect mobility, on-to-off current ratio, low subthreshold swing, threshold voltage close to zero and its full drain modulation within the used bias window the DPPDTT was chosen for further investigation in **Chapter 4** and **Chapter 5**.

Chapter 4 looks at the development and study of an array of EGOFET integrated into a microfluidic cell to confine and deliver the electrolyte to the device. The four fluidic channels and the multiple gate terminal allow high-throughput and multianalyte detection in parallel. By tuning the surface properties of individual gate with self-assembled-monolayer coupled with a capturing 19 base deoxyribonucleic acid its transformation to a DNA biosensor was demonstrated. The biosensor's electrical performance reproducibility and operational stability are assessed in flowing electrolyte condition. The *in operando* specific detection of DNA hybridization with EGOFET based on DPPDTT is reported for the first time with high specificity within a physiological like milieu. The developed system paves the way for the development of a universal low power

consumption and high throughput label free point of need testing device for molecular diagnosis and prognosis as well as chemical hazardous molecule detection.

Chapter 5 study the transferability of the technology to printed electronics. Here the DPPDTT was printed and the electrical performance, reproducibility and long-term operational stability of the device are discussed.

The thesis is terminated with a conclusion of the scientific findings and possible future avenues in **Chapter 6**.

References

1. Fu, E., Yager, P., Floriano, P. N., Christodoulides, N. & McDevitt, J. T. Perspective on diagnostics for global health. *IEEE Pulse*. **2,** 40–50 (2011).

2. Sacristàn, J. A. & Avendano-Slà, C. On heterogeneity of treatment effects and clinical freedom. *Int J Clin Pract*. **69,** 6–8 (2015).

3. Gorshkov, K., *Chen, C. Z., Marshall, R. E., Mihatov, N., Choi, Y., Nguyen, D. T., Southall, N., Chen,. K. G., Park, J. K. & Zheng, W*. Advancing precision medicine with personalized drug screening. *Drug Discov.* **24,** 272–278 (2019).

4. Liao, W. & Tsai, F. Review article Personalized medicine : A paradigm shift in healthcare. *BioMedicine* **3,** 66–72 (2013).

5. Florence, A. T. & Lee, V. H. L. Personalised medicines : More tailored drugs, more tailored delivery. **415,** 29–33 (2011).

6. Veer, L. J. V. & Bernards, R. Enabling personalized cancer medicine through analysis of gene-expression patterns. *Nature.* **452,** 564–570 (2008).

7. Tsimberidou, A., Iskander, N. G., Hong, D. S., Wheler, J. J., Falchook, G. S., Fu, S., Piha-Paul, S., Naing, A., Janku, F., Luthra, R., Ye, Y., Wen, S., Berry, D. & Kurzrock, R. Personalized Medicine in a Phase I Clinical Trials Program : The MD Anderson Cancer Center Initiative. *Clin. Cancer Res.* **18,** 6373–6384 (2012).

8. Deng, X. & Nakamura, Y. Cancer Precision Medicine : From Cancer Screening to Drug Selection and Personalized Immunotherapy. *Trends Pharmacol. Sci.* **38,** 15–24 (2017).

9. Berto, M., Diacci, C., D'Agata, R., Pinti, M., Bianchini, E., Di Lauro, M., Casalini, S., Cossarizza, A., Berggren, M., Simon, D., Spoto, G., Biscarini, F. *& Bortolotti, C. A.* EGOFET Peptide Aptasensor for Label-Free Detection of Inflammatory Cytokines in Complex Fluids. *Adv. Biosyst.* **2,** 1700072 (2017).

10. Doumbia, A., Webb, M., Turner, M. L., Behrendt, J. M. & Wilson, R. A printed electronic platform for the specific detection of biomolecules. *Proc. SPIE 10364, Organic Sensors and Bioelectronics X*, **103640N,** 1–10 (2019).

11. Desbief, S., Di Lauro, M., Casalini, S., David, G., Tortorella, S., Barbalinardo, M., Kyndiah, A., Murgia, M., Cramer, T., Biscarini, F. & Vuillaume, D. Electrolyte-gated organic synapse transistor interfaced with neurons. *Org. Electron.* **38,** 21–28 (2016).

12. Foschi, G., Leonardi, F., Scala, A., Biscarini, F., Kovtun, A., Liscio, A. &Casalini, S.

Electrical release of dopamine and levodopa mediated by amphiphilicamphiphilic β -cyclodextrins. *Nanoscale*. **7,** 20025–20032 (2015).

13. Mulla, M. Y., Tuccori, E., Magliulo, M., Lattanzi, G., Palazzo, G., Persaud, K. & Torsi, L. Capacitance-modulated transistor detects odorant binding protein chiral interactions. *Nat. Commun.* **6,** 1–9 (2015).

Blank page

Chapter 2: Review of the electrolyte-gated organic field-effect transistor as a versatile bioelectronic tool

2.1. Introduction (Biosensor)

A biosensor is an analytical device that offers the potential to study and understand life by collecting information from the interaction between chemical and biological substances and processes. For example, asbestos is a silicate mineral composed of tiny fibers. These fibers can get into the lung through the respiratory systems to cause gene mutations, followed by abnormal biological processes that lead to the lung cancer known as mesothelioma[1]. Biosensors can be used at all steps, from exposure to the foreign substance (e.g. asbestos) to the treatment of the disease (e.g. mesothelioma). A biosensor can identify the toxin[2] and detect the gene mutations[3] in order to prevent the disease or diagnose it in its early stage. It can also help to understand the biological processes and aid the development of appropriate drug therapy. In addition, to healthcare and drug discovery, potential applications of biosensors are homeland security, food safety and environmental protection[4,5,6 and 7].

A biorecognition element coupled to a transducer is the basic building block of a biosensor (**Figure 2-1**)[8 and 9].

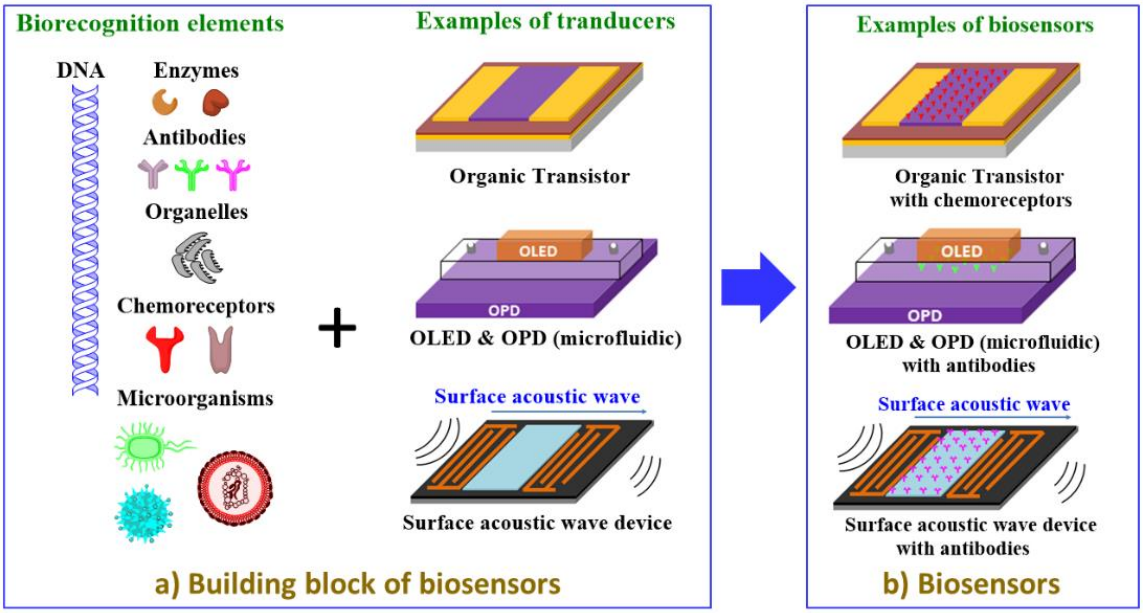

Figure 2-1: B*iosensors: a) the building blocks of a biosensor consisting of biorecognition elements that interact specifically with a target analyte; a transducer for translating chemical stimulus to a quantifiable physical signal. Integrating the biorecognition element onto a transducer surface give rise to b) a biosensor that translates the biological event (biorecognition element – analyte interaction) into an analysable physical signal(s).*

The biorecognition element assures that a specific biological or chemical event is recorded, while the transducer converts this event into a convenient analysable physical signal. The biorecognition element is typically an antibody, enzyme, nucleotide, cell, microorganism, tissue or synthetic molecule that interacts specifically with the substance to be identified (e.g. antigens, genetic materials) called the analyte[8]. Depending on the nature of the biorecognition element the interaction with the analyte can be a simple affinity binding (e.g. antibody-antigen, nucleotides cell-substrate interaction type), or electrostatic interaction, or can involve catalytic reactions (enzyme/microorganism/cell-substrate interaction type) that transform the substance to be detected into a chemical product. This specific interaction, whether electrostatic, catalytic or affinity – binding, prompts a change in at least one physio-bio-chemical parameter of the transducer, converting the recognition into a quantifiable signal. The signal is amplified, processed and displayed by a readout system.

L.C. Clark *et al*. devised the first biosensor in the early sixties[10]. It was a two-electrode system immersed into an electrolyte subject to a difference of potential that could measure the level of glucose present in liquids. Ag/AgCl was used as the reference electrode. A platinum (Pt) foil covered with an oxygen permeable membrane and an enzyme glucose oxidase layer was employed as the working electrode (**Figure 2-2**). A galvanometer was connected to the two electrodes to measure the ionic current flowing between them.

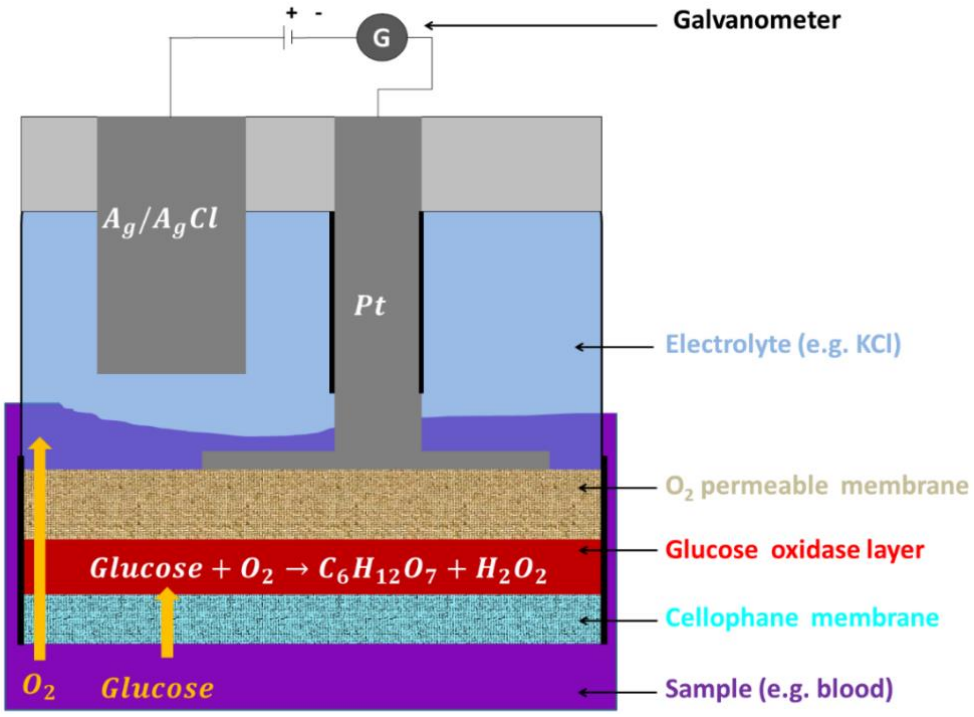

Figure 2-2: *Schematic representation of L.C. Clark glucose sensor.*

The sensing relies on the following reaction on the working electrode:

$$Glucose + O_2 \xrightarrow[\boldsymbol{GOx}]{} C_6H_{12}O_7 + H_2O_2 \quad (2.1)$$

This reduces the amount of O_2 that reaches the electrolyte and the current measured by the galvanometer. Hence, with this technology, the quantity of glucose present in a sample is determined by measuring the depletion of oxygen. Since then, the field of biosensors has expanded with the development of numerous bio-sensing mechanisms and devices[8]. Solid-state microelectronic systems based on inorganic and organic semiconductors are the backbone of these technologies[11,12 and 13]. Biosensors based on organic semiconductors (organic small molecules and polymeric semiconductors) have attracted significant attention during the last three decades owing to the new and unique perspective they offer[7,14,15,16 and 17].

2.2. Organic semiconductors

Organic semiconductors are soft materials consisting of carbon and hydrogen surrounded by other elements including nitrogen, sulphur and phosphorus. They can display adjustable electronic and optoelectronic properties[18 and 19]. These come from carbon atom's extraordinary ability to hybridize and to undergo extensive catenation.

2.2.1. Origin of the conducting nature of organic semiconductors

In atomic physics, carbon is a chemical element that contains six electrons occupying two allowed spin states in a total of five orbitals[20]. In the ground state, this gives a general electronic configuration of $1s^2$, $2s^2$, $2p^2$. The numbers (1 and 2 before the letter) specify the state, the letter stands for the shape of the orbitals ("s" and "p"), and the subscript indicates the number of electrons it contains. Stable molecules exist in nature show carbon binding covalently to four (CH_4), three (C_2H_4) or two (C_2H_2) other atoms. The binding can be considered as a mixing of the 2s and 2p orbitals of carbon to generate sp, sp^2, or sp^3 hybrid orbitals[21]. When the 2s orbital combines with one of the 2p orbitals two sp hybrid orbitals form. The mix up of the 2s orbital with two 2p orbitals generates three sp^2 hybrid orbitals. Four sp^3 hybrid orbitals are produced once the 2s orbital unites with the three 2p orbitals.

For organic semiconductors, the sp^2 configuration is of interest. The structure of ethylene introduces how carbon in sp^2 hybridization states bond to their neighbours (**Figure 2-3**). In this molecule, the three sp^2 hybrid orbitals of each carbon atom overlap with the 1s

orbital of its two nearest hydrogen atoms and the sp^2 orbital of the second carbon atom, to form six σ bonds. The p_z orbital of the two carbons (perpendicular to the sp^2 orbitals) overlap side by side to form delocalized double π bonds (**Figure 2-3**).

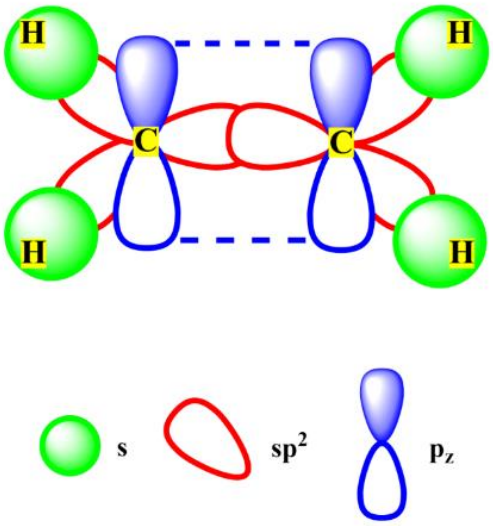

Figure 2-3: Hybridization in *ethylene: two carbon atoms with three sp^2 hybrid orbital and one $2p_z$ each, surrounded by four hydrogen atoms with 1s orbital. The sp^2 hybrid orbitals of the carbon share their electron with the s orbital of two hydrogen atoms and sp^2 of the other carbon to form three σ bond ($\sigma(s\text{-}sp^2)$ and $\sigma(sp^2\text{-}sp^2)$ and the p_z orbitals share their electrons to form a delocalised π bond*.

Long chains of carbon in sp^2 hybridization contain delocalized π-bonds. The delocalization of the electrons over the molecule (see **Figure 2-4** for the linear polyacetylene), leads to a Lowest Unoccupied Molecular Orbital (LUMO) and Highest Occupied Molecular Orbital (HOMO) of the molecule, that are the least antibonding and bonding orbitals. The gap between the molecular orbitals (HOMO and LUMO) must be < 4 eV for molecules to be called an organic semiconductor[20].

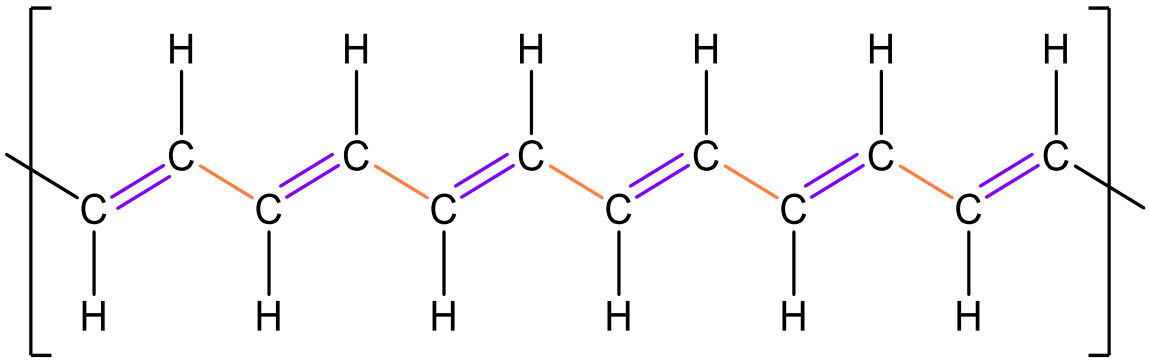

Figure 2-4: A segment of *polyacetylene showing alternation of σ-bond (light brown) and delocalised π-bond (violet) in the polymeric backbone.*

For bulk transport, in addition to the intramolecular charge transport along the backbone of the organic semiconductor, the molecules need to pack together in the solid state so charges can transfer from one molecule to another. At present, no solid-state theory fully

explains this mechanism. Although, whether the organic semiconductor adopts a crystalline, polycrystalline or amorphous structure in thin film, basic models help in the interpretation of experimental results[22,23,24 and 25]. The following section introduces the Polaron and Bässler Gaussian disorder models[26,27 and 28]. .

2.2.2. Basic models of charge transport in thin films of organic semiconductors

2.2.2.1. Polaron model

In ideal crystalline small molecules and polycrystalline polymers, free of defects and impurities, the charge transport mechanism could be explained by polaron models (a combination of band-like and a phonon-assisted models). Fundamentally, the polaron model is summarized as follows. The extraction of an electron from the HOMO of the molecule leaves a positive charge, known as hole, which distorts the electronic cloud by increasing the density of electron around it. Under an external force (Electrical or Magnetic Fields), the hole can move to a second molecule via hopping or tunneling. This leads to the relaxation of the first molecule when the second became distorted as it is charged. And so forth through the whole film. The created positive charge with its associated electronic cloud is a so-called "hole polaron", or an "electron polaron", in case of an electron injected into the LUMO. These species will propagate between adjacent molecules whose frontier orbitals overlap.

In general, at very low temperature, as nuclear vibration is frozen, the transport becomes a coherent movement in a periodic potential, such as the band-like transport in inorganic semiconductors (mobility increases with temperature). Near room temperature, there is competition between the band-like and phonon-assisted transport because the lattice vibration becomes non-negligible. Above room temperature, as the hole-phonon coupling is stronger, phonon-assisted transport becomes dominant (mobility decreases with temperature). Recently, Y. Krupskaya *et al.* demonstrated that, in single crystals of fluorinated tetracyanoquinodimethane (TCNQ, F 2 -TCNQ, and F 4 –TCNQ), both the band-like and phonon assisted transport take place[29]. An increase of mobility with increasing temperature was observed between 180 – 280 K, and a decrease of mobility in the range 290 – 320 K, was demonstrated by Y. Yamashita *et al.* for the polycrystalline hexadecyl-substituted cyclopentadithiophene-benzothiadiazole (CDT-BTZ-C16)[30].

2.2.2.2. Bässler Gaussian disorder model

The disorder model pioneered by Bässler[31], can be used to interpret charge transport in amorphous semiconductors if the contribution of phonons are negligible when compared to the static disorder (weak charge-phonon interaction). In amorphous polymers, the molecules pack in a random fashion in a thin-film, this leads to the creation of a disordered distribution of localised density of states in the solid-state (thin film). Bässler postulated that the distribution follows a Gaussian shape with different levels and varying distance between the localized states (**Figure 2-5)**. Hence charge carriers move across the solid-state film by a combination of tunnelling and hopping with a certain probability.

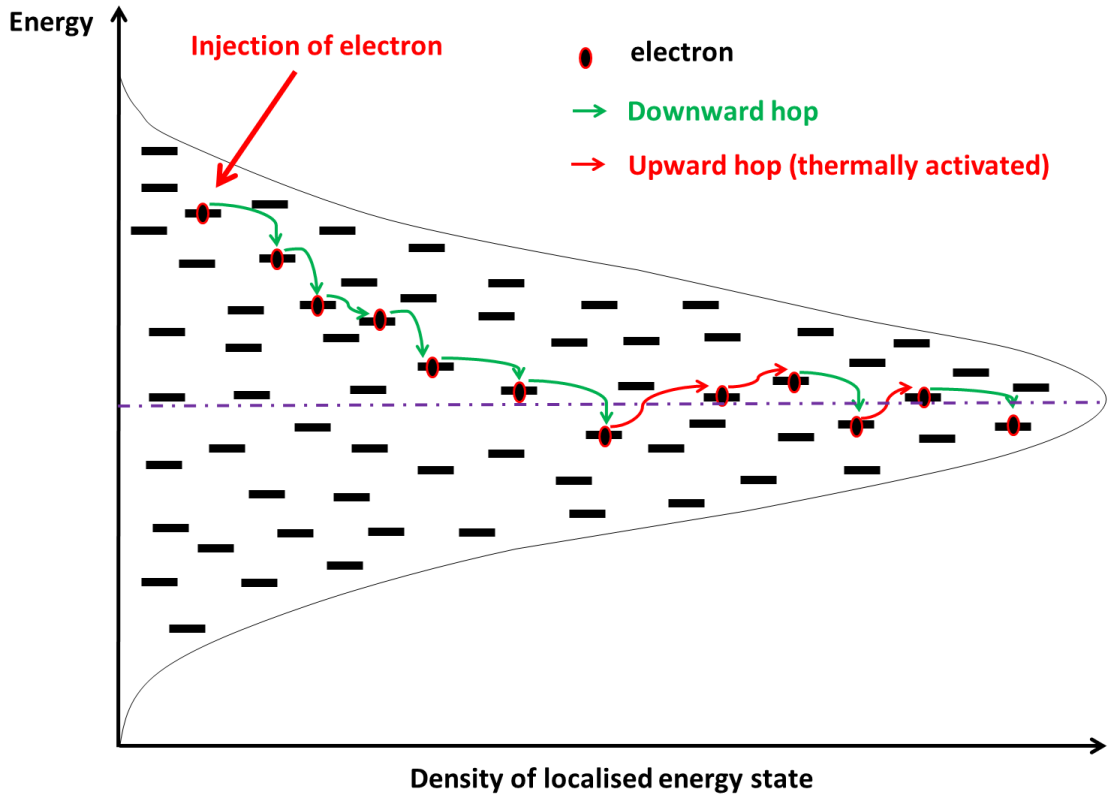

Figure 2-5: *Gaussian distribution of energetic states. The black lines represent free energetic states and the violet indicates the level of the transfer energy. Upon injection of an electron in one of the energetic states, it hops between closes state which probability is descripted by Miller-Abrahams formula.*

Such transition rate of hops (υ_{ij}) between localized states (from site i to j), is commonly described by Miller-Abrahams formula[32]:

$$\upsilon_{ij} = \upsilon_0 exp^{-2\gamma R_{ij}} \begin{cases} exp^{-\frac{(\varepsilon_j - \epsilon_i)}{\kappa T}} & \forall \varepsilon_j > \varepsilon_i \\ else \end{cases} \quad (2.2)$$

The first term of the Miller-Abrahams equation ($\upsilon_0 exp^{-2\gamma R_{ij}}$) represents the tunnelling contribution. It denotes the frequency of translation of the charge carrier between two

adjacent aligned states (i and j) or from an initial state i higher in energy than the final state j. One can notice that the maximum transition rate (υ_0) which correspond to the phonon vibration frequency, is multiplied by an exponential which decay with the distance between states (R_{ij}) and the inverse of their localization radius ($1/\gamma$). Hence, according to this expression, tunnelling between closes states (small R_{ij}) with large localization radius should be more frequent in thin-film of amorphous semiconductors. The second term of the Miller-Abrahams equation ($\exp^{-\frac{(\varepsilon_j-\varepsilon_i)}{\kappa T}}$), is a Boltzmann factor, account for the hopping upwards in energy of the charge. It evidences that the frequency of charge transfer from an initial state i lower in energy than the final state j becomes exponentially more difficult with the increase of the difference of energy ($\varepsilon_j - \varepsilon_i$) between the two states. However, such a penalty, arising from the energetic barrier between state i and j, can be reduced by increasing the temperature of the system. Therefore, hopping rats (υ_{ij}) is temperature dependant.

A range of mobility, a principal figure that describes the charge movement in materials, was observed for the same organic semiconductor[33 and 34]. This is because the transport of charges in these films depends on the morphology adopted by the molecules[34] and can be affected by factors including the surrounding environment (defects, impurities) and external forces (*e.g.* temperature, pressure, electric or magnetic fields)[35]. While the physics of charge transport in these materials is not fully understood, the unique properties they display are attracting attention for the development of low cost and/or low power consumption electronic and optronic systems[36,37 and 38].

2.2.3. Advantages of organic semiconducting materials in electronic biosensor applications

Organic semiconductors offer a set of advantages for applications including bio-sensing[39 and 40]. For instance, the physical and chemical properties of these materials are easily adjustable. The synthesis route can be altered, and post-film deposition treatment employed to develop novel and improved (opto-)electronic properties, as well as to deliver biocompatible and bio-stable interfaces[41]. Thus, new and interesting sensing mechanisms can be explored with preserved native biofunction of biological specimens[40].

Organic semiconductors are held together in thin film by Van der Waal's forces (weak interactions). While this is a limitation for charge transport, it confers a certain flexibility[42] that can be exploited to develop systems that can fit to an arbitrarily shaped

object over a large area with cost-effective techniques such as printing[43]. This can facilitate and improve the communication between the electronic and the biological systems as well as reducing the device manufacturing cost.

Several transducers based on organic semiconductors have been successfully employed as biosensors. During the last two decades, the electrolyte gated organic field effect transistor, known as EGOFET, is emerging as a versatile key technology of biosensors[17] and [44].

2.3. Electrolyte-gated organic field-effect transistors (EGOFET)

Electrolyte gated organic field effect transistors are solid state devices built with an organic semiconductor, an electrolyte and at least three terminals for connections to external circuits. Note: the terminals are in most cases made of conducting materials (*e.g.* gold (Au), silver (Ag), aluminium (Al)). A thin film of the organic semiconductor links the two terminals labelled source and drain. This defines the channel region of the device. The source and drain terminals are used to inject and collect the majority charge carriers into and from the device channel. The electrolyte separates the third terminal, termed the gate, from the organic semiconductor (**Figure 2-6**)[45].

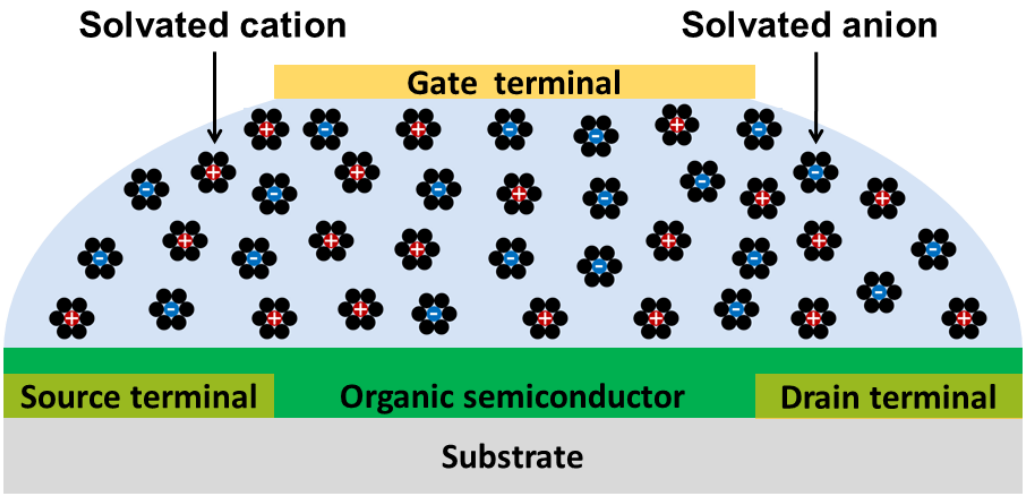

Figure 2-6: *Cross section of an electrolyte gated organic field effect transistor. It consists of three terminals (labelled source, drain, and gate), organic semiconductor between source and drain and insulated from the gate terminal by an electrolyte. Here the electrolyte is a salt dissolved in water for illustration, but other electrolytes have been reported.*

In this device, the resistivity of the channel between the source and drain terminal is indirectly controllable by the potential of the gate electrode.

In fact, in an EGOFET the electrolyte interfaces with the gate terminal and the organic semiconductor. Applying a potential to the gate terminal (source grounded), results in the

accumulation of charges on its surface (excess or deficiency of electrons). This disrupts the distribution of ions in the electrolyte to maintain the neutrality of the gate terminal/electrolyte interface. Ions of opposing sign to the surface charges of the gate electrode are electrostatically attracted towards the interface while the co-ions are repulsed. Due to strong coulombic interaction, near the electrode-electrolyte interface, this results in the formation of a compact and organised ionic layer called Stern or stationary layer. The Stern layer does not completely screen the surface charge of the gate terminal[46]. A second ionic layer, containing mobile and unorganised ions, is located beyond the Stern layer, this is known as the Gouy-Chapman diffusion layer. The ions concentration (c_i: concentration of ion i) in this diffuse ionic layer results from the interplay between the exceeding electrostatic force of the gate surface charges and the random thermal motion. It decays exponentially with the distance from the Stern layer following a Boltzmann distribution[47]:

$$c_i = c_i^0 exp^{-\frac{z_i e\varphi(\vec{r})}{\kappa T}} \tag{2.3}$$

c_i^0 and z_i stand for the concentration and valence of ion species "i" in the bulk solution, e is the elementary charge, $\varphi(\vec{r})$ is the potential at position r, κT is the product of the Boltzmann constant time the temperature of the system. The profile of the electric field of the Gouy-Chapman diffuse layer is usually derived from the solution of the Poisson-Boltzmann equation[47 and 48]. The Poisson equation expresses as the variation of potential with the distance from the Stern layer as a function of the density of ionic charge ($\rho(\vec{r})$):

$$\nabla^2\varphi = -\frac{\rho(\vec{r})}{\varepsilon\varepsilon_0} \tag{2.4}$$

The density of ionic charge is the number of ionic charges per volume and is related to the ionic concentration:

$$\rho(\vec{r}) = \sum_i z_i e c_i = \sum_i z_i e c_i^0 exp^{-\frac{z_i e\varphi(\vec{r})}{\kappa T}} \tag{2.5}$$

By combining equation (2.4) and (2.5) the Poisson-Boltzmann equation is obtained:

$$\nabla^2\varphi = -\frac{e}{\varepsilon\varepsilon_0}\sum_i z_i c_i^0 exp^{-\frac{z_i e\varphi(\vec{r})}{\kappa T}} \tag{2.6}$$

The solutions to this equation (2.6) give the variation of the potential with the distance from Stern layers. Note: the surface charges of the gate terminal coupled to the Stern and Gouy-Chapman layer is called the electrical double layer[44].

The co-ions (ions with the same sign of gate surface charges) that have been displaced toward the semiconductor layer induce opposite charges (holes or electrons) to accumulate in the organic channel. This leads to the formation of a second electrical double layer (EDL) at the semiconductor interface, as schematically shown in **Figure 2-7**.

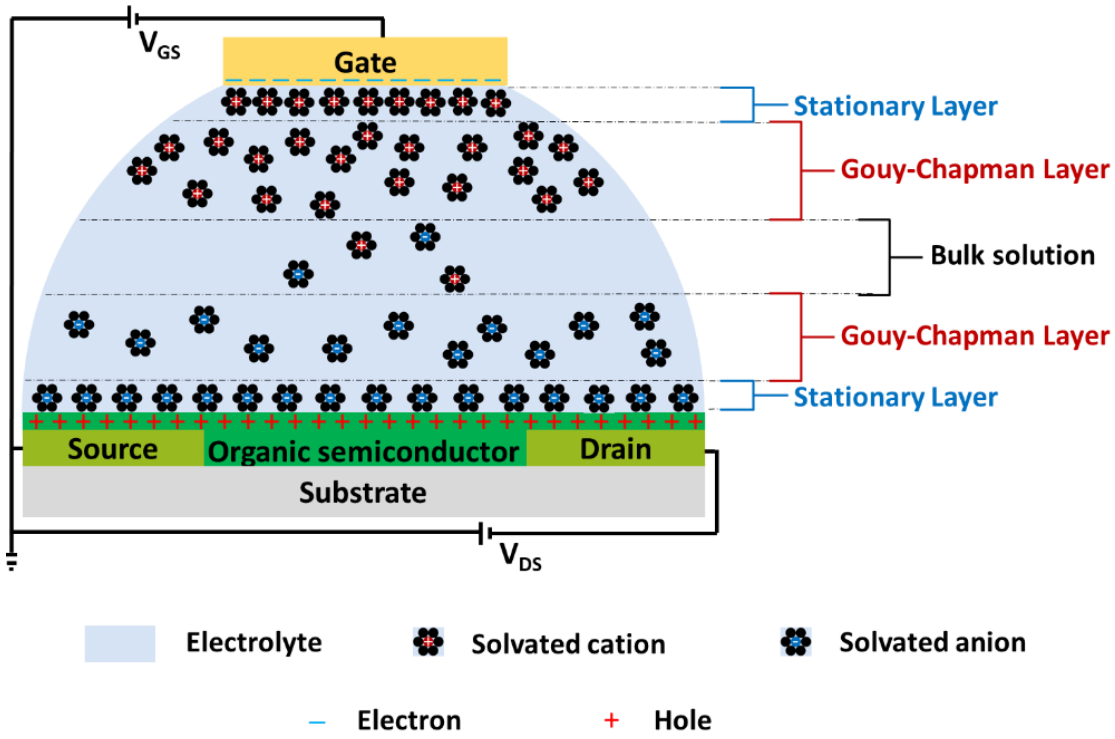

Figure 2-7: *Cross-section view of an electrolyte gated organic field effect transistor showing the electrical double layer (stationary + Gouy-Chapman plan) that forms at the interface between the electrolyte and the organic semiconductor and the gate terminal. The picture is not to scale.*

It is these two EDLs, controlled by the gate potential, that dictate the conductivity of the organic channel at a given voltage applied to the drain terminal.

2.3.1. Fundamentals of the electrolyte-gated organic field-effect transistor

The current understanding of the fundamentals of EGOFET is the physics of organic field-effect transistor (OFET) in which the concepts of electrical double layer capacitance is incorporated[49 and 50]. An OFET converts voltage into a drain current (I_{DS}) via capacitive coupling. The magnitude of I_{DS} is proportional to the quantity of accumulated mobile charges in the conducting channel. It is adjustable by the voltage of the drain (V_{DS}) and gate (V_{GS}) terminals (source grounded). A widely accepted theory that describes this transduction of voltages into current in an OFET is the charge drift model. In this model, the number of mobile charges that accumulate (Q_{mob} (x)) in the channel at a given position x through the gate capacitance (C_{gate}) is given as:

$$Q_{mob}(x) = C_{gate}(V_{GS} - V_{th} - V(x)) \quad (2.7)$$

V_{th}, termed the threshold voltage, denotes the fact that not all the accumulated charges are mobile due to the presence of trapping sites (e.g. defect, dipoles present in or at the interface of the conducting channel with the gate insulator). It is the minimum voltage required to outmatch the potential mismatch between the work function of the gate and the conducting channel, from which a further increase of V_{GS} induces a significant number of mobile charges to accumulate. And V(x) is the potential of the conducting channel induced by V_{DS} at a given position x.

In EGOFETs, the EDLs at the interface of the gate and conducting channel with the electrolyte controls the number of accumulated charges in the channel. Stern in his Gouy-Chapman-Stern model provides the distribution of ions and charges in the EDLs. In this model the capacitance of the EDL (C_{EDL}) is the series sum of the capacitance of the stationary (C_{Stat}) and Gouy-Chapman (C_{G-C}) layer:

$$\frac{1}{C_{EDL}} = \frac{1}{C_{stat}} + \frac{1}{C_{G-C}} \quad (2.8)$$

C_{Stat} and C_{G-C} are the capacitances proposed by Helmholtz[51] and Gouy-Chapman[52 and 53] for the two components of the EDL. They are dependent on the relative and vacuum permittivity (ε and ε_0), the ionic strength (c_∞) of the electrolyte, Boltzmann's constant (κ), the temperature (T), the elementary charge (e), as well as the electrode potential (φ_0) and the thickness of the Stern layer (d) according to:

$$C_{stat} = {\varepsilon\varepsilon_0}/{d} \text{ and } C_{G-C} = \varepsilon\varepsilon_0 / \sqrt{\varepsilon\varepsilon_0 \frac{\kappa T}{2e^2 c_\infty}} \cosh\left(\frac{e\varphi_0}{2\kappa T}\right) \quad (2.9)$$

Tu *et al* combined this definition of EDL capacitance with the charge drift model of OFET to describe the current versus voltage behaviour of EGOFETs in both linear ($V_{DS} < V_{GS}-V_{th}$) and saturation ($V_{DS} > V_{GS}-V_{th}$) device operation regime[49]. The Tu model considers the device as an electronic circuit consisting of resistors whose resistivity is controlled by a non-linear gate voltage dependent capacitor (C_{EDL}). The capacitive coupling is assumed to be purely electrostatic, hence C_{EDL} contains a voltage independent (C_0) and dependent component (C_V) to reflect respectively the Helmholtz and Gouy-Chapman capacitors of the EDLs in the EGOFET:

$$C_{EDL} = C_0 + C_v(V_{GS} - V_{th} - V(x))^{\chi} \quad (2.10)$$

The non-linear voltage-dependent capacitance factor is accounted for χ. Substituting C_{gate} of the OFET by C_{EDL} and considering other factors such as the channel length, gate voltage dependent contact resistance, the authors provide equations that describe quantitatively and qualitatively I_{DS} vs V_{GS} and I_{DS} vs V_{DS} (transfer and output characteristic) dependence of the EGOFET. These characteristics fit well the experimental electrical performances of poly(2,5-bis(2-thienyl)-3,6-dihexadecylthieno[3,2-b]thiophene) (PTTTT) and to the saturation on-state drain current of poly(3-hexylthiophene-2,5-diyl) (P3HT) based EGOFET (**Figure 2-8**)[49].

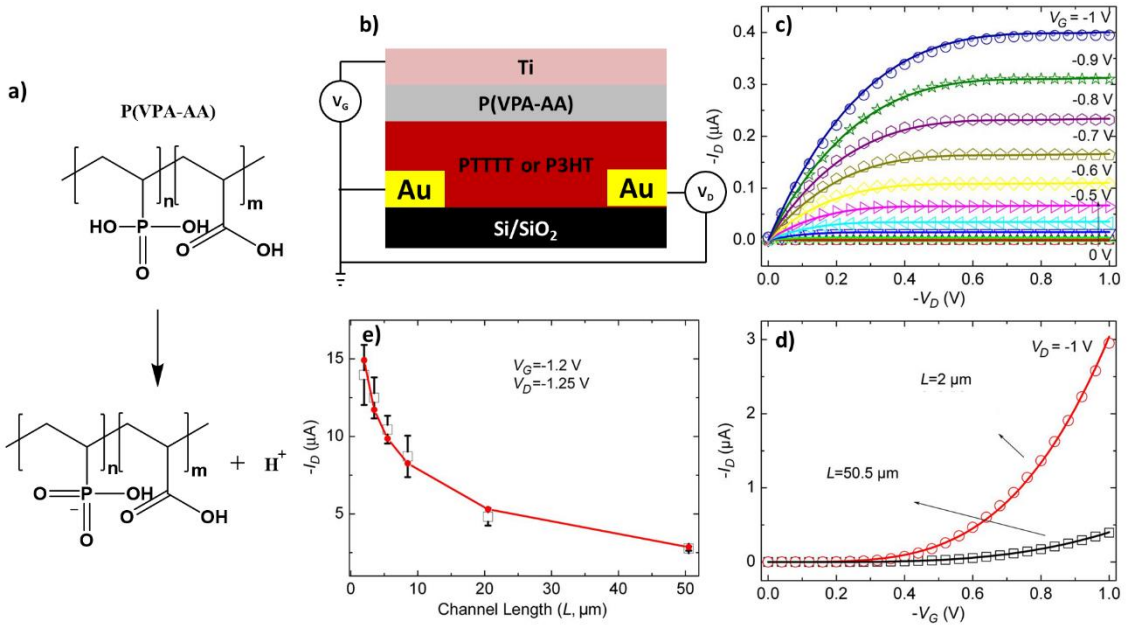

Figure 2-8: *a) Chemical structure of the electrolyte employed: a random copolymer of vinyl phosphonic acid and acrylic acid (P(VPA-AA) and its deprotonated process under a negative bias. b) Cross-section view of the EGOFET employed in the Tu et al. work*[49]*, together with c) the transfer (PTTTT), d) output characteristics (PTTTT) and e) drain current (P3HT) at different channel length (L) of EGOFET showing the fitting of experiment results (dots) with theoretical simulation (line). Note L, V_D, V_G stand for the channel length, drain voltage and gate voltage respectively. Figure c), d) and e) Reprint from Tu et al.* [49] *with the permission of IEEE, copyright © 2011, IEEE*

However, in Tu model, the contribution of the EDL that forms at the gate-electrolyte interface (C_{ge}) to the overall capacitance felt by the channel was not considered. Such an approximation works for the devices used by the authors, as the capacitance of the EDL of the semiconductor-electrolyte (C_{se}) is much smaller than C_{ge} (protons are very small as compared to anions in P(VPA-AA)). To be general, the model needs to take into consideration the capacitance of the EDL that forms at the gate/electrolyte interface, and the movement of the ions as well as the electrochemical doping phenomena that may occur in the device (even minor), during and after biasing the terminals. This may be possible by the reconciliation of the physics of OFET with that of the OECT and including the parameters that can be modulated to balance between the two models. This is

important because a better understanding of device operation logically yields an improved ability to better performance, operational stability and expanded applications.

An interesting property of EGOFET is its ability to effectively transduce small voltages (≤ 1 V) into high drain currents (few μA). This is possible because the capacitance of the electrical double layer, dictated by the Debye screening length ($\delta = \frac{\epsilon\epsilon_0\kappa T}{2e^2C_\infty}$), can be made higher than that of metal oxide as well as organic and hybrid high-k dielectrics by increasing the ionic strength/concentration of the electrolyte. Thus allowing the induction of higher quantity of charge carriers in the conducting channel at low voltage for EGOFET device as compared to standard OFETs[54,55 and 37]. This transduction of voltage to current is evaluated by the determination of several parameters including the normalized trans-conductance (product of field-effect mobility, μ with electrical double layer capacitance, C_{EDL}) ($\mu.C_{EDL}$), the on-to-off drain current ratio (I_{on}/I_{off}), the subthreshold swing (SS = $1/S_{Slope}$) as well as the transient off-to-on and on-to-off switching time (τ_{on} and τ_{off}).

The V_{th} and $\mu.C_{EDL}$ are obtained from linear fits to equations 2.11 or 2.12.

$$I_{DS} = \mu.C_{EDL}.V_{DS}.(V_{GS} - V_{th})W/L \text{ (Linear regime: } V_{DS} \ll V_{GS} - V_{th}) \quad (2.11)$$

$$\text{or } \sqrt{I_{DS}} = \sqrt{\mu.C_{EDL}.\frac{W}{2L}}.(V_{GS} - V_{th}) \text{ (Saturation regime: } V_{DS} \geq V_{GS} - V_{th}) \quad (2.12)$$

Where W and L represent the width and length of the channel. V_{th} is determined from the intercept of the fitted line with the gate voltage axis and the $\mu.C_{EDL}$ is obtained from the slope (B^2) following equations: $\mu.C_{EDL} = \frac{BL}{W}$ (when $V_{DS} \ll V_{GS} - V_{th}$) or $\mu.C_{EDL} = \frac{2BL}{W}$ (when $V_{DS} \geq V_{GS} - V_{th}$). This widely used technique of extracting $\mu.C_{EDL}$ and V_{th} is applicable to EGOFET when the $\sqrt{I_{DS}}$ increases linearly with the gate voltage. However, this is not always the case as μ[56] and C_{EDL}[53 and 52] can be gate voltage dependent. This may affect the linearity of $\sqrt{I_{DS}}$ curves, thus making the fitting procedure subjective. An alternative to this extraction technique consists of calculating μ from the density of injected charge in the device 2D channel (Q')[57] and determining the C_{EDL} via techniques such as Cyclic Voltammetry (CV)[58] and Electrochemical Impedance Spectroscopy (EIS)[59].

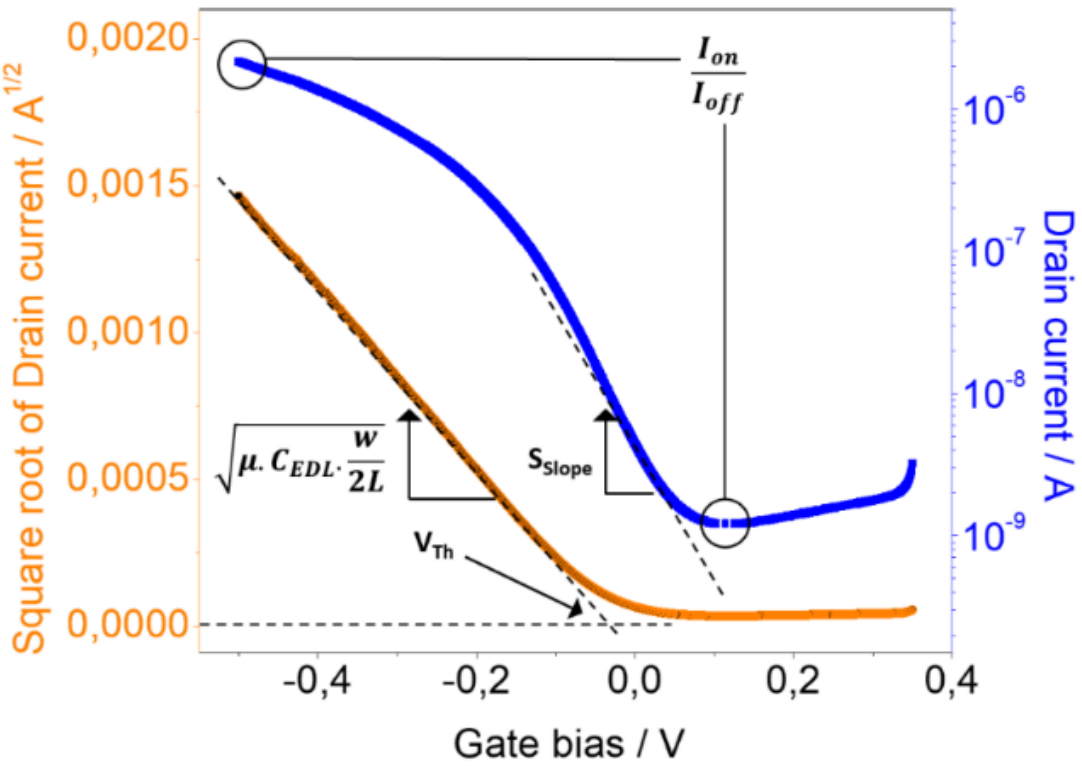

Figure 2-9: A *typical drain current-gate voltage characteristic for an EGOFET based on a p-type semiconductor at V_{DS} = -0.5 V and its square root exemplifying how the electrical figures of merit: $\mu.C_{EDL}$, V_{th}, I_{on}/I_{off}, and SS (=1/S_{Slope}) are obtained.*

The on-off ratio ($\frac{I_{on}}{I_{off}}$) is simply the ratio of the maximum to the minimum source-drain currents. The inverse of the slope of the linear fit of I_{DS} vs V_{GS} curve at the sub threshold region gives the subthreshold swing (SS). This indicates how fast the device switches from the off to the on-state. **Figure 2-9** illustrates the extraction of the mentioned parameters from I_{DS} and $\sqrt{I_{DS}}$ versus the gate bias curve. The magnitude of all these figures of merit depends on the device architecture and the materials employed as terminals (source, drain and gate), electrolyte and the conducting channel.

A few organic semiconductors are suitable for use as the channel of EGOFETs. This is due to the fact that the capacitive coupling between the conducting channel and the electrolyte must be solely electrostatic to guarantee pure field effect behaviour. The semiconductor needs to be impermeable to the ions of the electrolyte and chemically stable in order to prevent the electrochemical doping phenomenon. Otherwise, the device does not act as an EGOFET but as an organic electrochemical transistor (OECT). In contrast to EGOFETs, OECTs are devices where electrolyte penetration into the conducting channel is necessary for voltage to current transduction[44 and 60]. For this reason, the materials of choice for EGOFETs have been single crystal, small molecules and polycrystalline polymeric organic semiconductors. In fact, at optimum processing

conditions, these materials can display a good range of homogeneous compact crystallites (few tens of nanometres to a few tens of microns) in the solid state with few or undetectable amorphous domains. This crystalline nature may reduce the likelihood of electrolyte penetration into the conducting channel[58]. The hydrophobicity and organisation of the side chains of polymers need to be considered to protect the semiconductor from ions as well as improve the rigidity of the structure. Spectroscopy studies reveal that the degree of order of the semiconductor surface may alter when interfacing with liquid electrolytes[61]. **Figure 2-10** shows some of the most used organic semiconductors in EGOFET.

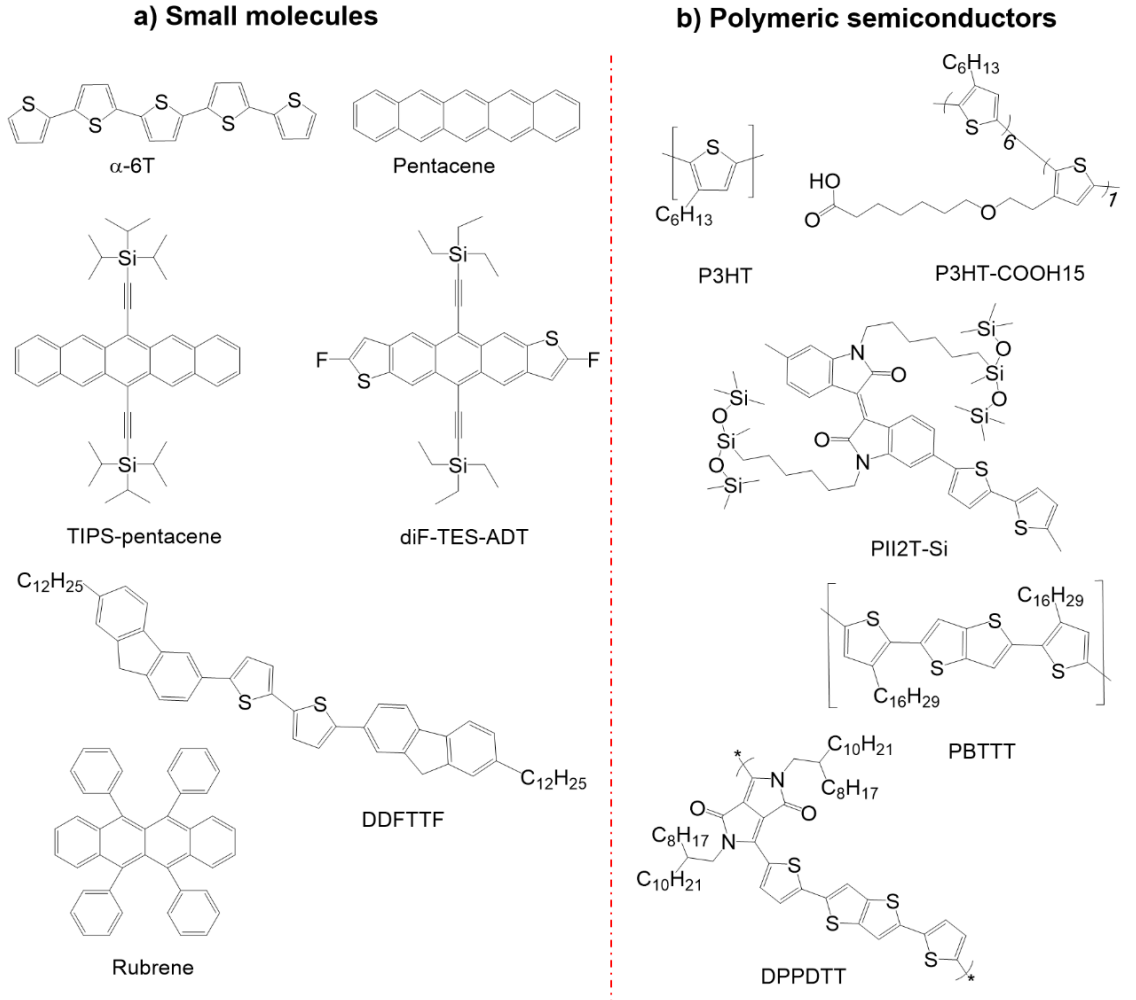

Figure 2-10: *A selection of organic small molecules and polymeric semiconductors explored in liquid gated organic field effect transistors (EGOFET).*

P3HT is to date the most studied organic semiconductor used in EGOFETs[45, 17 and 62]. P3HT is a thiophene (sulphur heterocycle) based polymer with a six-carbon linear alkyl group at the third position as displayed in **Figure 2-10**. It can be synthesized electrochemically[63] or chemically by using procedures such as oxidative polymerization[64] or catalytic cross-coupling reactions of bromothiophenes[65]. The latest chemical synthesis yields P3HT with excellent regioregularity, which in concert with a high polymeric

molecular weight are fundamental for the production of highly crystalline films[66]. P3HT processed from various solvents with a diversity of deposition techniques have been shown to perform reasonably in EGOFETs[45, 58 and 67]. Mobility values higher than 0.1 $cm^2.V^{-1}.s^{-1}$ (range: 10^{-3} – 0.16 $cm^2.V^{-1}.s^{-1}$) and drain current modulated over five orders of magnitude at a low gate voltage ($|V_{GS}| < 1$ V) were achievable in EGOFETs. Though P3HT is a benchmark material to advance the device physics of EGOFETs, its low ionization potential (HOMO around -5 eV) is rather a limitation for applications requiring long-term stability. It is worth mentioning that multiple single crystal nanofiber (few tens of nanometers to a couple of tens of microns long) of P3HT can be processed[68 and 69]. Such films have been shown to display a field-effect mobility as high as 2 $cm^2.V^{-1}.s^{-1}$ in an EGOFET[70]. The single crystalline nature can greatly improve the stability of these materials.

More environmentally stable polycrystalline polymeric semiconductors with superior charge conducting properties have also been explored in EGOFET devices[71 and 72]. Poly(2,5-bis(3-alkylthiophen-2-yl)thieno[3,2-b]thiophene), known as PBTTT, is a good example. The distinction between P3HT and PBTTT is the presence of two fused thiophene rings in the PBTTT π-conjugated backbone (**Figure 2-9**). For this reason, PBTTT has a slightly deeper HOMO (≈ -5.2 eV) and a more rigid polymer backbone when compared to P3HT. While both form an ordered lamellar structure, the size and morphology of the crystallites are different[73 and 74]. The former displays a terrace phase with an order of magnitude larger crystallite domains when thermally treated above its liquid crystal phase temperature (130˚ C)[75]. Such structures perform well in EGOFETs with field effect mobility in an excess of 3 $cm^2.V^{-1}.s^{-1}$ [75]. The ribbon phase of PBTTT has also been observed when their films were annealed above the polymer isotropic phase temperature (235˚ C) and then cooled. With such an improved crystalline structure Ito *et al.* reported an EGOFET with two-digit mobility (≈ 10 $cm^2.V^{-1}.s^{-1}$)[75]. In addition, to the improved performance, PBTTT is one the few polymeric semiconductors for which the electrical stability has been tested in EGOFET. Reasonably stable drain currents for up to two-hours of continuous bias stress measurement has been reported for PBTTT[76]. The authors applied -1 V bias to the terminals (V_{DS} and V_{GS}) up to 2 h while recording the drain current under a continuous flow of the electrolyte (water at 250 μL/min). After a decrease of 70 percent for about 1 h, the I_{DS} remained unchanged for 1 h. The initial decrease in I_{DS} was probably due to the removal of some dopants present in the PBTTT film. This improved operational stability is likely due to the crystalline nature of PBTTT

in concert with the interdigitated side chain that reduce the probability of ion penetration within the PBTTT film.

Small molecule organic semiconductors are considered to be the ideal materials for high-performance and stable EGOFETs, as they are known to organize well into polycrystalline films and single crystals, with much smaller, fewer or undetectable amorphous domains than in the polycrystalline polymeric semiconductors[77 and 78]. TIPS-pentacene (6,13-bis(triisopropylsilylethynyl)pentacene) (**Figure 2-10**) can be considered as a benchmark organic small molecule in organic electronics. In contrast to the majority of small molecules, TIPS-pentacene can be processed from a range of organic solvents (e.g. toluene, tetrahydrofuran, xylene) with a wide range of solution deposition techniques[79,80 and 81]. Techniques such as drop-casting and bar-assisted meniscus shearing (BAMS) have been used to deposit TIPS-pentacene also as a blend with polystyrene (ratio 4:1 in chlorobenzene solution) in the development of EGOFETs[82 and 59]. In both cases, the device performed reasonably with the field-effect mobility of 0.1 (a blend of TIPS-pentacene and PS) and 0.01 $cm^2.V^{-1}.s^{-1}$ (pristine TIPS-pentacene), for the BAMS and drop-casted films respectively. In addition, EGOFET devices based on the blend film displayed an on-to-off current ratio of about 10^3. This is an order of magnitude superior to that of the drop casted, pristine TIPs-pentacene device. These variations in the figures of merit confirm that the processing condition of the organic semiconductors, its nature and the device channel geometry are pivotal for the development of high-performance EGOFETs. Other small molecules including (5,50 -bis-(7-dodecyl-9Hfluoren-2-yl)-2,20 –bithiophene (DDFTTF) performed well in EGOFETs[83]. However, due to the absence of solubilising side chains, the majority cannot be processed from solution.

High-performance donor-acceptor (D-A) polymeric semiconductors may be promising materials in EGOFETs. These polymers consist of an array of alternating electron rich (donor) and deficient (acceptor) unit[30]. By carefully choosing the donor and acceptor unit one can build polymers via aromatic hetero coupling techniques (e.g. Suzuki reaction, Stille polycondensation) to obtain the desired structural and optoelectronic properties[84]. These materials display very small π–π stacking distance with excellent air stability due to more planar and/or rigid polymer backbone and deeper HOMO energy level. For these characteristics, D-A polymers should be considered for operation in EGOFETs.

Numerous electrolytes, including polyelectrolyte[85], ionic gel[86], and ionic liquids[87] have been employed in EGOFET devices. These devices were used for a diversity of purposes ranging from studying of charge transport properties of organic semiconductors[57] to applications including complementary integrated circuits[72], gas sensing[88], as well as stretchable electronics[89]. For bioelectronic applications, the electrolyte adopted is one based on salts dispersed into a polar solvent. To set the benchmark, figures of merits of EGOFETs obtained with various organics semiconductors when liquid electrolyte (e.g. purified water and saline solution) are employed are summarized in **Table 2-1**.

Polymers	Electrolyte	C μF/cm^2	μ × 10^{-2} cm^2/(Vs)	V_{th} V	I_{on}/I_{off}	SS mV/dec	Ref
Rubrene	water	-	0.67	-0.09	8 × 10^4	-	45
P3HT	water	3.0	0.59	-0.16	150	200	45
PII2T-Si	NaCl (10 μM)	-	0.1 ± 0.08	-0.72 ± 0.02	10^3	-	90
DB-TTF:PS	water	1.2	6 ± 5	0.86 ± 0.08	-	-	91
PCBM	water	1.0	0.8	0.18	-	-	72
PBTTT	water	0.6	8	0	10^2	-	58
TIPS-pentacene	water DPBS	3.8 1.8	1.3 0.17	-0.14 0.5	10^3 10^3	- -	82
TIPS-pentacene:PS (1:2 ratio)	water 1 M NaCl	- -	12 7	0.01 ± 0.002 -0.166 ± 0.005	7.3 × 10^3 1.0 × 10^4	87 ± 3 77 ± 6	59
diF-TES-ADT	water 1 M NaCl	- -	0.4 2	-0.028 ± 0.004 -0.120 ±0.002	1.6 × 10^2 5.5 × 10^2	121 ± 1 90 ± 4	59
diF-TES-ADT:PS (4:1 ratio)	water	5.3	4.3	0.39	5 × 10^3	-	92
α-6T	HEPES Buffer (5 mM)	2-8	2.2	-	-	245	93
P3HT:PMMA (3:7 ratio)	water	-	5	0.38	1.5 × 10^3	-	67

Table 2-1: *Summary of figure of merits of EGOFET gate with liquid electrolyte (water, NaCl, HEPES buffer and Dulbecco's Phosphate-Buffered Saline (DPBS).*

2.3.2. Electrolyte-gated organic field-effect transistor in ion sensing

According to the Stern model, the electrical double layer structure depends on parameters including the nature and surface state of the electrodes, the electrolyte properties (e.g. nature and quantity of ions, viscosity) as well as external stimuli such as the temperature. Adding of new charged species (e.g. ions, small molecules) or increasing existing electrolyte ions alter the structure of the electrical double layer (e.g. decreases of Debye screening length, viscosity). This can affect the magnitude of the EDL capacitance that controls the density and movement of charge carriers induced in the channel of the EGOFET. Therefore, the presence and quantity of charged species in aqueous media can be determined by simply comparing the electrical figures of merit of EGOFETs between a reference and the sample to be analysed.

Based on this observation, EGOFETs were applied for the identification and quantification of ions in liquid environments[90]. For instance, Buth *et al.* fabricated an α-sexithiophene based EGOFET and demonstrated the utility of this device for the detection of the concentration of three monovalent salts (KCl, NaCl, and KBr)[91] (**Figure 2-11**).

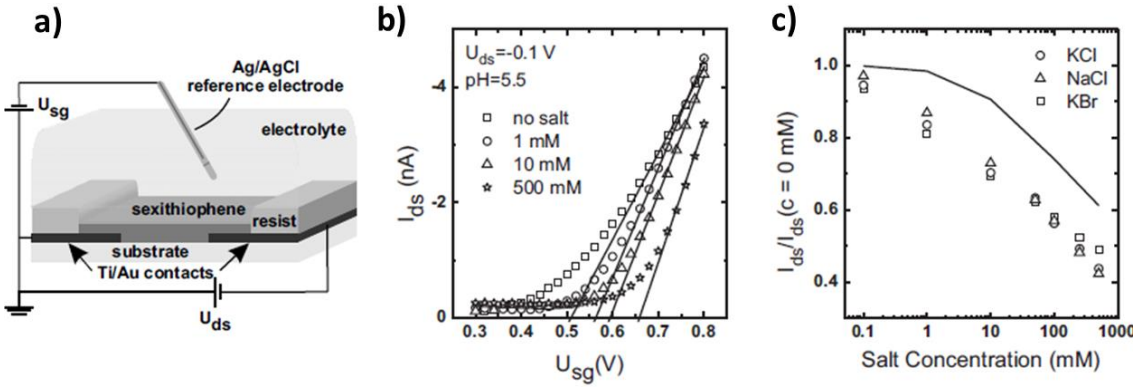

Figure 2-11: *Buth et al.* [91] *monovalent salts (KCl, NaCl, and KBr) sensor: a) Schematic representation of the EGOFET, b) Impact of salt concentration on the transfer characteristics of the developed devices and c) the dose curve showing a correlation between relative drain current response of the sensor as a function of salt concentration. Reprint from Buth et al.* [91] *with the permission of AIP Publishing, copyright © 2011, AIP Publishing.*

A decrease in the normalized on-state drain current with increasing salt concentration can be seen in the reported data (**Figure 2-11.c**). Interestingly the decrease in the drain current observed was accompanied by a threshold voltage shift, a decrease of the subthreshold swing in concert with an increase of mobility (**Figure 2-11.b**). These variations in electrical figures of merit are provoked by the change in the electrolyte ionic strength. The increase in the concentration of salts in the electrolyte augments the quantity of ions, which in turn allows a more effective screening of the surface charges. This translates into a shift in device threshold voltage, as more charges are required to fill the trap states induced by an increased number of positive ions in the Stern layer or inside the semiconductors due to ionic penetration. However, the device was unable to clearly discriminate between the three salts.

The presence of a sensitive layer is fundamental to enable EGOFETs to identify specific ions of interest. Some organic semiconductors interact with ions specifically up to a certain degree (e.g. electrostatic or electrochemical coupling). For instance, Zhang *et al.* fabricated an EGOFET that can quantify and differentiate Hg^{2+}, an environmentally toxic ion, from other divalent cations (Zn^{2+}, Mn^{2+}, Ca^{2+}, Fe^{2+}, $Cu^{2+,}$ and Pb^{2+})[92](**Figure 2-12**).

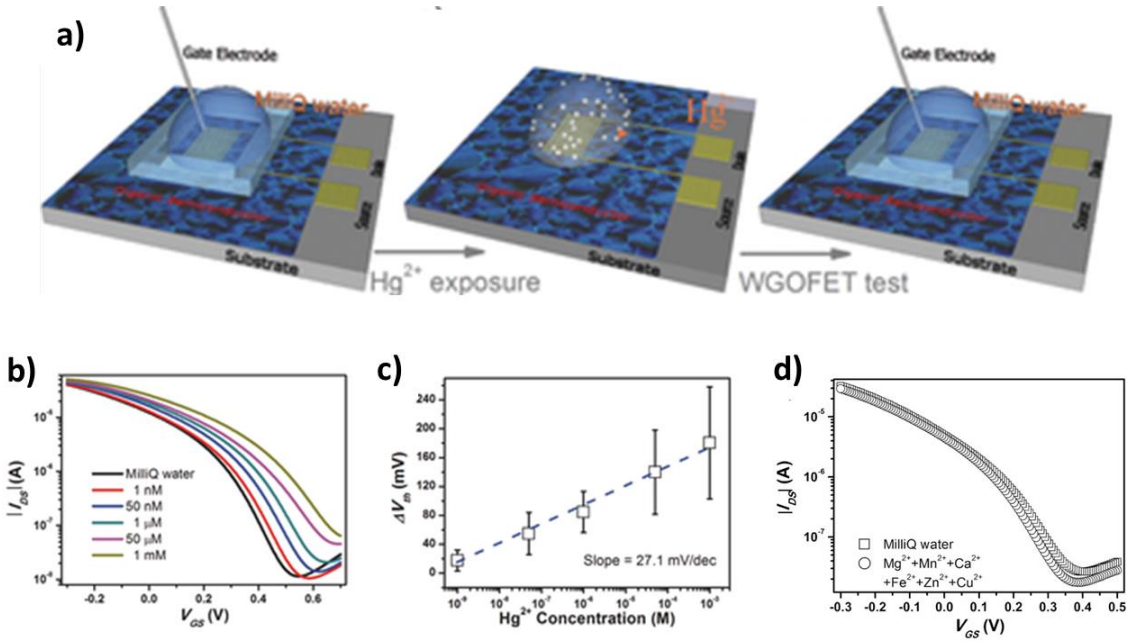

Figure 2-12: *Zhang et al.*[92] *mercury (Hg^{2+}) sensor: a) Schematic representation of the EGOFET and its utilisation procedure, b) Impact of mercury concentration on the transfer characteristics of the developed devices, c) the dose curve showing a correlation between relative variation of the threshold voltage of the sensor as a function of Hg^{2+} concentration and d) the control experiment with other divalent cations. Reprint from Zhang et al.*[92] *with the permission of John Wiley and Sons, Copyright 2017, © WILEY-VCH Verlag GmbH & Co. KGaA, Weinheim.*

The authors reported a positive V_{th} shift of the water gated OFET after exposure to Hg^{2+} (**Figure 2-12.b**). As can be seen in **Figure 2-12.c**, the shift in V_{th} observable in **Figure 2-12.b** scales linearly with the logarithm of the concentration of Hg^{2+} used. When the device was exposed to the mixture of the other divalent cations in the absence of Hg^{2+}, no major variation was observed (**Figure 2-12.d**). This specific detection is guaranteed by the fact that Hg^{2+} in contrast to the employed divalent cations electrochemically react with the chosen semiconductor due to its high oxidation potential.

Knopfmacher *et al.* demonstrated the specific detection of the same ion (Hg^{2+}) by decorating the surface of the organic semiconductor with "DNA-functionalized gold nanoparticles" (**Figure 2-13.a**)[93]. The electrolyte was confined to the surface of the device in a PDMS flow cell (**Figure 2-13.b**). In this study, the specific detection of Hg^{2+} was carried out *in situ* by measuring the transient behaviour of I_{DS} at a fixed V_{DS} and V_{GS}.

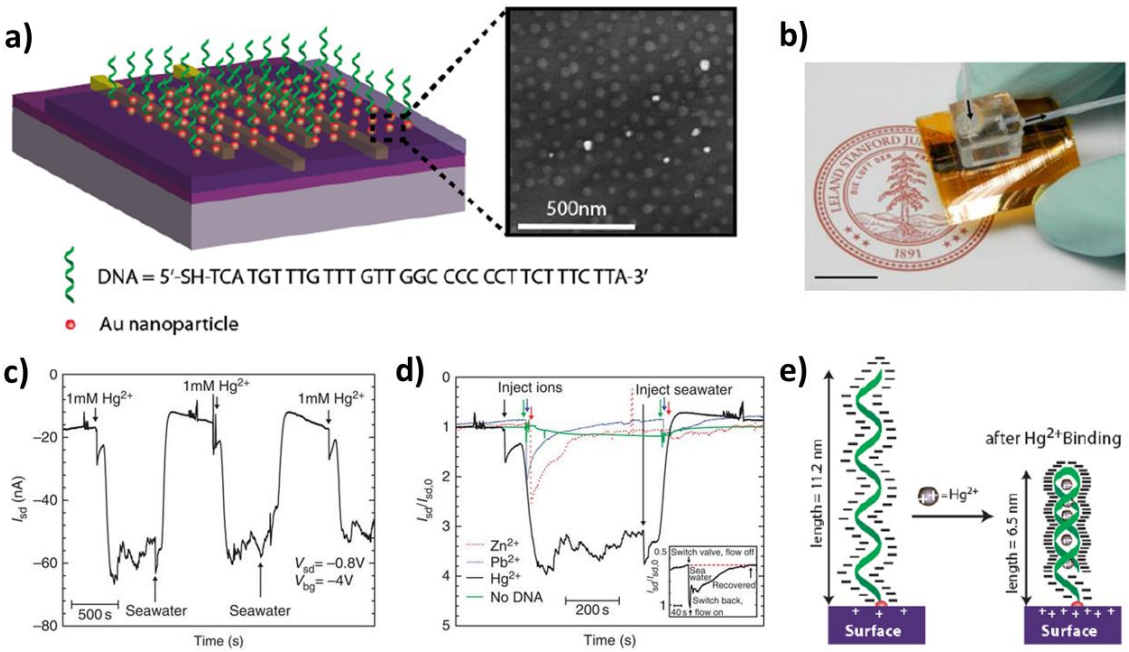

Figure 2-13: *Knopfmacher et al.* [93] *mercury (Hg^{2+}) sensor: a) Schematic representation of the EGOFET, the inset displays a scanning electron microscopy picture of the device surface displaying nanostructure (gold nanoparticle with ssDNA) b) a photograph of the sensor, c) the device drain current response to 1 mM Hg^{2+} injection and seawater as a function of times, d) control experiments showing drain current response to the injection of other divalent cations and without ssDNA on the device surface, and e) illustration of the conformational change of ssDNA upon interaction with Hg^{2+}. Reprint from Knopfmacher et al.* [93] *with the permission of Springer Nature , copyright © 2014, Springer Nature.*

The authors recorded a three-time increase of I_{DS} upon 1 mM Hg^{2+} injection into the flow cell (**Figure 2-13.c**). It can be noticed that their sensor displays a negligible response to the divalent cations Zn^{2+} and Pb^{2+} in comparison to Hg^{2+}(**Figure 2-13.d**). In the absence of DNA on the organic semiconductor, the sensor response to Hg^{2+} was weak. This selectivity was attributed to the fact that Hg^{2+} induces a conformational change of the DNA by binding to it (**Figure 2-13.e**). This reorganisation of the DNA molecules may affect the surface potential of the channel (*e.g.* charge variation and re-distribution), thus the electrical response of the EGOFET. The same principle has been applied to monitor interactions between biological molecules.

2.3.3. Electrolyte-gated organic field effect transistors in bioelectronics

The application of EGOFETs in bioelectronics is driven by the advantages of organic semiconductors (e.g. biocompatible, conformal, and tailorable with new function) combined with the simple device architecture (e.g. the sample to analyse can act as the electrolyte, an integral part of the device), it is also compatible with current microfabrication techniques and operates at low voltage (< 1 V)[71].

2.3.3.1. Biomolecule interaction monitoring

EGOFETs were successfully fabricated that show potential for applications in the field of medicine for molecular diagnosis and prognosis[94 and 95]. For example, Seshadri *et al.* built an immunosensor based on an EGOFET with a physisorbed biorecognition layer on the channel surface (P3HT)[62]. The biorecognition layer comprised an antibody that can interact with the target molecules specifically interspaced with bovine serum albumin (BSA). In this work, the authors used BSA to fill the gaps between bioreceptors (anti-procalcitonin) in order to prevent nonspecific interaction that can induce a false positive in the sensor response (**Figure 2-14.a**). With this architecture, the EGOFETs were able to detect procalcitonin, a biomarker that can be used for the diagnosis of bacterial infections by taking advantage of the specific antibody-antigen affinity coupling.

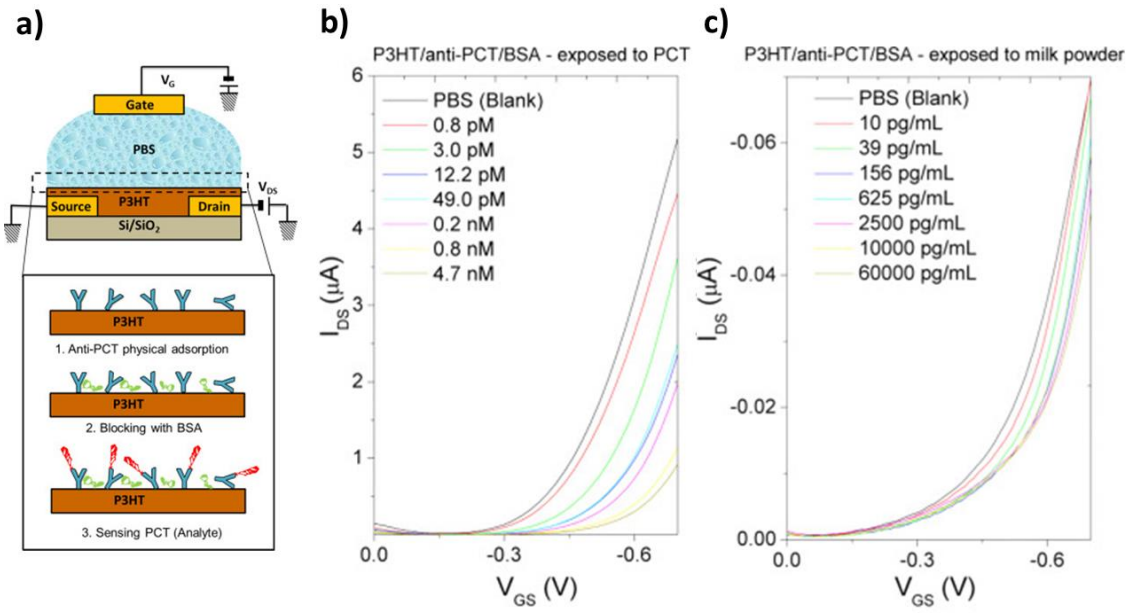

Figure 2-14 : *Seshadri et al.* [62] *procalcitonin biosensor : a) Schematic representation of the EGOFET, the inset displays how the P3HT surface has been functionalized b) the device drain current response after exposure to different centration of procalcitonin for 20 minutes and d) the control experiments showing drain current response after exposure to various concentration of milk powder (20 minutes exposure). Reprint from Seshadri et al.* [62] *with the permission of Elsevier, copyright © 2018, Elsevier.*

As can be seen from transfer curves (**Figure 2-14.b**), the drain current of the device decreases after exposure to procalcitonin molecules (20 minute exposure) when characterised with phosphate buffered saline solution as compared to the blank measurement. The higher the concentration of procalcitonin (PCT) used during the exposure time the larger the drain current decrease. These decreases in drain current are dominated by a shift in device threshold voltage which was induced by binding of PCT to anti-PCT according to the authors. In fact, the binding of PCT to the EGOFET surface may induce a change in charge distribution and quantity on the semiconductor surface

which in turn generates more trap sites to be filled. This required a larger gate voltage to turn the device fully on. The specificity of the sensor was tested with an increasing concentration of milk powder (same experimental condition to PCT detection). While the response seems to decrease with the increasing concentration of milk powder, the variations were weak compared with the sensing of PCT molecules (**Figure 2-14.c**).

Other approaches to integrate the biorecognition layer to EGOFETs at the electrolyte and semiconductor interfaces were demonstrated. Mulla *et al.* used 1-Ethyl-3-(3-dimethylaminopropyl)-carbodiimide (EDC) /N-hydroxysulfoxuccinimide (sulfo-NHS) chemistry (EDC/sulfo-NHS) to immobilize the bio-receptor on a UV crosslinked poly(acrylic acid) layer deposited onto PBTTT via a pendant carboxylic acid group (amine coupling)[96]. The sensor detects streptavidin binding to biotin (bio-receptor) down to 10 pM. Kergoat *et al.* employed the same chemistry to immobilize single-stranded DNA directly on the pendant carboxylate group of [3-(5-carboxypentyl)thiophene-2,5-diyl] (P3PT-COOH) and the device was able to detect the hybridization of DNA in water and phosphate buffered saline solution[97]. The detection of DNA hybridization was obvious in the water, while it was weak in PBS solution likely due to the charge screening effect.

Note that EDC/sulfo-NHS coupling, in theory, is a robust integration of biorecognition elements in comparison to the physisorption techniques. This is because the EDC/sulfo-NHS chemistry results in a covalent binding of the bio-receptor to the device surface, which is stronger than an electrostatic or Van der Waals interaction in physisorbed biomolecules. A drawback in functionalising the EGOFET at the organic semiconductor surface is that its electrical performance is likely to degrade. This may be due to the deterioration and, or structural variations of the organic semiconductor caused by the chemical employed in concert with the duration of the functionalisation procedure.

An alternative to functionalising the organic semiconductor surface is to use the gate terminal for biorecognition layer integration in to EGOFETs. The nature and surface state of the gate strongly affects the performance of water gated field effect transistors[98,99 and 100]. Less than a microelectronvolt changes in the work function (minimum energy required to pull an electron out of a material) results in a major shift in device figures of merit[100]. Accordingly, integration of the biorecognition layer at the interface of the gate and electrolyte was explored. Diacci and co-workers demonstrated two approaches to incorporate the sensitizer on the gate surface[101]. One strategy consisted of immobilising his-tagged antibody binding protein (protein G) on a gold wire serving as the gate

terminal, followed by fixing the bioreceptor (anti interleukin-6). In the second, a peptide aptamer that interacts specifically with the analyte was directly bound onto the gate electrode (**Figure 2-15.a**).

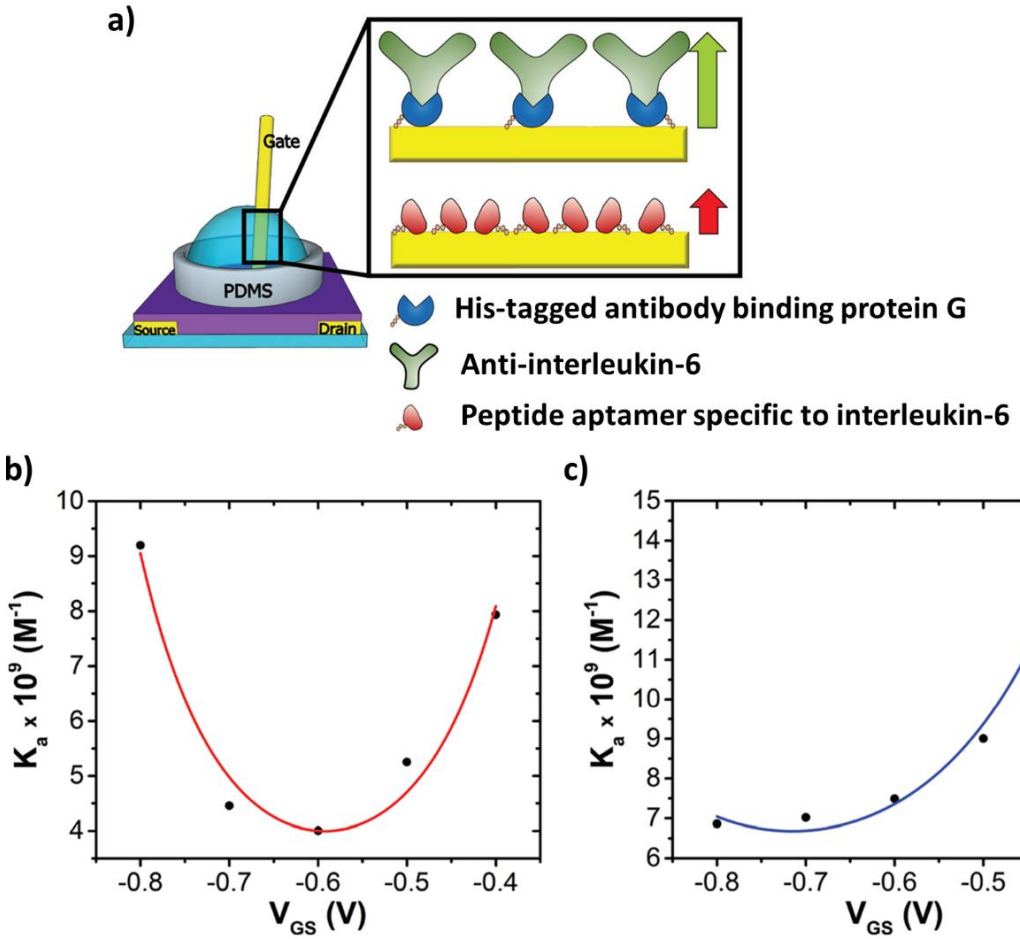

Figure 2-15: *Diacci and co-workers[101] interleukin-6 biosensor: a) Schematic representation of the EGOFET, the inset illustrates the two strategy of gate electrode functionalization, and the surface affinity constant (K_a) of the biosensor to interleukin-6 as a function of the gate bias for the two strategy (b and c). Reprint from Diacci et al[101] with the permission of AIP Publishing, copyright © 2017, AIP Publishing.*

The former immobilisation technique results in a well-orientated bio-recognition element. This improves the probability of analyte-bioreceptor interaction. The latter integration procedure guaranteed that the recognition events take place closer to the gate electrode, and thus improves the sensor response to a subtle surface change. Both of the integration strategies display similar calculated limit of detection (≈ 1 pM). In addition, the surface affinity constant, known as K_a, which is the strength of analyte-bioreceptor binding, a parameter that characterise the thermodynamics of binding of the target molecules to the receptor of the two sensors were within the same range. This parameter can be extracted by fitting the Langmuir or Hill models[102 and 103] to the sensor response curves (e.g. drain current as a function of analyte concentration). The authors found that the magnitude of the bias applied can modulate such a parameter (**Figures 2-15.b** and **Figures 2-15.b**) for

both of the sensors. This implies that the magnitude of the potential of the gate terminal can be used to improve the sensitivity of EGOFET by tuning, catalysing analyte-receptor interaction and that the device can also provide information on the thermodynamics of the biorecognition event.

Under certain circumstance, the length of the Gouy-Chapman diffusion layer, known as Debye screening length of the electrolyte has to be considered in functionalising the gate or the semiconductor surface in a liquid gated field-effect transistor. It has been observed that liquid-gated field-effect transistors drop in sensitivity when the bio interaction takes place outside the Debye screening length[104]. This is because ions present in the EDL likely screen the influence of the recognition event on the surface state of the gate or organic semiconductor layer. Two solutions were proposed in the literature to circumvent this problem[105 and 106]. The first consists of increasing the density of bioreceptor on the gate or semiconductor surface sufficiently to generate a third EDL capacitance at the bioreceptor/electrolyte interface known as a Donnan capacitor. This was demonstrated by Palazzo *et al*. in[106]. In this work, the authors show the detection of protein binding (*e.g.* streptavidin-biotin) at ~20 nm from the organic semiconductor in the serum with a Debye length of about 0.7 nm. The Donnan capacitance is smaller than the capacitance of the EDLs that form at the gate and semiconductor interface with the electrolyte, thus dominate the device capacitance. The second solution was reported by Piro and co-workers[105]. Instead of sensing the association of the target molecules (Bisphenol A) to the receptor on the surface of the sensor, the authors identified and quantified the analyte via a competitive exchange immunoassay. The method consists of detecting desorption of the receptor from the channel upon binding of the analyte (**Figure 2-16.a**).

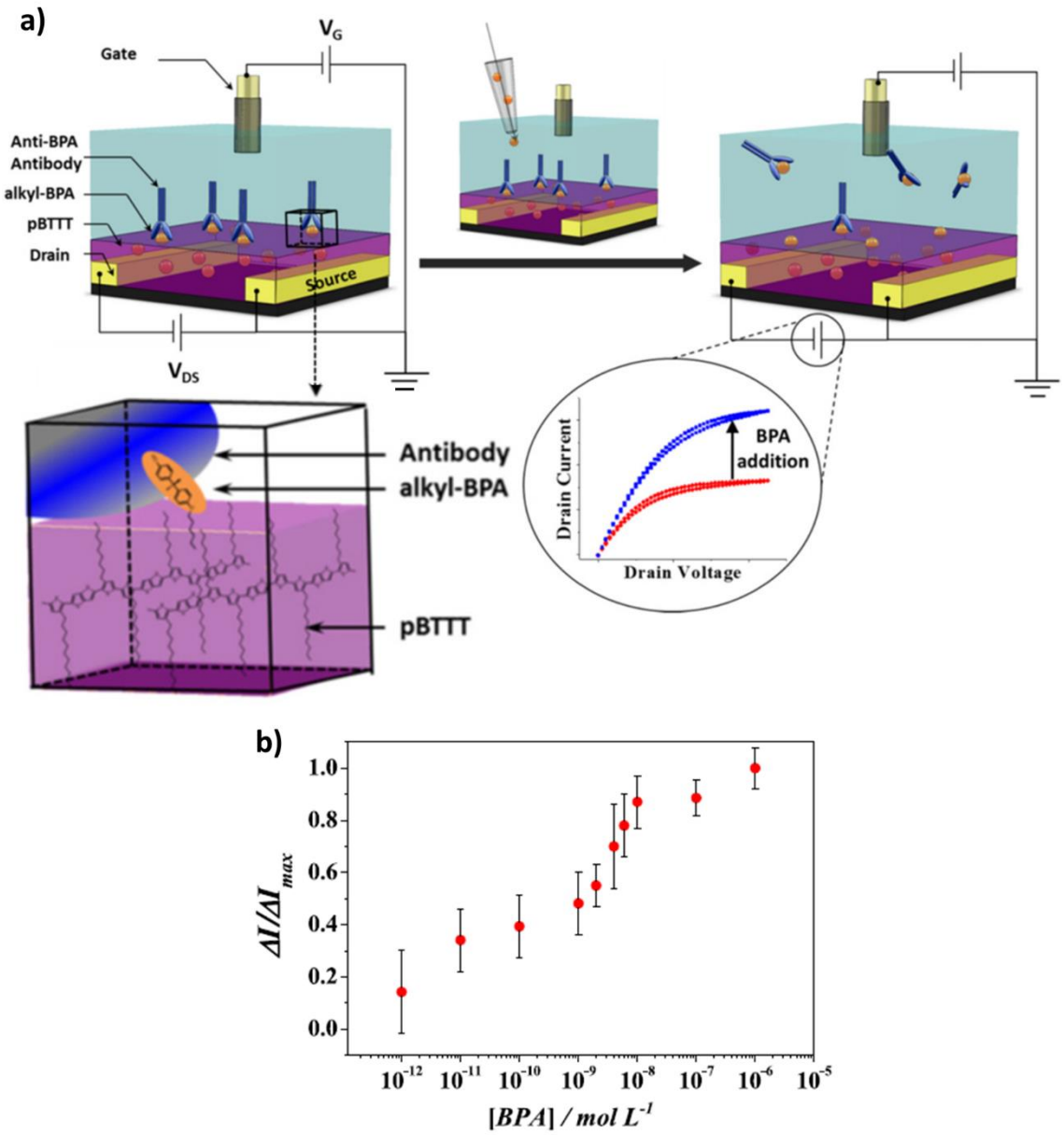

Figure 2-16: *Piro et al.*[105] *bisphenol A (BPA) biosensor: a) Schematic representation of the EGOFET showing the sensing mechanism, the inset illustrated how BPA binds to the alkyl BPA of the thin film blend of PBTTT: alkyl BPA and the device response before (red curve) and after addition of BPA (blue curve). b) the dose curve showing a correlation between relative variation of the drain current of the sensor as a function of BPA concentration. Reprint from Piro et al.*[105] *with the permission of Elsevier, copyright © 2017, Elsevier.*

This induces an increase in the capacitance of the EDL at the semiconductor/electrolyte interface which in turn leads to a rise of the device on-state drain current. The magnitude of the increase of drain current scales with the concentration of the target molecule present in the phosphate buffered saline solution (**Figure 2-16.b**). In addition to be a versatile tool for the identification of target-analyte interactions with single molecule detection sensitivity[107]; EGOFETs were reliable in simulating, mimicking and recording other biological phenomena.

2.3.3.2. Stimulating and recording of neuronal activity

EGOFETs have been interfaced with cells to stimulate and/or record their electrophysiological activities[108 and 109]. For instance, Cramer *et al.* devised a pentacene based EGOFET on top of which the different stages of a neuronal stem cell (urine NE-4C/GFP-NE-4C) differentiation into densely interconnected neurons was possible[108]. This was probably due to the biocompatibility of the pentacene in concert with the electrolyte employed (water). The authors demonstrated that bioelectronic signalling of the neural network can be stimulated and recorded. By applying a pulsed voltage to the gate terminal (V_{sim}), the physiological action of the neurons was triggered. This induced a variation in the electrostatic potential established between the neuron networks and the semiconductor channel, thus a change in the drain current of the EGOFET. The authors used the variation in the current to record and evaluate the behaviour of the stimulated neurons. However, stimulating and recording neural signalling simultaneously were not possible, as the application of V_{sim} induced a variation in the electrolyte capacitance which the authors found required several milliseconds to stabilise prior to recording the activity of the neurons. This may be problematic, as the response of the neurons to the stimulus can be instantaneous resulting in low detection sensitivity and or information lost. In addition, the device was not sensitive enough to study the differentiation of the neural stem cell into a network.

Benfenati and co-workers designed an EGOFET with a second bottom gate terminal to study the extracellular activity of dorsal root ganglion (DRG) primary neurons *in situ*[109]. In this report, the bidirectional recording of the neuronal bioelectric response was carried out simultaneously. The transient increase of the drain current, avoided by Carmer *et al.* by delaying the signal record after simulation, was removed by the authors during data processing. The technology displays a signal-to-noise ratio four times higher than the established microelectrode arrays (MEAs) in a similar experimental condition. Furthermore, the device was able to manipulate, stimulate and record the bioactivity of a single neuron. These works imply that EGOFETs can potentially deliver the required sensitivity and reliability for the study of cell differentiation, intercommunication as well as their interaction with therapeutic drugs.

2.4. Summary

An EGOFET is an OFET in which the gate terminal is insulated from the conducting channel of the device by an electrolyte. This device exploits the electrical double layer

phenomena to modulate the electrical characteristics of semiconductors below 1 V. The physics of these devices is describable by the Tu model, a combination of the current physics of OFETs with an EDL theory proposed by Stern. The Tu model can be improved by, for instance, taking into consideration the EDL that form at the gate terminal-semiconductor interface, the electrochemical doping that may happen, and ionic movement during the device operation.

Although a generalised theory that describe the physics of EGOFETs have yet to be established, it is known that the choice of the conducting channel material and device operation window are pivotal to warrant a pure or dominant field-effect charge transport. In this regard, crystalline and semi-crystalline organic semiconductors were investigated in EGOFET devices. These materials can be processed to yield uniform film with excellent degree of order, an important factor to suppress the penetration of ions into the conducting channel. Consequently, the studies of new crystalline and semi-crystalline materials as the active layer of EGOFET in concert with the use of technique that induces excellent crystallite formation (e.g. blending, solution deposition technique (BAMS)) leads to an improvement of device figures of merit. For instance, field-effect mobility was improved from ~10^{-3} to 10^{-2} $cm^2.V^{-1}.s^{-1}$ and on-to-off current ratio was about 10^2 when water acted as electrolyte. Such improvement of performance via the introduction of new materials and new processing condition is interesting. However, it is important to determine the ratio of field-effect to electrochemical transport contribution to charge transport. Because, recent works highlight that the degree of crystallinity is not the only criterion for improved performance and stability in electrolyte operation. Side chain engineering must also be considered. Particularly it is clear that these chains could be sufficiently hydrophobic and well-structured to protect the organic semiconductor from disorder induced by the contact with the liquid electrolyte. The planarity and rigidity of the organic semiconductor backbone, the π-π stacking inter-distance, orientation and organisation as well as the molecular energy levels could be very important parameters to further improve the performance and operational stability of EGOFETs. To investigate this, one can, for instance benchmark the electronic properties of organic semiconductors with these characteristics but least crystalline against a well-established semi-crystalline polymer in the field (e.g. PBTTT). This may lead to the development of better performing and operationally stable EGOFETs, which surely will fortify the potential of the device in bioelectronics and related fields. But also, to help to further understand the design characteristics the channel material as to fulfil for excellent in electrolyte operation.

Few works have been implemented to stimulate and record the bioelectric activity of cells with EGOFET devices. These works focused on the stimulation and recording of the physiological activity of neural cells via applying a bias to the gate terminal and record the drain current. The current that flows between the drain and gate terminal, which is the sum of the displacement and gate leakage currents, may provide additional information on a physiological activity. In fact, the potential generated by the cells in response to a stimulus is induced by the gradient of ions. This ionic gradient builds up within a few milliseconds via the movement of ions present in the electrolyte which are the resultant of the gate current. Thus, by following the gate current in-situ one may learn more for instance about the manner and exact timescale of how cells respond to an extracellular stimulus.

Ground-breaking works have been accomplished in identifying and quantifying various biological and chemical molecules with excellent sensitivity (single molecule level) using EGOFET device. This included dangerous chemicals, antibodies, and small molecules. The specificity of the sensors was addressed by the immobilisation of a probe molecule on either the gate-electrolyte or semiconductor-electrolyte interfaces. The reported work shows that EGOFET is becoming a key building block of bio-detection microsystems for applications in sector including healthcare, environmental protection and homeland security. Because, EGOFET technology is versatile, short assay-to-results time and its sensitivity is superior or at least equal to that of traditional technique and is within the clinically relevant range (**Table 2-2**).

Biomolecules	LOD required	LOD EGOFET	LOD Standard method	Ref
Procalcitonin (*Established marker for differential sepsis*)	≥ 4 pM	2.2 pM - 4.7 nM	0.02 - 100 ng/ml *BRAHMS PCTs II GEN*	*110,62* and *111*
Tumor necrosis factor alpha (*inform regarding diagnosis, stage and prognosis of cancer, cardiovascular, neurologic diseases.*)	-	1 – 1000 pM	1.7 – 1000 pg/mL *ELISA kit (ThermoFisher)*	*112*
Interleukin-6 (*levels associated with chronic inflammatory pathologies and cancer*)	≥ 5 pM	1 pM - 10 nM	0.057 – 50 pg/ml *ELISA kit (Enzo)*	*101*
Dopamine *Levels associated with Parkinson's and Alzheimer's diseases*	~ nM	1 pM – 1 mM	3 nM - 3 µM *ECL mehods	*113* and *114*

Table 2-2*: Sensitivity of EGOFET versus conventional methods in the detection of some biomolecules.*

References

1. McDonald, J. C. & McDonald, A. D. The epidemiology of mesothelioma in historical context. *Eur. Respir. J.* **9,** 1932–1942 (1996).

2. Kuroda, A., Alexandrov, M., Nishimura, T. & Ishida, T. Rapid on-site detection of airborne asbestos fibers and potentially hazardous nanomaterials using fluorescence microscopy-based biosensing. *Biotechnol. J.* **11,** 757–767 (2016).

3. García-Mendiola, T., Bravo, I., López-Moreno, J., M., Pariente, F., Wannemacher, R., Weber, K., Popp, J. & Lorenzo, E. Carbon nanodots based biosensors for gene mutation detection. *Sensors and Actuators, B Chem.* **256,** 226–233 (2018).

4. Neethirajan, S., Ragavan, V., Weng, X. & Chand, R. Biosensors for sustainable food engineering: Challenges and perspectives. *Biosensors.* **8,** 1–34 (2018).

5. Shafiee, A., Ghadiri, E., Kassis, J., Pourhabibi Zarandi, N. & Atala, A. Biosensing Technologies for Medical Applications, Manufacturing, and Regenerative Medicine. *Curr. Stem Cell Reports.* **4,** 105–115 (2018).

6. Mishra, G. K., Sharma, V. & Mishra, R. K. Electrochemical aptasensors for food and environmental safeguarding: A review. *Biosensors.* **8,** 1–13 (2018).

7. Chen, S. & Shamsi, M. H. Biosensors-on-chip: A topical review. *J. Micromechanics Microengineering.* **27,** 1–15 (2017).

8. Thevenot, D. R., Klara Toth, Richard A. Durst & Wilson, G. S. Electrochemical biosensors: recommended definitions and classification. *Biosens. Bioelectron.* **34,** 635–659 (2001).

9. Cammann, K. Bio-Sensors Based on Ion-Selective Electrodes. *Fresenius Z. Anal. Chem.* **9,** 1–9 (1977).

10. Clark, L. C. & Lyons, C. Electrode Systems for Continuous Monitoring in Cardiovascular Surgery. *Ann. N. Y. Acad. Sci.* **102,** 29–45 (1962).

11. Sang, S., Wang, Y., Feng, Q., Wei, Y., Ji, J. & Zhang, W.. Progress of new label-free techniques for biosensors: A review. *Crit. Rev. Biotechnol.* **36,** 465–481 (2016).

12. Chen, J. & Rosen, B. P. Biosensors for inorganic and organic arsenicals. *Biosensors.* **4,** 494–512 (2014).

13. Kassal, P., Steinberg, M. D. & Steinberg, I. M. Wireless chemical sensors and biosensors: A review. *Sensors Actuators, B Chem.* **266,** 228–245 (2018).

14. Strakosas, X., Bongo, M. & Owens, R. M. The organic electrochemical transistor for biological applications. *J. Appl. Polym. Sci.* **132,** 1–14 (2015).

15. Simon, D. T., Gabrielsson, E. O., Tybrandt, K. & Berggren, M. Organic Bioelectronics: Bridging the Signaling Gap between Biology and Technology. *Chem. Rev.* **116,** 13009–13041 (2016).

16. Patel, S., Park, H., Bonato, P., Chan, L. & Rodgers, M. A review of wearable sensors and systems with application in rehabilitation. *NeuroEngineering Rehabil.* **20,** 1–17 (2012).

17. Wang, D., Noël, V. & Piro, B. Electrolytic Gated Organic Field-Effect Transistors for Application in Biosensors—A Review. *Electronics* **5,** 9 (2016).

18. Hu, Y., Cao, D., X., Lill, A., T., Jiang, L., Di, C., Gao, X., Sirringhaus, H. & Nguyen, T. Effect of Alkyl-Chain Length on Charge Transport Properties of Organic Semiconductors and Organic Field-Effect Transistors. *Adv. Electron. Mater.* **4,** 1–8 (2018).

19. Liu, Q., Surendran, A., Feron, K., Manzhos, S., Jiao, X., McNeill, C., R., Bottle, C., E., Bell, J., Leong, W., L. & Sonar, P. Diketopyrrolopyrrole based organic semiconductors with different numbers of thiophene units: Symmetry tuning effect on electronic devices. *New J. Chem.* **42,** 4017–4028 (2018).

20. Köhler, A. & Bässler, H. *Electronic Processes in Organic Semiconductors*. (Wiley-VCH Verlag GmbH & Co. KGaA, 2015).

21. Brown, M. G. Atom hybridization and bond properties. Some carbon-containing bonds. *Trans. Faraday Soc.* **55,** 694–701 (1959).

22. Lu, N., Li, L., Geng, D. & Liu, M. A review for polaron dependent charge transport in organic semiconductor. *Org. Electron. physics, Mater. Appl.* **61,** 223–234 (2018).

23. Coropceanu, V., Cornil, J., Da Silva Filho, D., A., Olivier, Y., Silbey, R. & Brédas, J-L. Charge Transport in Organic Semiconductors. *Chem. Rev.* **107,** 926–952 (2007).

24. Ortmann, F., Bechstedt, F. & Hannewald, K. Charge transport in organic crystals: Interplay of band transport, hopping and electron-phonon scattering. *New J. Phys.* **12,** 023011 (2010).

25. Liu, C., Huang, K., Park, W-T., Li, M., Yang, T., Liu, X., Liang, L., Minari, T. & Noh, Y-Y. A unified understanding of charge transport in organic semiconductors: The importance of attenuated delocalization for the carriers. *Mater. Horizons.* **4,** 608–618 (2017).

26. Manu Jaiswal & Reghu Menon. Polymer electronic materials: a review of charge transport. *Polym. Int.* **55,** 1371–1384 (2006).

27. Tessler, N., Preezant, Y., Rappaport, N. & Roichman, Y. Charge transport in disordered organic materials and its relevance to thin-film devices: A tutorial review. *Adv. Mater.* **21,** 2741–2761 (2009).

28. Sirringhaus, H., Sakanoue, T. & Chang, J. F. Charge-transport physics of high-mobility molecular semiconductors. *Phys. Status Solidi.* **249,** 1655–1676 (2012).

29. Krupskaya, Y., Gibertini, M., Marzari, N. & Morpurgo, A. F. Band-Like electron transport with record-high mobility in the TCNQ family. *Adv. Mater.* **27,** 2453–2458 (2015).

30. Yamashita, Y., Hinkel, F., Marszalek, T., Zajaczkowski, W., Pisula, W., Baumgarten, M., Matsui, H., Müllen, K., & Takeya, J. Mobility Exceeding 10 $cm^2/(V{\cdot}s)$ in Donor-Acceptor Polymer Transistors with Band-like Charge Transport. *Chem. Mater.* **28,** 420–424 (2016).

31. Bässler, H. & Anna Köhler. in *Unimolecular and Supramolecular Electronics II.* **313,** 1–67 (2012).

32. Miller, A. & Abrahams, E. Impurity Conduction at Low Concentrations. *Phys. Rev.* **120,** 745–755 (1960).

33. Minari, T., Nemoto, T. & Isoda, S. Temperature and electric-field dependence of the mobility of a single-grain pentacene field-effect transistor. *J. Appl. Phys.* **99,** 1–6 (2006).

34. Tsao, H. N., Cho, D., Andreasen, J. W., Rouhanipour, A., Breiby, D. W., Pisula, W. & Müllen, K. The influence of morphology on high-performance polymer field-effect transistors. *Adv. Mater.* **21,** 209–212 (2009).

35. Fishchuk, I. I., Kadashchuk, A. K., Genoe, J., Ullah, M., Sitter, H., Singh, T. B., Sariciftci, N. S. & Bässler, H. Temperature dependence of the charge carrier mobility in disordered organic semiconductors at large carrier concentrations. *Phys. Rev. B - Condens. Matter Mater. Phys.* **81,** 1–12 (2010).

36. Inganäs, O. Organic Photovoltaics over Three Decades. *Adv. Mater.* **30,** 1–26 (2018).

37. Sirringhaus, H. 25th anniversary article: Organic field-effect transistors: The path beyond amorphous silicon. *Adv. Mater.* **26,** 1319–1335 (2014).

38. Geffroy, B., le Roy, P. & Prat, C. Organic light-emitting diode (OLED) technology: Materials, devices and display technologies. *Polym. Int.* **55,** 572–582 (2006).

39. Inal, S., Rivnay, J., Suiu, A. O., Malliaras, G. G. & McCulloch, I. Conjugated Polymers in Bioelectronics. *Acc. Chem. Res.* **51,** 1368–1376 (2018).

40. Magnus Berggren & Agneta Richter-Dahlfors. Organic Bioelectronics. *Adv. Mater.* **19,** 3201–3213 (2007).

41. Du, W., Ohayon, D., Combe, C., Mottier, L., Maria, L. P., Ashraf, R. H., Fiumelli, H., Inal, S. & McCulloch, I. Improving the Compatibility of Diketopyrrolopyrrole Semiconducting Polymers for Biological Interfacing by Lysine Attachment. *Chem. Mater.* **30,** 6164–6172 (2018).

42. Root, S. E., Savagatrup, S., Printz, A. D., Rodriquez, D. & Lipomi, D. J. Mechanical Properties of Organic Semiconductors for Stretchable, Highly Flexible, and Mechanically Robust Electronics. *Chem. Rev.* **117,** 6467–6499 (2017).

43. Sekitani, T. & Someya, T. Stretchable, large-area organic electronics. *Adv. Mater.* **22,** 2228–2246 (2010).

44. Kergoat, L., Piro, B., Berggren, M., Horowitz, G. & Pham, M. C. Advances in organic transistor-based biosensors: From organic electrochemical transistors to electrolyte-gated organic field-effect transistors. *Anal. Bioanal. Chem.* **402,** 1813–1826 (2012).

45. Kergoat, L., Herlogsson, L., Braga, D., Piro, B., Pham, M-C., Crispin, X., Berggren, M. & Horowitz, G. A Water-Gate Organic Field-Effect Transistor. *Adv. Mater.* **22,** 2565–2569 (2010).

46. Otto Stern. The theory of the electrolytic double-layer. *Zeitschrift für Elektrochemie* **30,** 508–516 (1924).

47. José Juan López-García & José Horno. Poisson À Boltzmann Description of the Electrical Double Layer Including Ion Size Effects. *Langmuir.* **27,** 13970–13978 (2011).

48. Gur, Y., Ravina, I. & Alexander J. Babchin. On the electrical double layer theory. I. A numerical method for solving a generalized Poisson—Boltzmann equation. *J. Colloid Interface Sci.* **64,** 326–332 (1978).

49. Tu, D., Herlogsson, L., Kergoat, L., Crispin, X., Berggren, M. & Forchheimer, R. A Static Model for Electrolyte-Gated Organic Field-Effect Transistors. *IEEE Trans. Electron*

Devices **58,** 3574–3582 (2011).

50. Melzer, K., Brändlein, M., Popescu, B., Popescu, D., Luglia, P. & Scarpaa, G. Characterization and simulation of electrolyte-gated organic field-effect transistors. *Faraday Discuss.* **174,** 399–411 (2014).

51. H. Helmholtz. Ueber einige Gesetze der Vertheilung elektrischer Ströme in körperlichen Leitern, mit Anwendung auf die thierisch-elektrischen Versuche (Schluss.). *Ann. Phys.* **165,** 353–377 (1853).

52. Chapman, D. L. LI . A contribution to the theory of electrocapillarity. *London, Edinburgh, Dublin Philos. Mag. J. Sci.* **25,** 475–481 (2010).

53. Gouy, M. Sur la constitution de la charge électrique à la surface d ' un électrolyte. *J. Phys. Theor. Appl.* **9,** 457–468 (1910).

54. Su, Y., Wang, C., Xie, W., Xie, F., Chen, J., Zhao, N., & Xu, J. Low-Voltage Organic Field-Effect Transistors (OFETs) with Solution-Processed Metal-Oxide as Gate Dielectric. *ACS Appl. Mater. Interfaces* **3,** 4662–4667 (2011).

55. Ortiz, P., Facchetti, A. & Marks, T. J. High- k Organic , Inorganic , and Hybrid Dielectrics for Low-Voltage Organic Field-Effect Transistors. *Chem. Rev.* **110,** 205–239 (2010).

56. Horowitz, G. Organic Field-Effect Transistors. *Adv. Mater.* **10,** 365–377 (1998).

57. Panzer, M. J. & Frisbie, C. D. Polymer electrolyte-gated organic field-effect transistors: Low-voltage, high-current switches for organic electronics and testbeds for probing electrical transport at high charge carrier density. *J. Am. Chem. Soc.* **129,** 6599–6607 (2007).

58. Porrazzo, R., Bellani, S., Luzio, A., Lanzarini, E., Caironi, M. & Antognazza, M. R. Improving mobility and electrochemical stability of a water-gated polymer field-effect transistor. *Org. Electron.* **15,** 2126–2134 (2014).

59. Zhang, Q., Leonardi, F., Casalini, S., Temiño, I. & Mas-Torrent, M. High performing solution-coated electrolyte-gated organic field-effect transistors for aqueous media operation. *Sci. Rep.* **6,** 1–10 (2016).

60. Rivnay, J., Inal, S., Salleo, A., Berggren, M. & Malliaras, G. G. Organic electrochemical transistors. *Nat. Rev. Mater.* **3,** 1–14 (2018).

61. Zhang, Y., Zhang, Y., Han, G., Qin, M., Shen, Y., Lu, X., Yi, Y. & Zhao, N. Spectroscopic

Study of Charge Transport at Organic Solid–Water Interface. *Chem. Mater.* **30,** 5422–5428 (2018).

62. Seshadri, P., Manoli, K., Schneiderhan-Marra, N., Anthes, U., Wierzchowiec, P., Bonrad, K., Di Franco, C. &Torsi, L. Low-picomolar, label-free procalcitonin analytical detection with an electrolyte-gated organic field-effect transistor based electronic immunosensor. *Biosens. Bioelectron.* **104,** 113–119 (2018).

63. Mizuno, M., Tateno, H., Matsumura, Y. & Atobe, M. Synthesis and molecular weight control of poly(3-hexylthiophene) using electrochemical polymerization in a flow microreactor. *React. Chem. Eng.* **2,** 642–645 (2017).

64. Amou, S., Haba, O., Shirato, K., Hayakawa, T., Ueda, M., Takeuchi, K. & Asai, M.. Head-to-tail regioregularity of poly(3-hexylthiophene) in oxidative coupling polymerization with FeCl3. *J. Polym. Sci. Part A Polym. Chem.* **37,** 1943–1948 (1999).

65. Tamba, S., Fuji, K., Meguro, H., Okamoto, S., Tendo, T., Komobuchi, R., Sugie, A., Nishino, T. & Mori, A. Synthesis of High-molecular-weight Head-to-tail-type Poly(3-substituted-thiophene)s by Cross-coupling Polycondensation with [CpNiCl(NHC)] as a Catalyst. *Chem. Lett.* **42,** 281–283 (2013).

66. Kline, R. J., McGehee, M. D., Kadnikova, E. N., Liu, J. & Fréchet, J. M. J. Controlling the field-effect mobility of regioregular polythiophene by changing the molecular weight. *Adv. Mater.* **15,** 1519–1522 (2003).

67. Kergoat, L., Battaglini, N., Miozzo, L., Piro, B., Pham, M-C., Yassar, A. & Horowitz, G. Use of poly(3-hexylthiophene)/poly(methyl methacrylate) (P3HT/PMMA) blends to improve the performance of water-gated organic field-effect transistors. *Org. Electron.* **12,** 1253–1257 (2011).

68. Thiburce, Q., Porcarelli, L., Mecerreyes, D. & Campbell, A. J. High performance photolithographically-patterned polymer thin-film transistors gated with an ionic liquid/poly(ionic liquid) blend ion gel. *Appl. Phys. Lett.* **110,** 233302 (2017).

69. Mun, S., Park, Y., Lee, Y. E. K. & Sung, M. M. Highly Sensitive Ammonia Gas Sensor Based on Single-Crystal Poly(3-hexylthiophene) (P3HT) Organic Field Effect Transistor. *Langmuir.* **33,** 13554–13560 (2017).

70. Zhu, Z., Wang, J. & Wei, B. Self-assembly of ordered poly(3-hexylthiophene) nanowires for organic field-effect transistor applications. *Phys. B.* **59,** 83–87 (2014).

71. Mulla, M. Y., Tuccori, E., Magliulo, M., Lattanzi, G., Palazzo, G., Persaud, K. & Torsi, L.

Capacitance-modulated transistor detects odorant binding protein chiral interactions. *Nat. Commun.* **6,** 1–9 (2015).

72. Porrazzo, R., Luzio, A., Bellani, S., Bonacchini, G. E., Noh, Y-Y., Kim, Y-H., Lanzani, G., Antognazza, M. R. & Caironi, M. Water-Gated n-Type Organic Field-Effect Transistors for Complementary Integrated Circuits Operating in an Aqueous Environment. *ACS Omega* **2,** 1–10 (2017).

73. Manoli, K., Dumitru, L. M., Mulla, M. Y., Magliulo, M., Di Franco, C., Santacroce, M. V., Scamarcio, G. & Torsi, L. A comparative study of the gas sensing behavior in P3HT- and PBTTT-based OTFTs: The influence of film morphology and contact electrode position. *Sensors* **14,** 16869–16880 (2014).

74. Alberga, D., Perrier, A., Ciofini, I., Mangiatordi, J. F., Lattanzi, G. & Adamo, C. Morphological and charge transport properties of amorphous and crystalline P3HT and PBTTT: Insights from theory. *Phys. Chem. Chem. Phys.* **17,** 18742–18750 (2015).

75. Ito, H., Harada, T., Tanaka, H. & Kuroda, S. I. Critical regime for the insulator-metal transition in highly ordered conjugated polymers gated with ionic liquid. *Jpn. J. Appl. Phys.* **55,** 1–5 (2016).

76. Algarni, S. A., Althagafi, T. M., Naim, A. Al & Grell, M. A water-gated organic thin film transistor as a sensor for water-borne amines. *Talanta.* **153,** 107–110 (2016).

77. Mannsfeld, S. C. B., Tang, M. L. & Bao, Z. Thin film structure of triisopropylsilylethynyl-functionalized pentacene and tetraceno[2,3-b]thiophene from grazing incidence x-ray diffraction. *Adv. Mater.* **23,** 127–131 (2011).

78. Murphy, A. R. & Fréchet, J. M. J. Organic semiconducting oligomers for use in thin film transistors. *Chem. Rev.* **107,** 1066–1096 (2007).

79. Choi, K. N., Kim, K. S., Chung, K. S. & Lee, H. Solvent effect on the electrical properties of triisopropylsilylethynyl (TIPS) pentacene organic thin-film transistors. *IEEE Trans. Device Mater. Reliab.* **9,** 489–493 (2009).

80. Giri, G., Park, S., Vosgueritchian, M., Shulaker, M. M. & Bao, Z. High-mobility, aligned crystalline domains of tips-pentacene with metastable polymorphs through lateral confinement of crystal growth. *Adv. Mater.* **26,** 487–493 (2014).

81. Lee, S. H., Choi, M. H., Han, S. H., Choo, D. J., Jang, J. & KiKwon, S. High-performance thin-film transistor with 6,13-bis(triisopropylsilylethynyl) pentacene by inkjet printing. *Org. Electron.* **9,** 721–726 (2008).

82. Lago, N., Buonomo , M., Imran, S., Bertani, R., Wrachien, N., Bortolozzi, M., Pedersen, M. G. & Cester, A.. TIPS-Pentacene as Biocompatible Material for Solution Processed High-Performance Electronics Operating in Water. *IEEE Electron Device Lett.* **39,** 1401–1404 (2018).

83. Roberts, M. E., Stefan, C., Mannsfeld, B., Queraltó, N., Reese, C., Locklin, J., Knoll, W. & Bao, Z. Water-stable organic transistors and their application in chemical and biological sensors. *PNAS* **105,** 12134–12139 (2008).

84. Zhang, J., Jin, J., Xu, H., Zhang, Q. & Huang, W. Recent progress on organic donor-acceptor complexes as active elements in organic field-effect transistors. *J. Mater. Chem. C* **6,** 3485–3498 (2018).

85. Thiburce, Q. & Campbell, A. J. Low-Voltage Polyelectrolyte-Gated Polymer Field-Effect Transistors Gravure Printed at High Speed on Flexible Plastic Substrates. *Adv. Electron. Mater.* **3,** 1600421 (2017).

86. Fillaud, L., Petenzi, T., Pallu, J., Piro, B., Mattana, G. & Noel, V. Switchable Hydrogel-Gated Organic Field-Effect Transistors. *Langmuir* **34,** 3686–3693 (2018).

87. Kim, S. H., Hong, K., Xie, W., Lee, K. H., Zhang, S., Lodge, T. P., Frisbie, C. D. Electrolyte-gated transistors for organic and printed electronics. *Adv. Mater.* **25,** 1822–1846 (2013).

88. Dumitru, L. M., Manoli, K., Magliulo, M., Palazzo, G. & Torsi, L. Low-voltage solid electrolyte-gated OFETs for gas sensing applications. *Microelectronics J.* **45,** 1679–1683 (2014).

89. Lee, S. W., Lee, H. J., Choi, J. H., Koh, W. G., Myoung, J. M., Hur, J. H., Park, J. J., Cho, J. H. & Jeong, U. Periodic array of polyelectrolyte-gated organic transistors from electrospun poly(3-hexylthiophene) nanofibers. *Nano Lett.* **10,** 347–351 (2010).

90. Schmoltner, K., Kofler, J., Klug, A., List-Kratochvil & J.W., E. Electrolyte-gated organic field-effect transistor for selective reversible ion detection. *Adv. Mater.* **25,** 6895–6899 (2013).

91. Buth, F., Kumar, D., Stutzmann, M. & Garrido, J. A. Electrolyte-gated organic field-effect transistors for sensing applications. *Appl. Phys. Lett.* **98,** 3–6 (2011).

92. Zhang, Q., Leonardi, F., Casalini, S. & Mas-Torrent, M. Mercury-Mediated Organic Semiconductor Surface Doping Monitored by Electrolyte-Gated Field-Effect Transistors. *Adv. Funct. Mater.* **27,** 1703899 (2017).

93. Knopfmacher, O., Hammock, M. L., Appleton, A. L., Schwartz, G., Mei, J., Lei, T., Pei, J. & Bao, Z. Highly stable organic polymer field-effect transistor sensor for selective detection in the marine environment. *Nat. Commun.* **5,** 1–9 (2014).

94. Suspène, C., Piro, B., Reisberg, S., Pham, M-C., Toss, H., Berggren, M., Yassar, A. & Horowitz, G. Copolythiophene-based water-gated organic field-effect transistors for biosensing. *J. Mater. Chem. B* **1,** 2090–2097 (2013).

95. Magliulo, M., De Tullio, D., Vikholm-Lundin, I., Albers, W. M., Munter, T., Manoli, K., Palazzo, G. & Torsi, L. Label-free C-reactive protein electronic detection with an electrolyte-gated organic field-effect transistor-based immunosensor. *Anal. Bioanal. Chem.* **408,** 3943–3952 (2016).

96. Mulla, M. Y., Seshadri, P., Torsi, L, Manoli, K., Mallardi, A., Ditaranto, N., Santacroce, M. V., Di Franco, C., Scamarcioc, G. & Magliulo, M. UV crosslinked poly(acrylic acid): a simple method to bio-functionalize electrolyte-gated OFET biosensors. *J. Mater. Chem. B* **3,** 5049–5057 (2015).

97. Kergoat, L., Piro, P., Berggren, M., Pham, M., Yassar, A. & Horowitz, G. DNA detection with a water-gated organic field-effect transistor. *Org. Electron.* **13,** 1–6 (2012).

98. Leonardi, F., Tamayo, A., Casalini, S. & Mas-Torrent, M. Modification of the gate electrode by self-assembled monolayers in flexible electrolyte-gated organic field effect transistors: Work function: Vs. capacitance effects. *RSC Adv.* **8,** 27509–27515 (2018).

99. Singh, M., Mulla, M., Y., Santacroce, M., V., Magliulo, M., Di Franco, C., Manoli, K., Altamura, D., Giannini, C., Cioffi, N., Palazzo, G., Scamarcio, G. & Torsi, L. Effect of the gate metal work function on water-gated ZnO thin-film transistor performance. *J. Phys. D. Appl. Phys.* **49,** 274101 (2016).

100. Fabiano, S., Braun, S., Fahlman, M., Crispin, X. & Berggren, M. Effect of gate electrode work-function on source charge injection in electrolyte-gated organic field-effect transistors. *Adv. Funct. Mater.* **24,** 695–700 (2014).

101. Diacci, C., Bertob, M., Di Lauro, M., Bianchini, E. & Pinti, M. Label-free detection of interleukin-6 using electrolyte gated organic field effect transistors. *Biointerphases* **12,** 05F401 (2017).

102. Irvinq Langmuir. THE ADSORPTION OF GASES ON PLANE SURFACES OF GLASS, MICA AND PLATINUM. *J Am Chem Soc.* **40,** 1361–1403 (1918).

103. A. V. HILL. The possible effects of the aggregation of the molecules of huemoglobin on its dissociation curves. *J. Physiol.* 4–6 (1910).

104. Stern, E., Wagner, R., Sigworth, F., J., Breaker, R., Fahmy, T., M. & Reed, M., A. Importance of the Debye Screening Length on Nanowire Field Effect Transistor Sensors. *Nano Lett.* **9,** 3405–3409 (2007).

105. Piro, B., Wang, D., Benaoudia, D., Tibaldi, A., Anquetin, G., Noël, V., Reisberg, S., Mattana, G. & Jackson, B. Versatile transduction scheme based on electrolyte-gated organic field-effect transistor used as immunoassay readout system. *Biosens. Bioelectron.* **92,** 215–220 (2017).

106. Palazzo, G., De Tullio, D., Magliulo, M., Mallardi, A., Intranuovo, F., Mulla, M., Y., Favia, P., Vikholm-Lundin, I. & Torsi, T. Detection Beyond Debye ' s Length with an Electrolyte-Gated Organic Field-Effect Transistor. *Adv. Mater.* **27,** 911–916 (2015).

107. Macchia, L., Manoli, K., Holzer, B., Di Franco, C., Ghittorelli, M., Torricelli, F., Alberga, D., Mangiatordi, G., F., Palazzo, G., Scamarcio, G. & Torsi, L. Single-molecule detection with a millimetre-sized transistor. *Nat. Commun.* **9,** 1–10 (2018).

108. Cramer, T., Chelli, B., Murgia, M., Barbalinardo, M., Bystrenova, E., De Leeuwb, D., M., & Biscarini, F. Organic ultra-thin film transistors with a liquid gate for extracellular stimulation and recording of electric activity of stem cell-derived neuronal networks. *Phys. Chem. Chem. Phys.* **15,** 3897–3905 (2013).

109. Benfenati, V., Toffanin, T., Bonetti, S., Turatti, G., Pistone, A., Chiappalone, M., Sagnella, A., Stefani, A., Generali, G., Ruani, G., Saguatti, D., Zamboni, R. & Muccini, M. A transparent organic transistor structure for bidirectional stimulation and recording of primary neurons. *Nat. Mater.* **12,** 672–680 (2013).

110. Pfäfflin, A. & Schleicher, E. Inflammation markers in point-of-care testing (POCT). *Anal. Bioanal. Chem.* **393,** 1473–1480 (2009).

111. A., F. A new sensitive automated assay for procalcitonin detection: LIAISON® BRAHMS PCT® II GEN. *Pract. Lab. Med.* **6,** 1–7 (2016).

112. Berto, M., Diacci, C., D'Agata, R., Pinti, M., Bianchini, E., Di Lauro, M., Casalini, S., Cossarizza, A., Berggren, M., Simon, D., Spoto, G., Biscarini, F. & Bortolotti, C., A. EGOFET Peptide Aptasensor for Label-Free Detection of Inflammatory Cytokines in Complex Fluids. *Adv. Biosyst.* **2,** 1700072 (2017).

113. Casalini, S., Leonardi, F., Cramer, T. & Biscarini, F. Organic field-effect transistor for

label-free dopamine sensing. *Org. Electron.* **14,** 156–163 (2013).

114. Liu, S., Zhang, X., Yu, Y. & Zou, G. A monochromatic electrochemiluminescence sensing strategy for dopamine with dual-stabilizers-capped CdSe quantum dots as emitters. *Anal. Chem.* **86,** 2784–2788 (2014).

Blank Page

Chapter 3: Benchmarking organic semiconductors in liquid gated organic field effect transistors

Contributors: ***A. Doumbia,*** *J. Tong and M. L. Turner*

Authors contributions:

A. Doumbia *conceived the idea presented. M. L. Turner and* ***A. Doumbia*** *discuss the choice of semiconductor interesting to investigate.* ***A. Doumbia*** *choose the semiconductors from literature review and discussion with M. L. Turner.* ***A. Doumbia*** *leads the project: designed, planned, carried out the experiments, and collected and analysed the data. J. Tong assisted* ***A. Doumbia*** *in the characterisation of the film morphology. All authors discussed the results.* ***A. Doumbia*** *took the lead in writing the manuscripts (Co-authors provided critical feedback).*

3.1. Abstract

The electrolyte-gated organic field effect transistor (EGOFET) is a highly regarded low power thin film electronic device that finds application in various areas including in aqueous media molecular detection. To maximise the performance and stability of EGOFETs, it is important to minimize or switch off electrochemical doping phenomena. In theory, this can be done by carefully choosing the conducting channel and gate terminal materials in concert with the device operational window (magnitude of drain and gate electrode bias). However, the ideal design characteristic that the channel materials must fulfil is not yet fully understood. Here, high performance donor-acceptor polymers, namely poly[2,5-(2-octyldodecyl)-3,6-diketopyrrolopyrrole-alt-5,5-(2,5-di(thien-2-yl)thieno [3,2-b]thiophene)] (DPPDTT) and indacenodithiophene-co-benzothiadiazole (IDT-BT), are evaluated in EGOFETs. Interestingly, the in-water field-effect operational performance of these materials turns out to be superior to that of the well-established liquid crystalline poly[2,5-bis(3-hexadecylthiophen-2-yl)thieno[3,2-b]thiophene] (PBTTT). The effective mobility of DPPDTT (μ = 0.18 $cm^2.V^{-1}.s^{-1}$), and IDT-BT (μ = 0.15 $cm^2.V^{-1}.s^{-1}$) were almost double that of the PBTTT (μ = 0.09 $cm^2.V^{-1}.s^{-1}$) based EGOFET. Equally, their on-to-off current ratio (I_{on}/I_{off}) were an order of magnitude (I_{on}/I_{off} (DPPDTT): 3×10^3) or two (I_{on}/I_{off} (IDT-BT): 2×10^4) higher than that of PBTTT ($I_{on}/I_{off} = 2 \times 10^2$). Furthermore, the switch-on time was found to be shorter in the donor-acceptor polymer based EGOFET (DPPDTT: 1.2 s; IDT-BT: 0.18 s) as compared to that of PBTTT (2.8 s). These results suggest that high performance donor-acceptor polymers can perform well in EGOFETs.

3.2. Introduction

The Electrolyte-Gated Organic Field-Effect Transistor (EGOFET) is an OFET in which an electrolyte acts as the gate insulator[1, 2 and 3]. These devices make use of the high capacitance (~μF.cm^{-2}) of the electrical double layer (EDL), a phenomenon described by Helmholtz[4], Gouy[5], Chapman[6], and Stern[7], which is established at the interface of an electrolyte and polarizable materials, to convert small voltages to field effect currents. The transduction efficacy is partly dependent on the capacitive coupling of the electrolyte with the organic semiconductor and the gate terminal. The coupling must be electrostatic to guarantee charge transport under dominant field-effect mode. This specificity differentiates the EGOFETs from an analogue device known as the Organic Electrochemical Transistor (OECT)[8], as the organic semiconductor must be impermeable to ions, and chemically as well as structurally stable when in direct contact with the electrolyte. Yet less is known about the characteristics the materials must fulfil to hinder such electrochemical doping and film restructuring phenomena. It has been suggested that a high degree of crystallinity with an interdigitated side chain to protect the polymer from the electrolyte ions was crucial for improved device performance[9]. With this in mind organic small molecule and liquid crystalline polymeric semiconductors were employed as conducting channels of EGOFET for a variety of bioelectronic applications including sensing[10 and 11], triggering[12] and mimicking biological or chemical phenomena[13 and 14].

Now, a class of organic semiconductors, known as donor-acceptor polymers (D-A polymers) are attracting a great deal of interest in organic electronics[15, 16 and 17]. These materials with easily tuneable backbone planarity but yet less crystalline (or undetectable) than semi-crystalline polymer films are displaying first-rate field-effect mobility in OFETs (> 1 cm^2.V^{-1}.s^{-1})[18 and 19]. Also, the air and bias stress operational stability of some of these materials are state-of-the-art in organic electronics. This superior charge transport and operational stability seems to originate from polymer backbone planarity, thin film π-π stacking inter-distance and organisation in concert with the molecular energy levels (HOMO-LUMO) of these polymers. These characteristic performances may well hold true in EGOFETs. In fact, a short intermolecular distance homogeneously distributed and oriented over the entire film can logically hinder ions getting into the vicinity of the polymer film therefore guaranteeing, pure or at least dominant field-effect charge transport.

Here the performances of EGOFETs based on two donor-acceptor polymers were evaluated (DPPDTT and IDT-BT). Specifically, the normalised transconductance, on/off current ratio, subthreshold swing, and switch-on time of these materials were determined and compared against that of well-established PBTTT. Both of the materials performed well with state-of-the-art electrical figures-of-merit as compared to PBTTT based water-gated EGOFET.

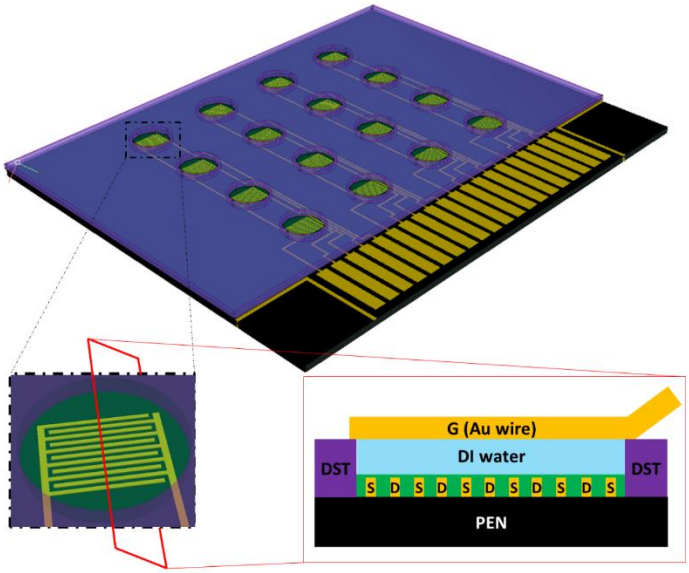

Figure 3-1: *AutoCAD 3D model of the array of electrolyte gated organic-field-effect transistors used in this work, a zoom of a single transistor (bottom left) and its cross sectional schematic representation (bottom right): featuring a PEN substrate (black), interdigitated contact electrode (yellow), organic semiconductor (green) and double-sided tape (violet), DI water (light blue) and Au wire serves as electrolyte and gate terminal, respectively.*

3.3. Results

Flexible substrates with an array of sixteen bottom contact top gate EGOFETs based on the three polymeric semiconductors were fabricated following procedures detailed in **Section 3-5**. **Figure 3-1**. displays the layout of a typical device, and consists of an array of interdigitated source/drain electrodes patterned on a flexible substrate fully coated with an organic semiconductor, which was either PBTTT, DPPDTT or IDT-BT. On top of this, holes designed in a double-sided tape was fixed. The device was terminated by filling the hole in the double-sided tape with purified tap water (6 µl) and a gold wire inserted in it acting as a gate electrode (bottom right panel of **Figure 3-1**). The double-sided tape was used to confine the electrolyte over the channel area and define the relative position of the gate electrode to the conducting channel. This is important for electrical performance comparison. Because the position of the gate electrode relative to the organic semiconductor affected the electrical performance of the EGOFET. In vertical direction, the closer the gate electrode was to the conducting channel the higher the drain current of

the device became (**Supporting information Figure S3-1**). This can be explained by the variation in the amount of gate electrode area immersed into the electrolyte which dictates the EDL capacitance that builds up at the gate/electrolyte interface. This in series with the EDL capacitance at the semiconductor/electrolyte interface controls the modulation of the current outputted by the device. Hence the same double-sided tape design and thickness are used for the entire device to minimise the impact of gate position errors on performance comparison.

3.3.1. AFM micrographs of thin film of PBTTT, DPPDTT and IDT-BT

The morphology of thin film of PBTTT, DPPDTT and IDT-BT deposited onto the contact electrodes was assessed by Atomic Force Microscopy (AFM) in tapping mode prior to the electrical characterisation of the devices. AFM height micrographs of thin films of these organic semiconductors are presented in **Figure 3-2**.

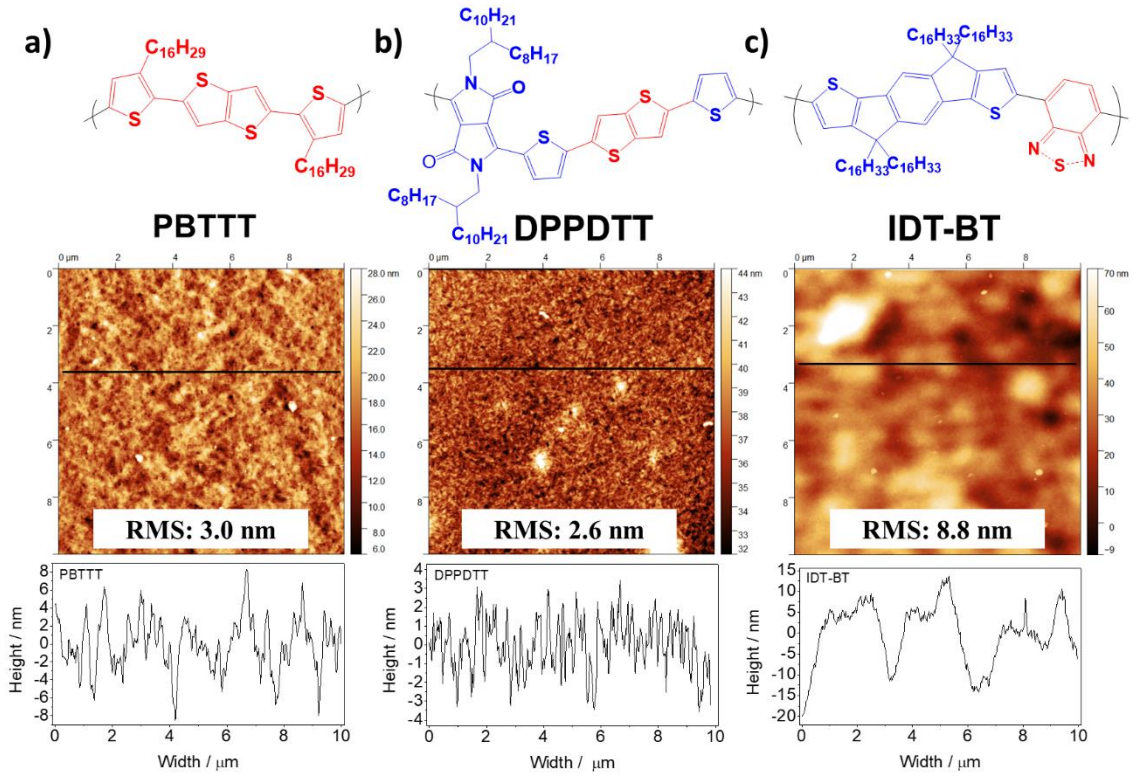

Figure 3-2: *Chemical structure and AFM height micrograph of a) PBTTT, b) DPPDTT and c) IDT-BT together with the line scan profile (Height vs width). The insets show the root-mean-square surface roughness (RMS) of the film. In the chemical structure of the donor-acceptor, the blue and red represent the electron donating and accepting unit, respectively.*

As expected, the surface morphologies of the three polymers film were different. IDT-BT was very rough (root-mean-square (RMS) of about 8.8 nm). In contrast, PBTTT and DPPDTT show smooth surface (RMS of 3 nm and 2.6 nm, respectively) with a network of structured aggregates that are homogeneously distributed over 10 µm^2. Differences in

the size and shape of the aggregates in PBTTT and DPPDTT film were observed. In DPPDTT, the aggregates appear as nanofibers. Similar morphology was recently observed by Y. Xi and co-worker for this polymer [20]. However, the authors deposited DPPDTT film from a mixture of chloroform with methanol at different methanol loading (10%, 15% and 20%). They suggested that, the mixture of polar poor solvent (methanol) with chloroform (good solvent for dissolving DPPDTT) was the reason for DPPDTT self-organisation into nanofibers[20]. Here, the nanofiber formation was probably due to the high concentration of DPPDTT (7 mg/ml) in a high boiling point solvent (1,2-dichlorobenzene (DCB)). In fact, high concentration of DPPDTT favours the formation of aggregates in the solution after taking off from the hot plate and prior to spin-coating onto the device. These aggregates may act as nucleation site on the substrate, and due to the high boiling point of DCB, long time for $\pi - \pi$ stacking interaction results into well structure nanofiber showed in **Figure 3-2.b**. For PBTTT, the interconnected aggregates resemble the expected semi-crystalline microstructure with well-defined terraces observed in room temperature PBTTT films after heating above its first thermal transition temperature (between ≥ 130° C and ≤ 180° C)[21, 22]. Here the thermal treatment was carried out at 140° C. The domain of the terraces in PBTTT appears about 2 to 3 times larger than that of nanofibers seen in the DPPDTT film (**Figure 3-2.a** and **b**). Note PBTTT film thermal treated at 180° C shows aggregates that are well structured and organise with sharp angle and larger than the ones reported in this work[23].

The absence of structured aggregates in the AFM of IDT-BT suggest that the film was amorphous. The nanofiber and terraced structures, respectively, seen in DPPDTT and PBTTT is an indication that DPPDTT and PBTTT chains are well ordered in the film. The domain is larger in PBTTT; previous reports have shown that PBTTT films are more crystalline than DPPDTT and IDT-BT films[24].

3.3.2. Electrical performance of droplet gated EGOFET

The output characteristics of EGOFETs based on PBTTT, DPPDTT and IDT-BT are presented in **Figure 3-3**. The electrolyte used was tap water purified with a Millipore Milli-Q system (resistivity of 18.2 MΩ.cm). The three devices display p-channel response with identifiable linear, pinch-off and saturation regions (**Figure 3-3**). No deviation from linearity at low drain voltage was observed. Hence, no evidence of charge injection problems was noticeable in these devices. The output characteristics of DPPDTT water-gated EGOFET, in contrast to that of the two other polymers, shows full saturation at all gate biases (**Figure 3-3).**

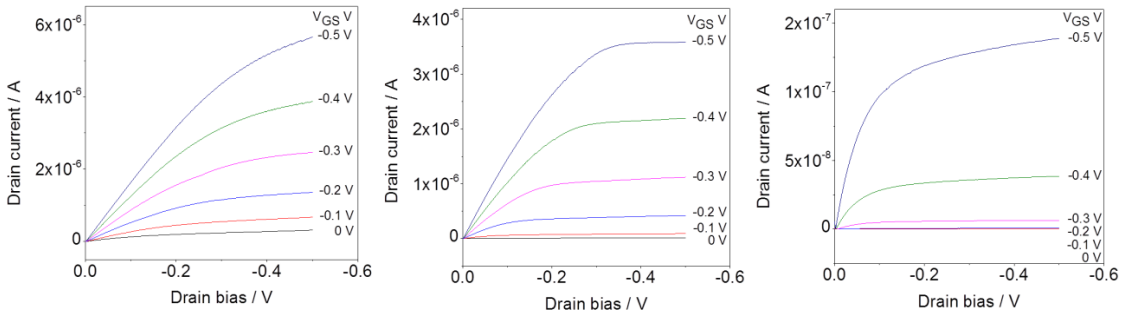

Figure 3-3: *Typical output characteristic of electrolyte gated organic field-effect transistor based on PBTTT, DPPDTT and IDT-BT (from left to right). The electrolyte employed was tap water purified with Milli-Q system (resistivity of 18 MΩ.cm). The sweep rate of the drain bias was -1 mV.s^{-1}.*

Transfer and gate current curves in **Figure 3-4** were measured by sweeping the gate voltage forward (from 0.35 V to -0.5 V) and backward (from -0.5 V to 0.35 V) at fixed drain bias (-0.5 V) to analyse drain current hysteresis and extract electrical figures of merit using commonly adopted fitting methods in saturation regime, as reported in **Chapter 2** equation (2.12). Minor drain current hysteresis was observed for all the fabricated devices. Among the polymers investigated PBTTT displays the highest on-state drain current (~7 µA). This is almost twice that of DPPDTT based devices (~3.6 µA) and more than an order of magnitude superior to the drain current of IDT-BT (~0.21 µA) at a gate bias of -0.5 V (**Table S3-1**).

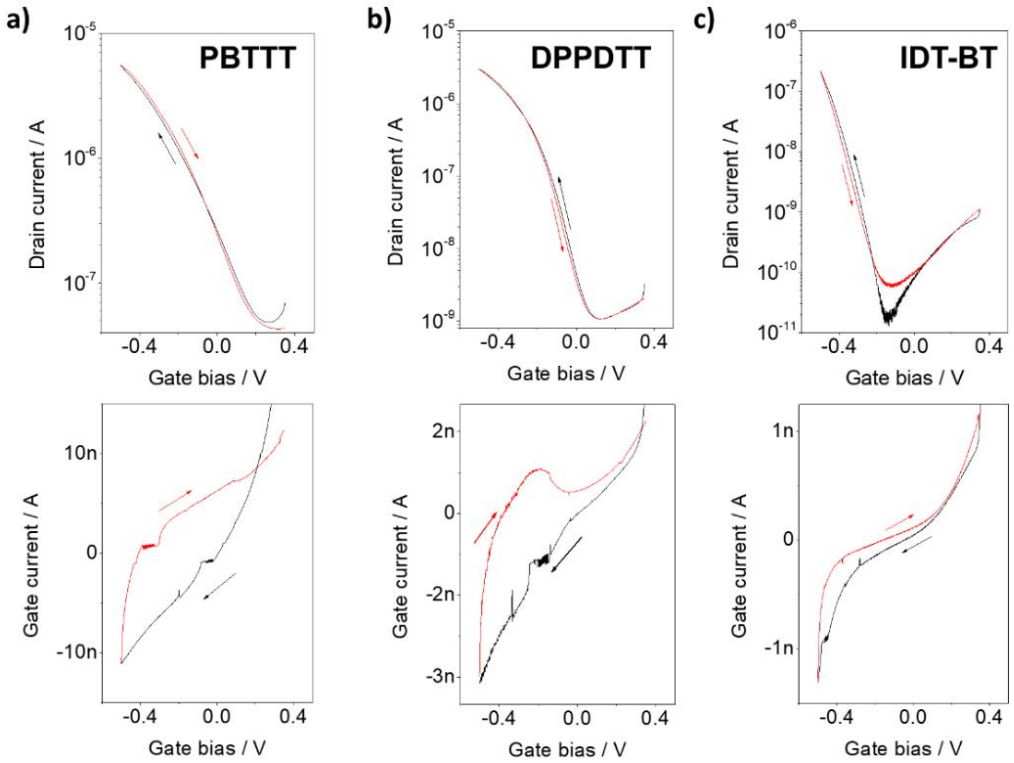

Figure 3-4: *Drain and gate current curves of EGOFET based on a) PBTTT, b) DPPDTT, and c) IDT-BT. The I-V curves were measured by sweeping the gate voltage between 0.35 V and -0.5 V at fixed drain bias of -0.5 V with steps of -1 mV. The sweeping of the gate bias has been carried out forward (from 0.35 V to -0.5 V) and backward (from -0.5 V to 0.35 V). The direction of the sweep is indicated by the arrows. The electrolyte used was tap water purified with Milli-Q microporous system (resistivity of 18. 2 MΩ.cm).*

Such a low on-state current observed in IDT-BT can be attributed to the fact that the voltage necessary to overcome the energy mismatch between the semiconductor and the gate work function is higher. As shown in **Figure 3-5**, the HOMO energy level of PBTTT (-5.1 eV) and DPPDTT (-5.2 eV) are closer to the work function of the gold gate terminal (~ -4.9 eV after solvent cleaning) in comparison to that of IDT-BT (-5.4 eV).

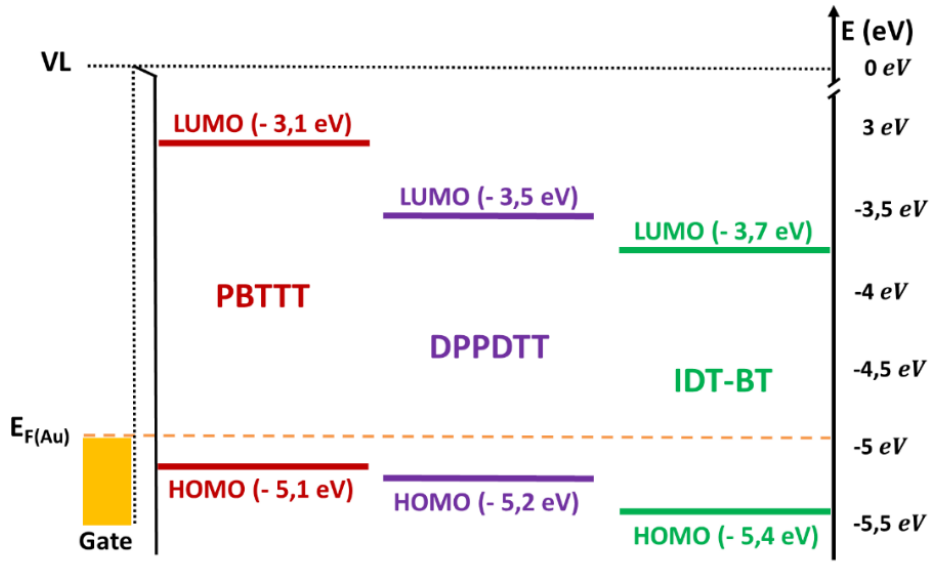

Figure 3-5: *Schematic representation showing how the Fermi level of the Au gate electrode ($E_{F(Au)}$= -4.9 eV) compares to the frontier orbitals (HOMO and LUMO) of PBTTT, DPPDTT and IDT-BT.*

Equally atomic force microscopy of the film showed that the surface roughness of IDT-BT (8.8 nm) was almost triple that of PBTTT (3 nm) and DPPDTT (2.6 nm) (**Figure 3-2)**. This roughness could accentuate the energetic difference of IDT-BT surface potential with the gate terminal by, for instance acting as charge trapping sites. Thus, preventing current saturation within the operating voltage window due to higher voltage required to fill the defect and remove the energetic difference between IDT-BT and gold gate terminal.

While all the polymers perform adequately in the water gated configuration, qualitatively, DPPDTT displayed the best transduction of voltage to current within the chosen characterisation window ($0V \geq V_{DS} \geq -0.5V$ and $0.35V \geq V_{GS} \geq -0.5V$). The output characteristics of the DPPDTT device, in contrast to those of the two other polymers, shows full saturation at all gate biases (**Figure 3-3).** Equally, the square root of the drain current as a function of gate bias is linear while that of PBTTT and IDT-BT present a small deflection toward high value at high negative gate bias (**Supporting information Figure S3-2**).

3.3.3. Comparison of electrical figures of merit in water gated EGOFET

EGOFETs based on PBTTT have been reported to exhibit a large off-state current (I_{off}) of about a few tens of nano-amperes when an electrolyte is used as a gate insulator[9 and 25]. Note: I_{Off} is considered as the minimum drain current in the forward gate voltage sweep. In the experiments reported in this work it was found to be ~50 nA, this is one and three orders of magnitude higher than that recorded for DPPDTT (~1 nA), and IDT-BT (~12 pA) device, respectively (**Figure 3-4.(a-c)**, **Figure 3-6.b** and **Table S3-1**).

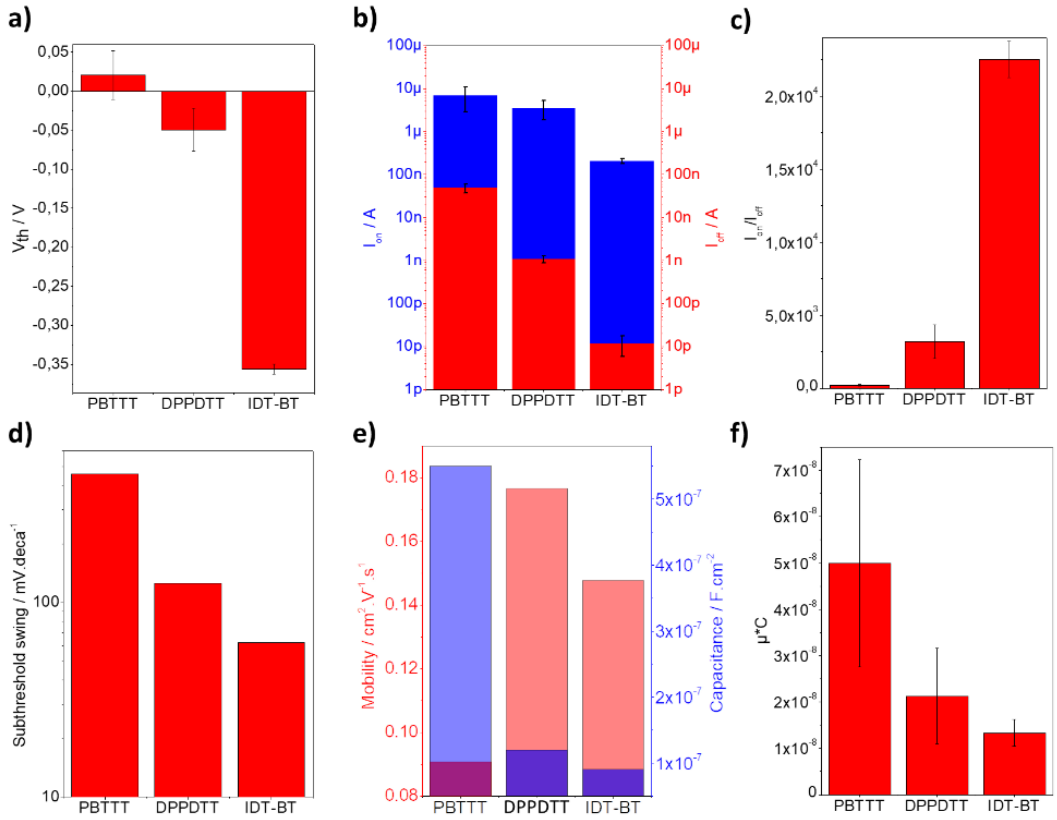

Figure 3-6: *Electrical figures of merit of EGOFETs based on DPPDTT, IDT-BT, and PBTTT. The data shows a) Threshold voltage, b) On, off-state drain current and c) their ratio, d) subthreshold swing e) Capacitance, mobility and f) their product when the device is operated in purified water. Errors bars represent device variations on the same substrates.*

The high off-state current degrades the on-to-off current ratio (I_{on}/I_{off}) of a PBTTT based water-gated OFET, which here and in most of the reported literature is about 10^2 (here $2.1 \pm 0.7 \times 10^2$)[9 and 25]. This is much lower than I_{on}/I_{off} displayed by DPPDTT ($3 \pm 1 \times 10^3$) and IDT-BT ($2.3 \pm 0.1 \times 10^4$) (**Figure 3-6.b** and **c**, and **Table S3-1**). Furthermore, the sub-threshold swing (SS) of the donor-acceptor polymers were lower than that of PBTTT (456 mV.deca^{-1}) reported in this work and in the literature[9] (**Figure 3-6.d**). Note: SS of PBTTT based device was ~106 mV.deca^{-1} lower than that reported in the literature. However, the product of mobility and capacitance (μ.C) of PBTTT was double that of DPPDTT and IDT-BT (**Figure 3-6.f**). To understand the high transconductance displayed by the PBTTT

as compared to the donor-acceptor polymers the capacitance and mobility were decoupled. Usually this is carried out by determining the capacitance of the electrical double via techniques such as cyclic voltammetry and electron impedance spectroscopy measurement[26 and 27]. The capacitance of the electrical double layer (C) that form at the interface between an electrolyte and an electrode is voltage dependent[28]. Basically, it quantifies the change in surface charge (σ) near the electrodes with the change in electric potential (φ_e). And it can be written as a differential capacitance:

$$C = \frac{d\sigma}{d\varphi_e} \tag{3.1}$$

by the introduction of a derivative of time, equation (3.1) becomes:

$$C = \frac{d\sigma}{dt} \times \frac{dt}{d\varphi_e} \tag{3.2}$$

Considering that a variation of charge with time is a current ($I = \frac{d\sigma}{dt}$), equation (3.1) can be rewritten as:

$$I = C \times \frac{d\varphi_e}{dt} \tag{3.3}$$

In EGOFET, the electrolyte is inserted between the conducting channel and the gate terminal. Hence, the current (I) in equation (3.3) is the gate current of EGOFET. Because of low hysteresis seen in transfer curves and the small recorded gate current, here the gate leakage can be neglected, thus "I" is the displacement current. Therefore, the effective capacitance of the electrical double layer is the slope of the displacement current as a function of gate sweeping rate. The peak gate current, which corresponds to a gate bias of -0.5 V was the current used to calculate the capacitance as it corresponds to the current at which the capacitance is close to the steady state value. Initially the gate current characteristic at different gate bias sweep rate was recorded (**Supporting information Figure S3-3 (a-c)**). Then, the peak currents at -0.5 V were extracted and plotted against gate sweep rate (**Supporting information Figure S3-3 (d-e)**). The slope of gate peak current against the sweep rate, the capacitance of the EDL, was extracted by linear fitting of data points. Dividing this by the source/drain electrode area, the capacitance per unit area of the electrical double layer of fabricated EGOFETs were obtained. The mobility and capacitance of all the materials obtained by this method are plotted in **Figure 3-6.e** and summarised **Table S3-1**.

The capacitances range from 0.55 µF.cm^{-2} for PBTTT, 0.12 µF.cm^{-2} to 0.09 µF.cm^{-2} for DPPDTT and IDT-BT respectively. These are within capacitance per unit area reported for EGOFETs with purified water acting as gate insulator[2, 25 and 29]. The high

transconductance of PBTTT originated from its superior capacitance rather than high mobility. The mobility of PBTTT obtained here was similar to that reported in the literature (0.09 $cm^2.V^{-1}.s^{-1}$)[25 and 9]. It is almost two times lower than that of DPPDTT and IDT-BT which were 0.18 $cm^{-2}.V^{-1}.s^{-1}$ and 0.15 $cm^{-2}.V^{-1}.s^{-1}$ respectively (**Table S3-1**). These results in concert with the high I_{on}/I_{off} ratio, the small SS of IDB-BT and DPPDTT based EGOFET as compared to PBTTT, indicate that the modulation of I_{DS} by the gate bias through the EDL was more effective with donor-acceptor polymers as conducting channels. The trends of the gate current, which is a combination of ionic (dominant) and electronic current, differ from that of the transfer characteristics (**Figure 3-4**). Also, I_{GS} were about two orders of magnitude lower than the on-state drain current of the corresponding device at maximum gate amplitude. Hence, the drain current modulations of water gated devices based on the three polymers were not influenced by the gate current. However, despite the channel and gate terminals superposition and that the geometry for all the fabricated device and the electrolyte employed were identical, the magnitudes of gate current recorded at -0.5 V gate bias differ. Gate current recorded with the PBTTT based device was 3 times higher than those of DPPDTT and IDT-BT which were in a similar range (< 3.5 nA).

Others figures of merit that provide information on the quality of the devices are the hysteresis, difference of pathway followed by drain current between forward (off to on-state) and backward (on to off-state) gate bias sweep, and the switching times. Zero hysteresis and fast switching are desired for applications including in-electrolyte sensing. The absence of hysteresis may guarantee stable long-term operation, and fast switching may be correlated to the device sensitivity and response time to external stimuli. Here minor hysteresis was noticeable in the transfer characteristics (**Figure 3-4.a, b** and **c**). In the on-state, devices-based on IDT-BT, show lower backward drain current (I_{DB}) compared to the forward current (I_{DF}). That of PBTTT show lower I_{DB} as compared to I_{DF} at gate bias from 0.4 V to about -0.2 V while the opposite was observed at other voltages. For DPPDTT, I_{DB} and I_{DF} were practically identical at gate bias between -0.2 V and -0.5 V, but I_{DB} becomes lower than I_{DF} at bias higher than -0.2 V. In EGOFETs, the hysteresis may originate from diverse physical phenomena. It can be induced by the presence of mobile ions in the electrolyte, the polarizability of Gouy-Chapman diffusion layer of the EDL, defect/impurity in the conducting channel, the penetration of ions into the semiconductor/gate terminal or release of them in the electrolyte. All or part of these phenomena may take place in the fabricated devices, determining the origin of the hysteresis is beyond the scope of this study.

As mentioned above, the switching times can provide valuable information on the dynamic behaviour of the device during for instance in situ transduction of external stimulus. The switch-on times (τ_{on}) were determined by monitoring the time-dependent drain current (I_{DS}) when the gate bias was switched from 0 V to -0.5 V. During the measurement the drain terminal was biased at -0.5 V. Typical transient responses of the devices along with the switch-on time are depicted in **Figure 3-7**.

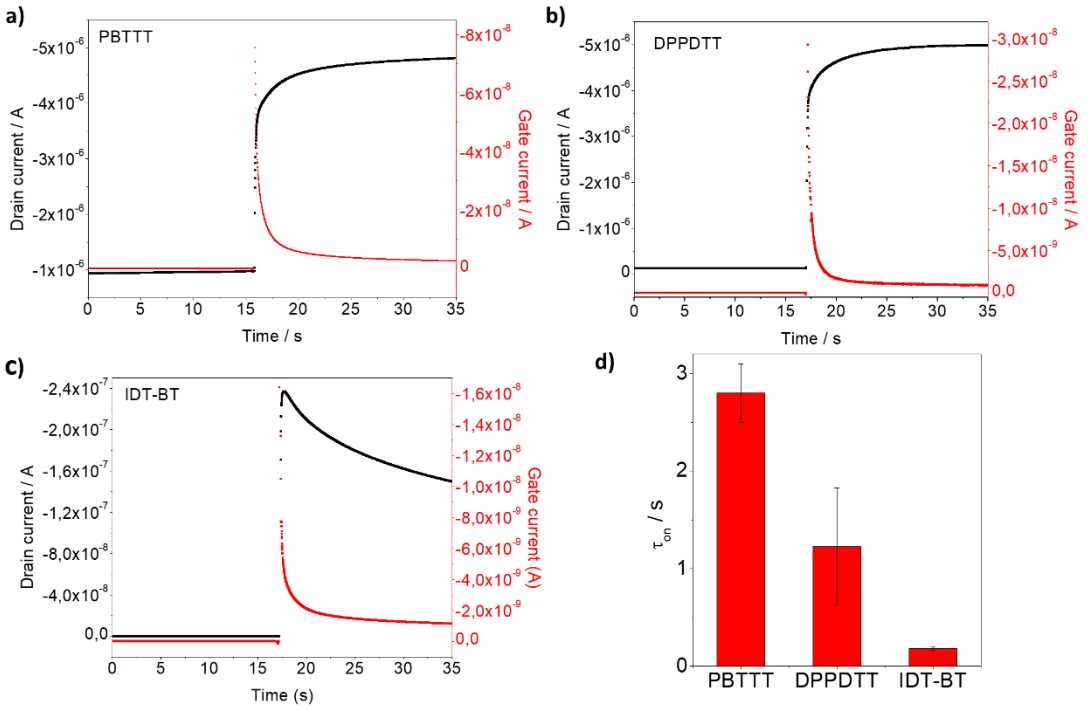

Figure 3-7: *Drain and gate current response to the switching of the gate terminal bias from 0 V to -0.5 V of an EGOFET based on a) PBTTT, b) DPPDTT, and c) IDT-BT. d) Time required to reach 90% of the saturation current. These experiments were conducted with purified water (resistivity of 18.2 MΩ.cm) with signal recorded every 10 ms.*

The curves obtained show very similar I_{DS} switch on behaviour (**Figure 3-7.a, b** and **c**) up on switching the gate bias to -0.5 V. They display a sharp increase of I_{DS} followed by a slow increase toward saturation. I_{DS} of IDT-BT based device, in contrast that of PBTTT and DPPDTT, decreased after saturation (**Figure 3-7.c**). Note: some points are missing in the rising part of the curves. This was attributed to the fact that the change in current were too fast to the Agilent reading. The increase of I_{DS} can be correlated with the change in the gate current. Upon switching the gate bias from 0 V to -0.5 V the gate currents increase sharply to reach a maximum value in less than 10 ms (**Figure 3-7** (**a-c**)). This corresponds to an ionic displacement under the effect of the field established between the gate and source-channel-drain. This is followed by an exponential decrease to the steady state value. The drain and corresponding gate currents reach steady state at the same times. The variation in the rate of increase of the drain current describes the state of coupling between the majority charge carriers in the semiconductor and ions present in

the electrical double layer. One explanation for this behaviour is that the EDL capacitance increases with a rate that dictates the response time of the device. Here this time (τ_{on}) depends on the conducting channel employed in the device (**Figure 3-7.d**). The times required to reach 90% of the maximum current were 2.8 s, 1.2 s and 0.18 s for PBTTT, DPPDTT and IDT-BT, respectively. These values are an order of magnitude higher than what was achieved for water gated devices based on P3HT[2]. The lowest reported response time for EGOFETs was about 1 ms with a blend of diF-TES-ADT: PS (4:1) deposited by means of the bar-assisted meniscus shearing technique[27]. Due to the fast response to gate bias change, ones may expect the donor-acceptor polymers DPPDTT and IDT-BT to be more sensitive to change in gate surface potential when compared to the PBTTT based EGOFET devices.

3.4. Conclusion

In this work, the electrical performances of three polymeric semiconductors were investigated in the electrolyte-gated transistor configuration. The results show that the donor-acceptor polymers, namely DPPDTT and IDT-BT can be water-gated to produce devices that operate in pure or at least dominant field-effect charge transport mode. The figures of merit of devices based on the two materials were systematically compared against that of an established polymer in the field, PBTTT. Except for the capacitance, the electrical characteristics of the devices based on D-A polymers were superior to those fabricated with PBTTT (**Table 3-1 and S3-1**). These findings widen the library of organic semiconductor that can be utilised in EGOFET.

	C $\mu F.cm^{-2}$	**μ** $cm^2.V^{-1}.s^{-1}$	**SS** $mV.deca^{-1}$	**I_{on}/I_{off}**	**Switch-on time** s
PBTTT	0.55	0.09	456	$2.1 \pm 0.7 \times 10^2$	2.8 ± 0.3
DPPDTT	0.12	0.18	125	$3 \pm 1 \times 10^3$	1.2 ± 0.6
IDT-BT	0.09	0.15	62	$2.3 \pm 0.1 \times 10^4$	0.18 ± 0.02

Table 3-1: *Summary of figures of merit obtained from EGOFET devices gated with purified water.*

Based on field-effect mobility, subthreshold swing, on-to-off current ratio and switch-on time achieved here **(Table 3-1 and Table S3-1)**, DPPDTT and IDT-BT should be preferred to PBTTT in developing a high performance EGOFET for applications including the detection of external stimuli.

3.5. Experimental: Device fabrication & characterisation

3.5.1. Substrate conditioning, contact electrode patterning and channel materials deposition

3.5.1.1. Substrate preparation

EGOFETs are fabricated in bottom contact top gate architecture (BCTG) by employing a combination of manufacturing techniques including laser cutting, photoresist lithography, spin-coating and lamination. Initially, a 125 µm polyethylene naphthalate (PEN) with 4 µm planarization layer and a platfix CS2325NA4 adhesive sheet (both provided by DuPont) were cut into rectangular pieces of 20 mm x 30 mm with a CO_2 laser cutter (100 W at 10 $mm.s^{-1}$). Then, a plain silicon substrate (obtained from Manchester Centre for Mesoscience and Nanotechnology) was cut into rectangular pieces of 22 mm x 32 mm with a diamond tip. The silicon carriers (22 mm x 32 mm) were sonicated in acetone and isopropanol (IPA) for 5 minutes each, rinsed with IPA and blown dry with a stream of nitrogen. PEN substrates (20 mm x 30 mm) were then laminated, using Bonsen Electronics Ltd. laminator Peach PL714, onto cleaned silicon carriers with the help of the platfix adhesive. This planarization of PEN substrates on silicon is necessary for improved device fabrication reproducibility and yields. **Figure 3-8** shows a schematic representation of the structure obtained after this process.

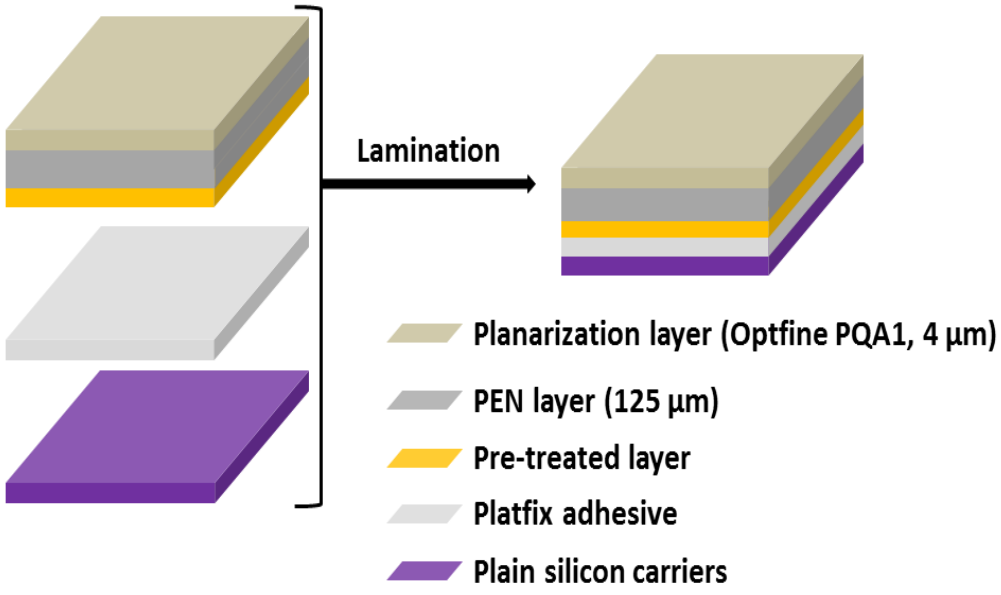

Figure 3-8: *Schematic representation of the substrate after lamination of the flexible substrate consisting of planarization, polyethylene naphthalate (PEN) and pre-treated layers, on a silicon carrier via platfix adhesive. Note: the layers are not to scale.*

3.5.1.2. Contact electrode patterning

The next step consists of generating source drain electrodes patterned onto the PEN substrate. Photoresist direct laser lithography in combination with metal evaporation and lift-off technique were employed in a yellow clean room. The substrate fixed on silicon carrier (PEN/Si) was sonicated in IPA (5 minutes), rinsed with a spray bottle full of IPA (about 30 seconds), blown dry with a stream of nitrogen (about 30 seconds) and heated on a hotplate at 110˚C (5 minutes) to prepare for photoresist deposition. At this stage, spin-coating was employed to deposit a sacrificial polymethylglutarimide (PGMI)) and positive imaging resist (S1805) layers on PEN/Si. Both resists were obtained from Manchester Centre for Mesoscience and Nanotechnology. Firstly, a solution of PGMI was spun onto PEN/Si (Speed: 1500 rpm, acceleration: 1000 rpm.s^{-1}, Time: 60s), then the substrate was heated up to 150 °C for 5 minutes to fully dry the produced film and improve its adhesion to the PEN substrate. Secondly, S1805 was spun onto PGMI coated substrates (Speed: 7000 rpm, acceleration: 1000 rpm.s^{-1}, time: 60s), followed by heating the substrate on a hotplate at 110 °C for a minute to remove residual solvent. Contact electrodes (source and drain) of sixteen transistors designed with AutoCAD (**Figure 3-9**) were used by a direct laser lithography machine (DLW405) to expose some part of the PEN/Si coated S1805/PGMI bilayer photoresist to a 405 nm laser beam. Then, the substrate was immersed in an MF-319 solution, and in water for 60s each, rinsed with water and blown dry with a stream of nitrogen to generate the same pattern as the design of the AutoCAD drawing exchange format file.

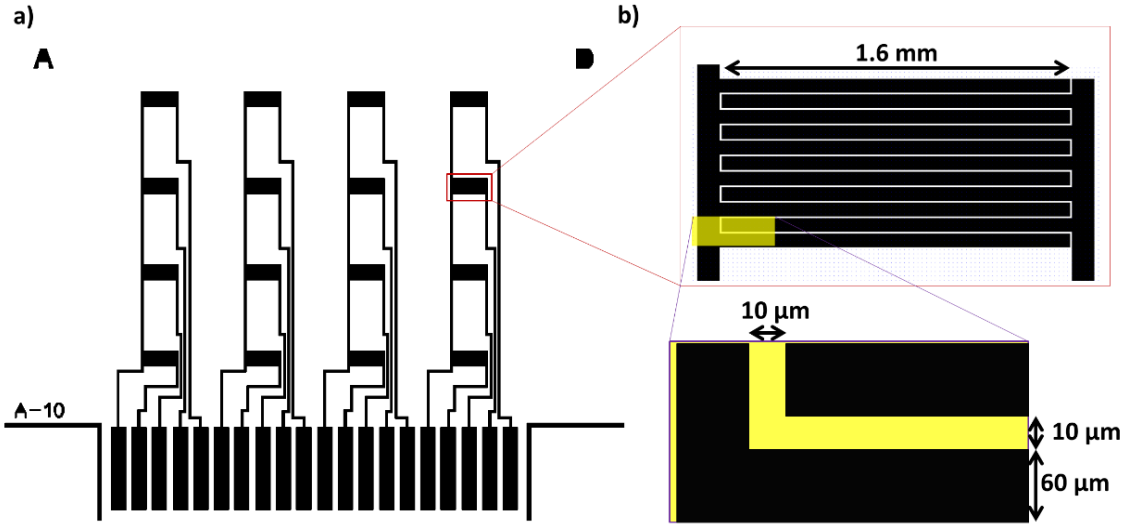

Figure 3-9: *a) Schematic representation of the mask used by the laser writer to produce interdigitated electrodes array. b) Zoom-in displays details of the interdigitation sizes and channel length.*

Note: MF-319 removes the exposed S1805 and etches, it underneath the PGMI layer. Here water was used to quench the etching, of PGMI. This was followed by thermally

evaporating 5 nm of chromium and 40 nm of gold with an Edward Auto 300 in high vacuum (10^{-7} mbar) at a rate of 0.1 nm per second. The last step to obtain the electrode pattern onto the PEN/Si consists of immersing the substrate in acetone for about 15 minutes of sonication to lift-off. The procedure for the patterning of the substrate with the contact electrode is schematised in **Figure 3-10**. The substrate is then peeled off the silicon carriers, sonicated in acetone and IPA for 15 minutes in each, rinsed with IPA, blown dry with a stream of nitrogen and treated by UV/O_3 for 15 minutes to remove organic contaminants. The contact electrode patterned substrates were then coated with semiconducting polymers.

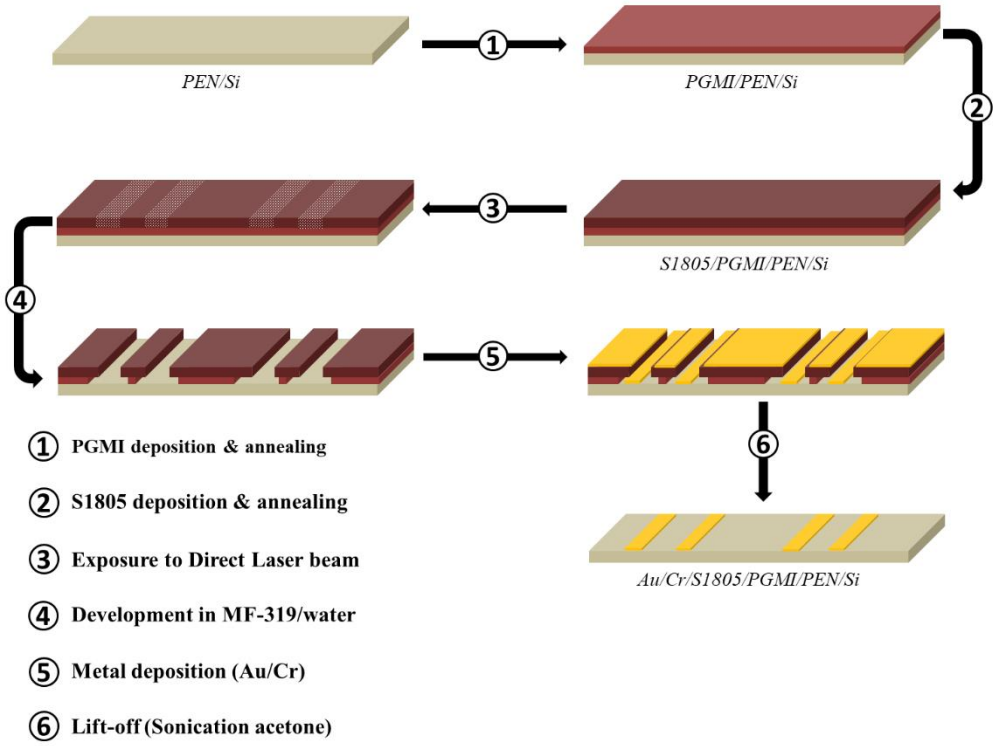

Figure 3-10: *Schematic representation of the procedure for patterning of the contact electrode on the PEN substrate.*

3.5.1.3. Organic semiconductor deposition

The three polymers, PBTTT (Ossila Ltd. – Mw ~39 507 Da and Mn ~20 260 Da), DPPDTT (Ossila Ltd. – Mw ~292 200 Da and Mn ~74 900 Da), IDT-BT (from Dr. D. Tate – Mw ~243 000 Da and Mn ~33 000 Da), were dissolved in 1-2, dichlorobenzene (heated at 80 °C for about an hour) to produce 7 $mg.ml^{-1}$ of solutions of each. The four solutions were deposited on different substrates with patterned contact electrodes with the same spin-coating parameters (speed: 1500 rpm, acceleration 1000 $rpm.s^{-1}$, time: 2 minutes). All the substrates, except otherwise stated, were heated at 140 °C for one hour to fully dry the films. A double-sided tape with circular holes, were laser cut and fixed on the substrate. The hole was filled with 6 µL of purified water (Milli-Q - resistivity of 18

MΩ.cm). A gold wire cleaned with isopropanol and water (1 mm width), serving as the gate electrode, was fixed on the double-sided tape.

3.5.2. Device electrical testing and surface properties metrology

3.5.2.1. Surface properties metrology

Olympus BX51 optical microscope was used for the inspection of the quality of the source-drain electrode pattern on the PEN substrate after the lift-off procedure. Atomic force microscope (Nasoscope V) was used to probe the organic semiconductor films surface properties in tapping mode.

3.5.2.2. Electrical characterisation

The electrical measurement, namely transfer, output curves, gate current, and transient characteristics, were conducted in air at ambient conditions with a semiconductor parameter analyser Agilent 1500B. The transfer and gate current curves consist of applying a constant voltage to the drain terminal (-0.5 V) while sweeping the bias applied to the gate terminal (forward and backward from 0.35 V to -0.5 V, at a sweeping rate of -1 mV/s) and recording the current at the drain and gate terminals. The output curves were obtained by measuring the drain current when sweeping the drain voltage (from 0.05 V to -0.5 V, at a sweeping rate of -1 mV/s) at different constant gate voltage (from 0 V to -0.5 V, step of -0.1 V). The gate curves used to calculate the capacitance were obtained by measuring the gate current with the same condition as for the transfer curves, however a set of 4 sweep rates were used (1 $mV.s^{-1}$, 2 $mV.s^{-1}$, 3 $mV.s^{-1}$ and 4 $mV.s^{-1}$). The response time measurements consist of recording the drain and gate currents (every 10 ms) over time when the gate bias was swept from 0 V to -0.5 V at constant drain voltage of -0.5 V.

Acknowledgment

I would like to acknowledge CDT Ltd. and EPSRC for generous financial support and Dr D. Tate for supplying IDT-BT.

References

1. Wang, D., Noël, V. & Piro, B. Electrolytic Gated Organic Field-Effect Transistors for Application in Biosensors—A Review. *Electronics* **5,** 9 (2016).

2. Kergoat, L., Herlogsson, L., Braga, D., Piro, B., Pham, M-C., Crispin, X., Berggren, M. & Horowitz, G. A Water-Gate Organic Field-Effect Transistor. Adv. Mater. 22, 2565–2569 (2010).

3. Kergoat, L., Piro, B., Berggren, M., Horowitz, G. & Pham, M. C. Advances in organic transistor-based biosensors: From organic electrochemical transistors to electrolyte-gated organic field-effect transistors. *Anal. Bioanal. Chem.* **402,** 1813–1826 (2012).

4. H. Helmholtz. Ueber einige Gesetze der Vertheilung elektrischer Ströme in körperlichen Leitern, mit Anwendung auf die thierisch-elektrischen Versuche (Schluss.). *Ann. Phys.* **165,** 353–377 (1853).

5. Gouy, M. Sur la constitution de la charge électrique à la surface d ' un électrolyte. *J. Phys. Theor. Appl.* **9,** 457–468 (1910).

6. Chapman, D. L. LI. A contribution to the theory of electrocapillarity . *London, Edinburgh, Dublin Philos. Mag. J. Sci.* **25,** 475–481 (2009).

7. Otto Stern. The theory of the electrolytic double-layer. *Zeitschrift für Elektrochemie* **30,** 508–516 (1924).

8. Rivnay, J., Inal, S., Salleo, A., Berggren, M. & Malliaras, G. G. Organic electrochemical transistors. *Nat. Rev. Mater.* **3,** 1–14 (2018).

9. Porrazzo, R., Bellani, S., Luzio, A., Lanzarini, E., Caironi, M. & Antognazza, M. R. Improving mobility and electrochemical stability of a water-gated polymer field-effect transistor. Org. Electron. 15, 2126–2134 (2014).

10. Berto, M., Diacci, C., D'Agata, R., Pinti, M., Bianchini, E., Di Lauro, M., Casalini, S., Cossarizza, A., Berggren, M., Simon, D., Spoto, G., Biscarini, F. & Bortolotti, C., A. EGOFET Peptide Aptasensor for Label-Free Detection of Inflammatory Cytokines in Complex Fluids. Adv. Biosyst. 2, 1700072 (2017).

11. Casalini, S., Leonardi, F., Cramer, T. & Biscarini, F. Organic field-effect transistor for label-free dopamine sensing. *Org. Electron. physics, Mater. Appl.* **14,** 156–163 (2013).

12. Foschi, G., Leonardi, F., Scala, A., Biscarini, F., Kovtun, A., Liscio, A. &Casalini, S. Electrical release of dopamine and levodopa mediated by amphiphilicamphiphilic β -cyclodextrins. Nanoscale. 7, 20025–20032 (2015).

13. Di Lauro, M., Berto, M., Giordani, M., Benaglia, S., Schweicher, G., Vuillaume, D., Bortolotti, C. A., Geerts, Y. H. & Biscarini, F. Liquid-Gated Organic Electronic Devices Based on High-Performance Solution-Processed Molecular Semiconductor. *Adv. Electron. Mater.* **3,** 1–6 (2017).

14. Desbief, S., Di Lauro, M., Casalini, S., David, G., Tortorella, S., Barbalinardo, M., Kyndiah, A., Murgia, M., Cramer, T., Biscarini, F. & Vuillaume D. Electrolyte-gated organic synapse transistor interfaced with neurons. Org. Electron. 38, 21–28 (2016).

15. Nielsen, C. B., Turbiez, M. & McCulloch, I. Recent advances in the development of semiconducting DPP-containing polymers for transistor applications. *Adv. Mater.* **25,** 1859–1880 (2013).

16. Lu, C. F., Shih, C. W., Chen, C. A., Chin, A. & Su, W. F. Tuning the Morphology of Isoindigo Donor–Acceptor Polymer Film for High Sensitivity Ammonia Sensor. *Adv. Funct. Mater.* **28,** 1–9 (2018).

17. Marszalek, T., Li, M. & Pisula, W. Design directed self-assembly of donor-acceptor polymers. *Chem. Commun.* **52,** 10938–10947 (2016).

18. Zhang, X., Bronstein, H., Kronemeijer, A. J., Smith, J., Kim, Y., Kline, R. J., Richter, L. J., Anthopoulos, T. D., Sirringhaus, H., Song, K., Heeney, M., Zhang, W. McCulloch, I. & DeLongchamp, D. M. Molecular origin of high field-effect mobility in an indacenodithiophene- benzothiadiazole copolymer. *Nat. Commun.* **4,** 1–9 (2013).

19. Venkateshvaran, D., Nikolka, M., Sadhanala, A., Lemaur, V., Zelazny, M., Kepa, M., Hurhangee, M., Kronemeijer, A. J., Pecunia, V., Nasrallah, I., Romanov, I., Broch, K., McCulloch, I., Emin, D., Olivier, Y., Cornil, J., Beljonne, D. & Sirringhaus, H. Approaching disorder-free transport in high-mobility conjugated polymers. *Nature* **515,** 384–388 (2014).

20. Xi, Y., Wolf, C. M. & Pozzo, L. D. Self-assembly of donor-acceptor conjugated polymers induced by miscible 'poor'' solvents'. *Soft Matter* **15,** 1799–1812 (2019).

21. Gaikwad, A. M., Khan, Y., Ostfeld, A. E., Pandya, S., Abraham, S. & Arias, A. C. Identifying orthogonal solvents for solution processed organic transistors. *Org. Electron. physics, Mater. Appl.* **30,** 18–29 (2016).

22. DeLongchamp, D. M., Kline, R. J., Lin , E. K., Fischer, D. A., Richter, L. J., Lucas, L. A., Heeney, M., McCulloch, I., Northrup, J. E. High carrier mobility polythiophene thin films: Structure determination by experiment and theory. *Adv. Mater.* **19,** 833–837 (2007).

23. McCulloch, I., Heeney, M., Bailey, C., Genevicius, K., MacDonald, I., Shkunov, M., Sparrowe, D., Tierney, S., Wagner, R., Zhang, W., Chabinyc, M. L., Kline, R. J., McGehee, M. D. & Toney, M. F. Liquid-crystalline semiconducting polymers with high charge-carrier mobility. *Nat. Mater.* **5,** 328–333 (2006).

24. Noriega, R., Rivnay, J., Vandewal, K., Koch, F. P. V., Stingelin, N., Smith, P., Toney, M. F. & Salleo, A. A general relationship between disorder, aggregation and charge transport in conjugated polymers. *Nat. Mater.* **12,** 1038–1044 (2013).

25. Porrazzo, R., Bellani, S., Luzio, A., Bertarelli, C., Lanzani, G., Caironi, M., & Antognazza M. R. Field-effect and capacitive properties of water-gated transistors based on polythiophene derivatives. *APL Mater.* **3,** (2015).

26. Panzer, M. J. & Frisbie, C. D. Polymer electrolyte-gated organic field-effect transistors: Low-voltage, high-current switches for organic electronics and testbeds for probing electrical transport at high charge carrier density. *J. Am. Chem. Soc.* **129,** 6599–6607 (2007).

27. Zhang, Q., Leonardi, F., Casalini, S., Temiño, I. & Mas-Torrent, M. High performing solution-coated electrolyte-gated organic field-effect transistors for aqueous media operation. *Sci. Rep.* **6,** 1–10 (2016).

28. Tu, D., Herlogsson, L., Kergoat, L., Crispin, X., Berggren, M. & Forchheimer, R. A Static Model for Electrolyte-Gated Organic Field-Effect Transistors. *IEEE Trans. Electron Devices* **58,** 3574–3582 (2011).

29. Cotrone, S., Ambrico, M., Toss, H., Angione, M. D., Magliulo, M., Mallardi, A., Berggren, M., Palazzo, G., Horowitz, G., Ligonzo, T. & Torsi, L. Phospholipid film in electrolyte-

gated organic field-effect transistors. *Org. Electron. physics, Mater. Appl.* **13,** 638–644 (2012).

Supporting information

Gate electrode position impact on water-gate device transfer characteristic

To evaluate the impact of the gate electrode position to the organic semiconductor on water gate EGOFET performance a simple device was developed. The device was fabricated on a glass substrate using thermal evaporated gold (40 nm) source drain contacts (channel length of 60 µm and width of 1 mm) with chromium (5 nm) as an adhesion promoter between gold and glass. The gold and chromium layer were deposited onto glass substrate, that was sonicated in acetone (5 minutes) isopropanol (5 minutes) and blown dry with a stream of nitrogen gun, with an Edward Auto 300 in high vacuum (10^{-7} mbar) at a rate of 0.1 nm per second. Then, PBTTT was spin-coated from 1,2-dichlorobenzene (7 mg/ml) at 3000 rpm for 2 minutes and the film was heated for 30 minutes at 160° C. The device was terminated by depositing 4 µL of purified water (Milli-Q - resistivity of 18 MΩ.cm) on the channel area and dipping a tungsten needle in it.

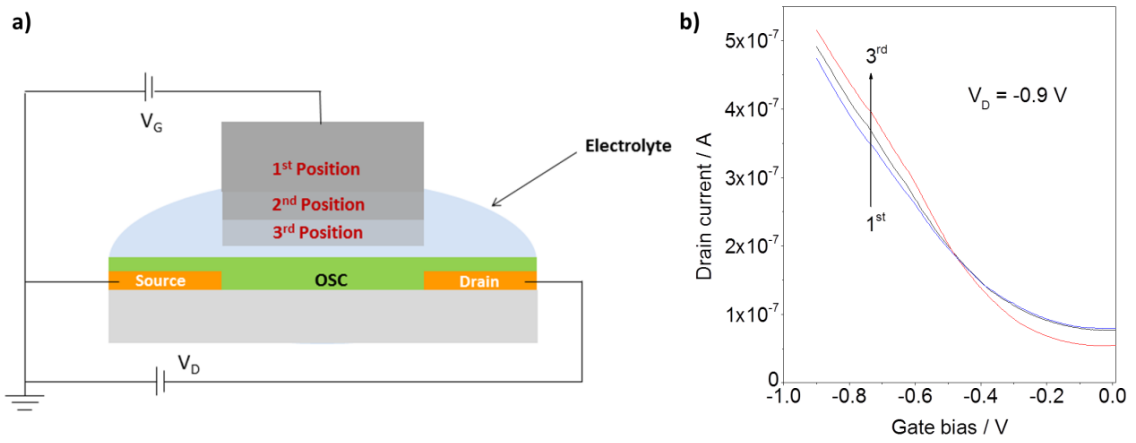

Figure S3-1*: a) Cross-section view of a water-gated organic field effect transistor showing the position of the gate electrode relative to the conducting channel in the vertical direction and b) the corresponding electrical transfer characteristic.*

The curves show a clear dependence of the transfer characteristic with the gate position relative to the conducting channel (**Figure S3-1**). Performance improves with the reduction of the distance between the gate and the semiconductor in the vertical direction. This may be due to the fact that the areas of gate immersed into the electrolyte increases, which increases the capacitance of the EDL at the gate/electrolyte interface, thus increasing the slope of the transfer curve resulting in higher drain current.

Comparison of water gated electrical performance of PBTTT, DPPDTT and IDT-BT based EGOFET.

The figures of merit summarised in **Table S3-1**, square root of drain current and gate peak current as a function of gate bias sweep in **Figure S3-2** and **Figure S3-3** were obtained from the EGOFETs array fabricated following procedure detailed in **Section 3.5**.

	$\mu.C \times 10^{-8}$ F/(Vs)	μ $cm^2/(Vs)$	C $\mu F/cm^2$	$I_{on}/I_{off} \times 10^3$	I_{on} µA	I_{off} nA	SS mV/Deca	V_{th} V	τ_{on} s
PBTTT	5 ± 2	0.09	0.55	0.21 ± 0.07	6.9 ± 4.0	48 ± 1	456	0.02 ± 0.03	2.8 ± 0.3
DPPDTT	2 ± 1	0.18	0.12	3 ± 1	3.6 ± 1.7	1.1 ± 0.2	125	-0,05 ± 0.03	1.2 ± 0.6
IDT-BT	1.3 ± 0.3	0.15	0.09	23 ± 1	0.21 ± 0.03	0.012 ± 0.006	62	-0,36 ± 0,01	0.18 ± 0.02

Table S3-1*: Summary of figures of merit obtained from EGOFET devices gated with purified water.*

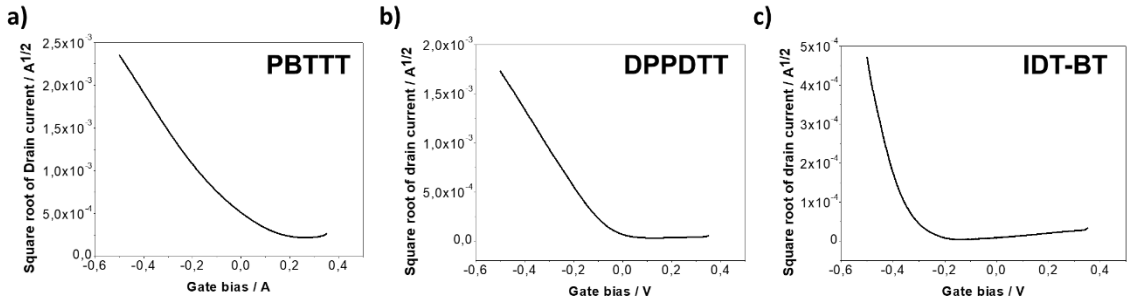

Figure S3-2*: Square root of drain current as a function of gate bias for EGOFETs based on a) PBTTT, b) DPPDTT, and c) IDT-BT. The drain bias was -0.5 V and the gate bias was swept from 0.35 V to -0.5 V at a rate of -1 mV/s*

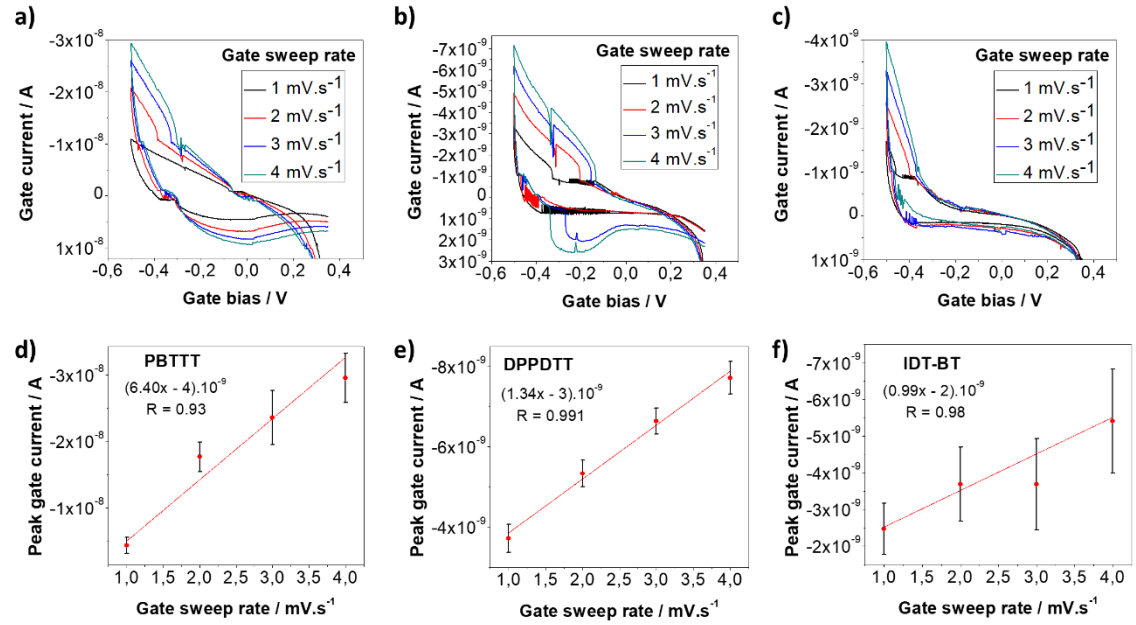

Figure S3-3*: Typical gate current characteristics at different gate sweep rate for water-gated devices based on a) PBTTT, b) DPPDTT and c) IDT-BT. (d-f) Average of the maximum gate currents as a function of the gate sweep rate. The error bars are the standard deviation from three devices. The variation of the peak current is linear with coefficient equal to the capacitance of the electrical double layer of the devices. The capacitances per unit area were obtained from the ratio of the slope to the surface area of the device (0.0116 cm)^2. This gives a capacitance of 0.55 µF.cm^2 for PBTTT, 0.12 µF.cm^2 and 0.09 for DPPTTT and IDT-BT, respectively.*

Optical microscope picture of the contact electrode after lift-off procedure

Figure S3-4*: Optical microscope picture of the interdigitated contact electrodes. The interfinger spacing is 10 µm.*

Blank Page

Chapter 4: Electrolyte gated organic field effect transistor array integrated with a microfluidic device as a platform for point of care testing

The following chapter is an adaptation of: ***A. Doumbia****, M. Webb, M. L. Turner, J. M. Behrendt, R. Wilson : "A printed electronic platform for the specific detection of biomolecules", Proc. SPIE 10364, Organic Sensors and Bioelectronics X, 103640N (25 August 2017); doi: 10.1117/12.2274038.*

Authors contributions:

M. L. Turner, M. Webb and ***A. Doumbia*** *conceived the presented idea (sensing of biochemical molecules with EGOFET). J. M. Behrendt, R. Wilson encouraged* ***A. Doumbia*** *to choose deoxyribonucleic acid (DNA) as the molecule to demonstrate the utility of the platform in point-of-care testing.* ***A. Doumbia*** *technically leads the project: conceived and designed the device, planned, carried out the experiments, and collected and analysed the data. All authors discussed the results.* ***A. Doumbia*** *took the lead in writing the manuscripts (Co-authors provided critical feedback).*

4.1. Abstract

Electrolyte gated organic field effect transistors (EGOFETs) are becoming an established technology in the field of biosensors and bioelectronics. Platforms based on this device that are capable of detection of chemical and biological molecules selectively with high sensitivity have been reported. However, the research presented to date have been dominated by EGOFETs in the droplet gated configuration in which the interaction between analyte and receptor took place before sensing was carried out. Here we present a stable EGOFET array integrated with a microfluidic device, for the in-line detection of the hybridization of deoxyribonucleic acid (DNA) *in operando*. The selectivity of individual EGOFET in the array toward the target DNA was addressed by functionalising the gate terminal with a self-assembled-monolayer coupled to a single strand of DNA. The performance, stability and inter-device reproducibility of the developed system is among the best reported for EGOFET gated with saline solution. The average normalised transconductance, on-to-off current ratio, and subthreshold swing were estimated to be 0.16 ± 0.03 $\mu F.V^{-1}.s^{-1}$, $1.5 \pm 0.7 \times 10^3$ and 110 $mV.decade^{-1}$, respectively. The platform successfully detected complementary target DNA diluted in physiological-like media selectively under a flow of analyte (210 $\mu L.min^{-1}$). The assay-to-results time was about 30 seconds and the relative standard deviation on the sensing reproducibility was less than fifteen percent. This detection is fast in comparison to current DNA Enzyme-linked Immunosorbent assay (ELISA) kits (~1 h) with similar reproducibility. The system is versatile, cost-effective and can be tailored for rapid detection of others biochemical molecules for in line point-of-care testing in sector including life science, healthcare, environmental protection and homeland security.

4.2. Introduction

The rising awareness of the needs of reliable portable easy-to-use and high-throughput tools for onsite environmental monitoring, disease diagnosis and prognosis are catalysing research in the fields of biosensors and bioelectronics. Miniaturised biological and biochemical sensing devices based on various detection modalities are under investigation to deliver point-of-need testing systems[1,2 and 3]. Among others, platforms based on organic field-effect transistors (OFETs) have sparked considerable attention due to several advantages they offer[4]. For instance, the characteristics of the output signal of OFETs are sensitive to subtle change in surface potential. By tailoring the interface with a specific biorecognition element, selective label-free identification and multiparametric quantification of target analyte is realisable[5, and 6]. The miniaturisation and integration of OFETs to other microsystems on various substrates are straightforward[7].

A class of OFETs known as electrolyte gated organic field-effect transistor (EGOFET) emerge lately as a cutting-edge in electrolyte label-free biosensing tool[8]. A particularity of EGOFET is the presence of an electrolyte in its architecture[9]. It insulates the gate terminal from the source-drain and channel layer. Upon biasing the gate and drain terminals (source grounded), the electrolyte acts as gate capacitor (~$\mu F.cm^{-2}$) via the exploitation of the Electrical Double Layer (EDL) phenomenon. Generally, in these devices a full modulation of the drain current from off to on-state with $\leq 1V$ is achieved[10]. Hence the biological medium is an integral part of the device, it is the electrolyte. Platforms based on this cutting-edge low power consumption technology were reported for various molecules[10] and ions[11, 12 and 13] detection with good selectivity and high sensitivity. Commonly, the selectivity is obtained by incorporating a biorecognition element at the semiconductor or gate terminal interface with the electrolyte[10]. This promotes a special interaction between the device and the analyte. Sensitivity achieved were within the relevant range for biological molecules detection[14 and 15].

So far, the developed platforms were dominated by EGOFETs in the droplet gated configuration in which the interaction between analyte and receptor took place before sensing was carried out (*ex-situ* sensing)[14,16 and 15]. Also, most of these devices have been limited to a single spot measurement by the EGOFET[17]. In fact, it is challenging to continuously bias the device terminals and to flow the electrolyte to reliably visualise the interaction between biomolecules in real-time. Because, the flow of the electrolyte on the

organic semiconductor can induce a shear force resulting in the degradation of the semiconductor or even the delamination of the components of the device. Also, constantly biasing the device can induce ions into the conducting channel. These ions can modify the distribution of charges in the organic semiconductor (electrostatic interaction with the charges), act as trapping sites or contribute to the output current of the device (ions transport). This can lead unstable device operation, making the results of real-time continuous sensing ambiguous to interpret.

In this work, we report a reliable platform based on an array of EGOFET devices integrated with a microfluidic device and demonstrated *in operando* specific detection of the hybridization of deoxyribonucleic acid (DNA) under flowing electrolyte condition. Note: the selectivity of individual EGOFET in the array toward the target DNA was addressed by functionalising the gate terminals with a self-assembled-monolayer of single strand capturing DNA (ssDNA-Cap). The developed system selectively detects the hybridization of 100 nM of ssDNA (19 bases) in about 30 seconds with a relative standard deviation of the sensing reproducibility of less than fifteen percent.

4.3. Reliability and Sensing Demonstration of EGOFET Integrated with a Microfluidic platform

4.3.1. Functionalisation of the EGOFET and investigation of device reliability

4.3.1.1. Design of the biosensor and bio-functionalisation

The label-free biosensing system, which comprise an array of bio-functionalised EGOFET integrated with a microfluidic device was developed by using a combination of polymer microfabrication and fast prototyping techniques (**Section 4.5.2**). Briefly, 16 interdigitated (IDE) gold contact electrodes (4 source lines for 16 independent drain terminals) were produced on a flexible polyethylene naphthalate (PEN) substrate via direct laser lithography, metallisation and lift-off techniques. The substrate was then coated with poly(diketopyrrolo-pyrrole-dithiophene-thienothiophene) (DPPDTT). This donor-acceptor polymer (DPPDTT) was chosen as the conducting channel because of the high performance and in air bias stress stability it exhibited in OFETs[18 and 19]. Following the coating of the gold patterned substrate with DPPDTT, a spacer was mounted on to the device to confine the analyte on its surface. The spacer used was a double-sided tape with four flow channels patterned by a CO_2 laser. Each flow channel contains a total of 4

interdigitated contact electrodes. The channels are sealed with a top cover that has 4 inlets and 4 outlets for supplying the devices with electrolyte and an array of 16 gold gate electrodes coated with self-assembled-monolayer of desired capturing molecule. The fluidic channels were sealed so that the gate electrodes were inside the flow cells and directly over the interdigitated source/drain electrodes. The parts for assembling of the biosensing systems, along with a schematic representation and a top view photograph of the device and a closer look to the biofunctionalized gate electrode are outlined in **Figure 4-1**.

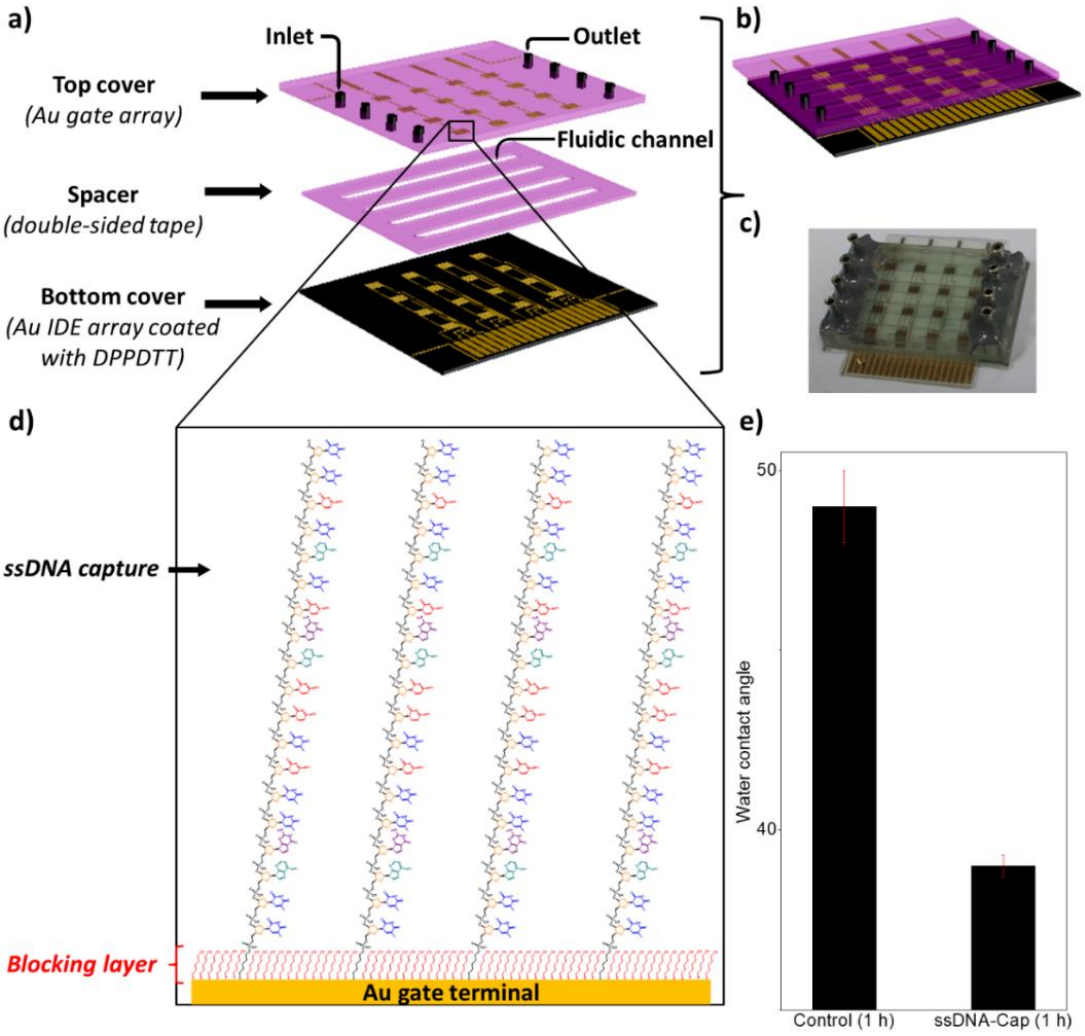

Figure 4-1: *a) Schematic of the parts of the label-free biosensor showing the top and bottom covers with a spacer in between. The top cover consists of 16 bio-functionalised gates patterned on PEN substrate that was stuck onto a polymethylmethacrylate (PMMA) sheet. The bottom cover comprises 16 interdigitated contact electrodes (IDE) coated with DPPDTT onto a PEN substrate. The gates are at 280 µm from the spin-coated DPPDTT film. b) 3D AutoCAD model of the device and c) a top view photograph. d) Schematic representation, not in scale for clarity, of the gate: the biofunctionalized layer on the gate surface is a self-assembled-monolayer comprising 6-mercaptohexanol (MCH) and a thiol-terminated ssDNA (ssDNA-Cap). e) Water contact angle of a clean gate, after incubation in phosphate buffer saline solution (1x PBS) with 100 µM of ssDNA-Cap (ssDNA-Cap) or without (control). Standard deviation (red) were obtained from 3 successive measurement.*

This choice of gate electrode for integration of the sensitive layer is linked in the fact that the incorporation of biorecognition and blocking elements at the surface of conducting channels may results in a degradation of the electronic performances of EGOFET. Because the solvents employed for covalent immobilization of these elements can change the structure of the semiconducting film via a dissolution and re-crystallisation process and/or doping it in the time scale of the experience. It is worth mentioning that solvent-free technique exists to functionalise the organic semiconductor (OS) interface with least significant impact on device figures of merit[20 and 16] as compared to the former technique. However, such a biorecognition layer may not remain stable during flowing electrolyte due to its weaker binding strength with the OS (electrostatic or Van dee Waals types). The shear force applied by the electrolyte during flow on the recognition layer can remove the recognition layer.

Here, the biofunctionalized layer consists of a mixture of a self-assembled-monolayer of capturing ssDNA-Cap and 6-mercaptohexanol (**Figure 4-1.d**). The terminus of the capturing ssDNA is an alkanethiol (**Supporting information Figure S4-1**). This promoted a spontaneous formation of a self-assembled-monolayer of ssDNA-Cap on individual gate terminal via gold-thiol chemistry[21]. In the aim of filling the space left after the immobilisation of ssDNA-Cap, thus minimising non-specific interactions of elements present in the sample to analyse with the gate terminal, the gate was subsequently covered with a diluted 6-mercaptohexanol (MCH) solution in 1x PBS. This treatment also removed non-specific adsorbed ssDNA-Cap molecules from the gate terminal[22 and 23]. To verify the modification of the surface properties of the gold electrode (e.g. surface energy, wettability), one reliable, quick, economic and simple approach is to measure the contact angle (CA) with a liquid droplet[24 and 25]. Thus, the formation of a self-assembled-monolayer of ssDNA-Cap on the gate electrode was confirmed by water contact angle measurement (**Figure 4-1.e** and **Table S4-1**). CA of a control gate after incubation in 1x PBS was 49° ± 1°. For a gate electrode after covering with ssDNA-Cap diluted in the same 1x PBS solution and duration it was 10° lower than the control (39.1° ± 0.3°). This suggest the effective immobilisation of ssDNA-Cap on the gate. Subsequent incubation of the functionalised gate in MCH diluted in 1x PBS improve ssDNA SAM orientation and fill the remaining free space[26, 22 and 21] on the gate.

4.3.1.2. Performance Reproducibility & Repeatability of the biosensing system

Current-voltage/time curves of the system were recorded while flowing 1x PBS at 210 µL.min^{-1} in the fluidic channel. See **Section 4.5.2** for a schematic representation of the characterisation set up. A typical I_{DS} vs V_{GS} is plotted in **Figure 4-2.a**. This behaviour of the drain current (I_{DS}) in respect to gate bias (V_{GS}) resembles that of p-channel OFETs[27]. This is normal as DPPDTT is an ambipolar semiconductor with pronounced p-type charge transport. At certain negative gate bias I_{DS} start increasing with the gate voltages to reach saturation with minor hysteresis. Moreover, the output curve presents obvious linear and saturation regime in I_{DS} (**Supporting information Figure S4-2**). These characteristics confirm the effective establishment of a stable EDLs and a dominant field-effect charge transport under flowing electrolyte condition.

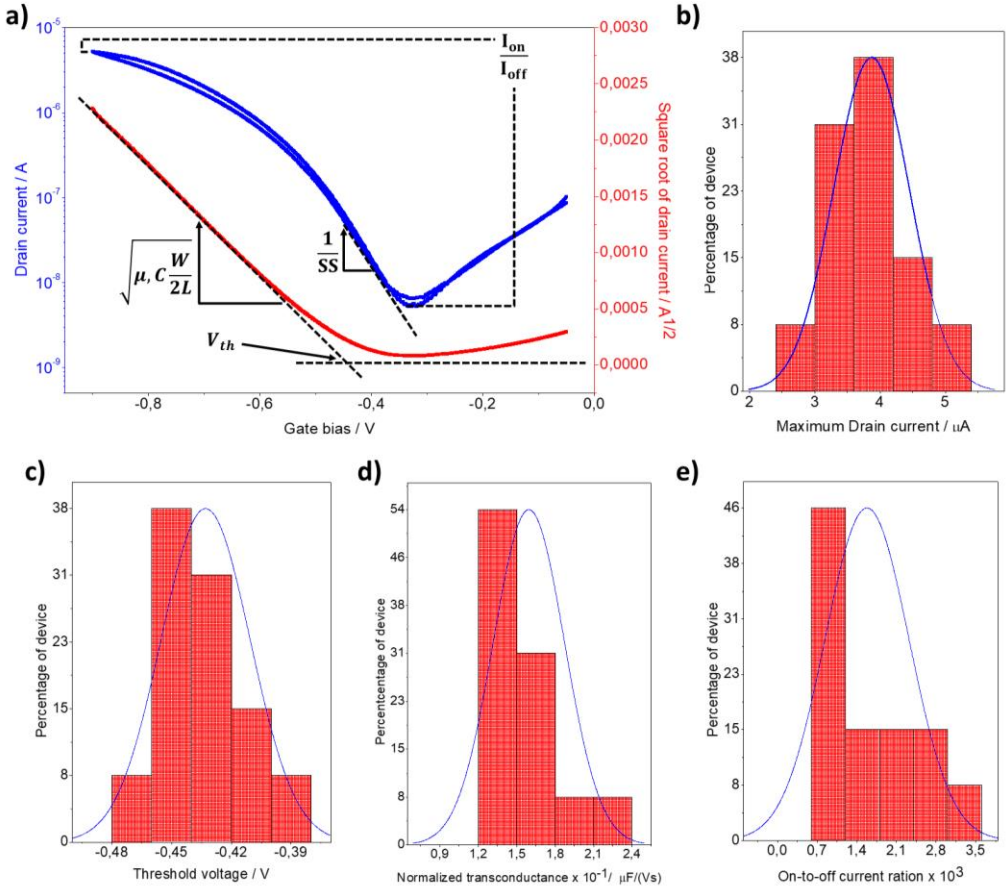

Figure 4-2: *Biosensing system gated with phosphate buffered saline solution (1x PBS) at flow rate of 210 µL.min^{-1}: distribution of electrical figures of merit extracted from the a) current voltage characteristics (V_{DS} = - 0.7 V) in the saturation regime, namely b) maximum drain current (V_{GS} = - 0.9 V) c) threshold voltage d) normalized transconductance and e) on-to-off drain current ratio.*

Several EGOFET in the array on 3 different devices were characterised similarly, to comprehensively study the reliability of the developed system. Device performance reproducibility, repeatability and long-term operational stability were chosen as criteria for operational reliability, as these are fundamental criteria a system has to fulfil prior to

realistic applications. In OFETs, these are investigated by extracting device figures of merit from current-voltage characteristics using standard Metal-Oxide-Field-Effect-Transistor (MOSFET) approximated equations[28 and 29]. These equations can be applied to the developed device, as $\sqrt{I_{DS}}$ scales linearly with the gate bias (**Figure 4-2.a**). Hence, the electrical parameters were extracted from the tested devices by linearly fitting equation (4.1) (saturation regime) to $\sqrt{I_{DS}}$ vs V_{GS} and calculating the slope of log (I_{DS}) vs I_{GS} at very low gate bias for the subthreshold swing (SS) as shown in **Figure 4-2.a**.

$$\sqrt{I_{DS}} = \sqrt{\mu . C_i . \frac{W}{2L}} (V_{GS} - V_{th}) \quad (4.1)$$

W, L, C_i, μ and V_{th} are the channel width and length, the EDLs area capacitance, the field-effect mobility and the threshold voltage, respectively. The distributions of the obtained figures, namely in the maximum drain current, V_{th}, normalized transconductance (μ.C) and on-to-off drain current ratio (I_{On}/I_{Off}), are displayed in **Figure 4-2**. The recorded drain currents lie between 2.9 μA and 5.2 μA at gate bias of -0.9 V (**Figure 4-2.b** and **Table S4-2**). The mean value was 3.9 μA with a relative standard deviation of about 12.8%, calculated from 36 devices over 3 systems (12 devices/system were characterised). The mean value of the drain current belongs to the high end of what were reported in solution gated EGOFET (e.g. water, saline solution) to date: few hundred of nA to a few μA are the usual drain current[30, 31, 32 and 33]. On the system, the estimated relative error on the drain current was equally reproducible, standard deviation was as good as 8% (**Figure S4-2 and Table 4-1**).

	I_{SD} (μA)	**V_{th}** (V)	**μ.C × 10^{-1}** ($\mu F.V^{-1}.s^{-1}$)
Substrate 1	4.0 ± 0.3	-0.42 ± 0.01	1.6 ± 0.2
Substrate 2	4.2 ± 0.7	-0.45 ± 0.01	1.7 ± 0.3
Substrate 3	3.6 ± 0.3	-0.43 ± 0.02	1.4 ± 0.003
Average	3.9 ± 0.5	-0.43 ± 0.02	1.6 ± 0.3

Table 4-1: *Average device figures of merit with standard deviation from 12 devices per substrate.*

Drain current in the devices off-state were low (~3 ± 2 nA) as was the subthreshold swing (~110 $mV.deca^{-1}$), yielded a high on-to-off current ratio of (1.5 ± 0.7) × 10^3 (**Figure 4-2.c**). The V_{th} and μ.C were reproducible and repeatable. The extracted V_{th} and μ.C values range from -0.39 V to -0.47 V and 0.13 $\mu F.V^{-1}.s^{-1}$ to 0.23 $\mu F.V^{-1}.s^{-1}$, respectively (**Figure 4-2.d** and **e**). Minor fluctuations from the mean values of device V_{th} of about 2 - 3% in the same substrate (0.43 ± 0.002 mV) and 5% between substrate were found. For μ.C the variations on the mean were 10% and 17% on the substrate and between substrate, respectively. Note: μ.C, on-to-off drain current ratio are comparable to the state-of-the-art performance reported recently[33], where the electrolyte used by the authors has

different composition to the one used here (1 M NaCl) and the semiconducting layer was a blend of TIPS-pentacene:PS (4:1 ratio). These small fluctuations in figures of merit, may be caused for example by the variation in the fabrication and assembly process of the system. The latter is less controlled, as it was conducted under a binocular microscope with hand tools (e.g. tweezer) and this can induce undetectable misalignment of the gate with the IDE at that resolution. Automating this step with submicrometric resolutions will further reduce the spread in the figures of merit of the device.

4.3.1.3. Operational stability of the biosensing system

With the electrical performance, reproducibility and repeatability criteria satisfied, the continuous operational stability of the developed device was investigated. This study is crucial, as it provides additional information on the threshold of the utility of the device figures of merit during *in operando* identification and quantification of the targeted molecule. Initially, the variation of the drain and gate currents under constant gate and drain bias (source grounded) as a function of time when the electrolyte was flowing in the fluidic channel at 210 µL.min^{-1} was recorded. The obtained drain current was normalised to allow direct estimation of percentage change in its value (**Figure 4-3**).

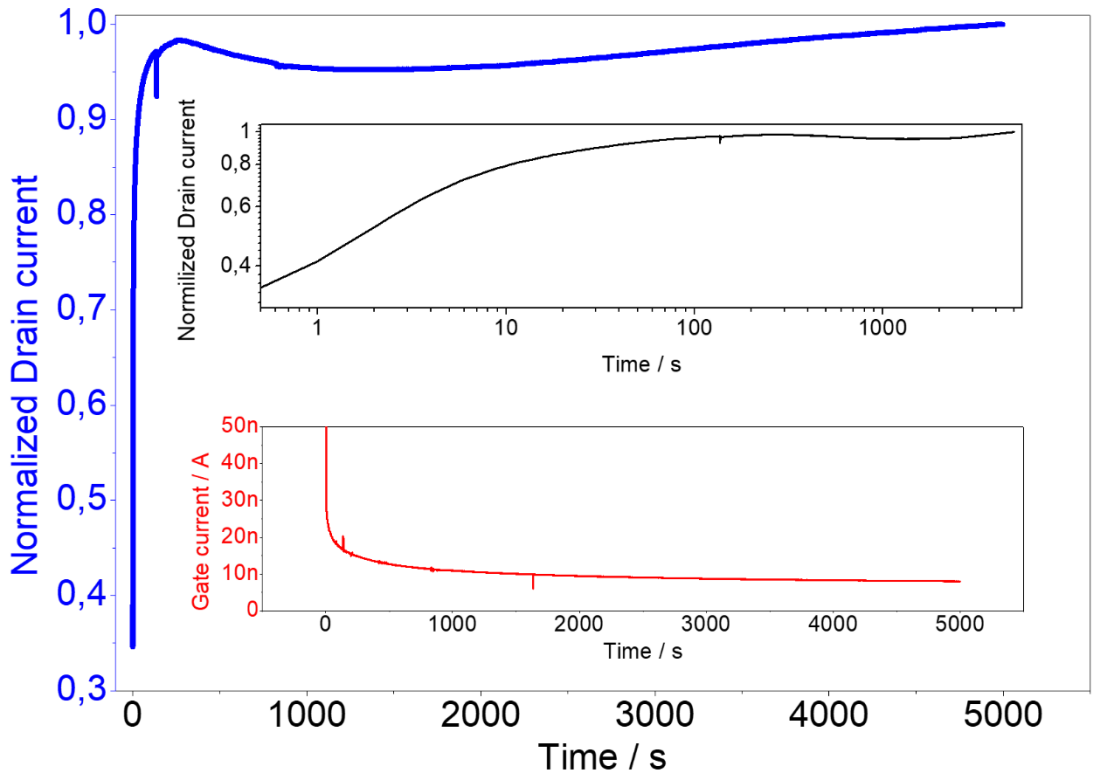

Figure 4-3: *Biosensing system with phosphate buffer saline solution at flow rate of 210 µL.min^{-1}: currents as a function of time at constant drain (-1.2 V) and gate bias (-0.7 V). The insets are the variation of the drain (upper panel in logarithmic plot) and gate (lower panel) current with time.*

The drain current, starting at about 35% of its maximum value, gradually increased to reach a maximum after 100 s and thus remained stable for up to 5000 s. A logarithmic

plot is presented in the upper panel of the inset of **Figure 4-3** showing a drift in the drain current of about 4% (between 500 s to 5000 s). Similarly, the gate current, decreased to reach 96% of its minimum value after 100 seconds (lower panel of the inset of **Figure 4-3**). While the drain current increased, that of the gate decreased and they plateaued simultaneously. Such a variation of the drain and gate currents may be correlated to the evolution of the electrical double layer structure. The drain current at t=0 was not null, thus the build-up of the electrical double layer was about few milliseconds, as a 500 ms was the time between two consecutive recorded drain current. While the electrical double layer build-up quickly, it required about 100 seconds to reach the maximum capacitance. This can be seen in the variation of the gate current as a function of time. If no electrochemical reaction takes place at the gate or the semiconductor interface with the electrolyte, I_{GS} is the resultant of the movement of ions from the electrolyte to the gate and the OS layer. The decrease of the gate current, therefore, means that the ionic movement in the electrolyte takes time. According to the current understanding of the operation of EGOFET[34, 10 and 9], these ions, become less mobile in the EDL and the capacitance increases with time. This increase of the capacitance induces an increase of the drain current over time as observed (inset upper panel of **Figure 4-3** from 0 to 100 s). Ultimately, the EDL capacitance reached steady state as the gate potential can not induces the addition of further ions, so the drain current plateaued with a small drift.

EGOFET biosensors can be multiparametric sensors[35]. In addition to the drain current, the other output parameters (e.g. μ.C, V_{th}) can be affected by chemical and biological events. To use these parameters in concert with the drain current for robust bio-detection it is vital to confirm their stability as a stable I_{DS} may not reflect a stable operating device. For instance, a decrease of drain current with time due to degradation of mobility could possibly be moved by a shift in the threshold voltage. Therefore, multiple I_{DS} vs V_{GS} curves, spaced with 1 min gate bias, were measured. The normalized I_{DS} vs V_{GS} obtained every 5 minutes and the evolution of I_{DS} (at gate bias of -1.2 V), V_{th} and μ.C are depicted in **Figure 4-4**.

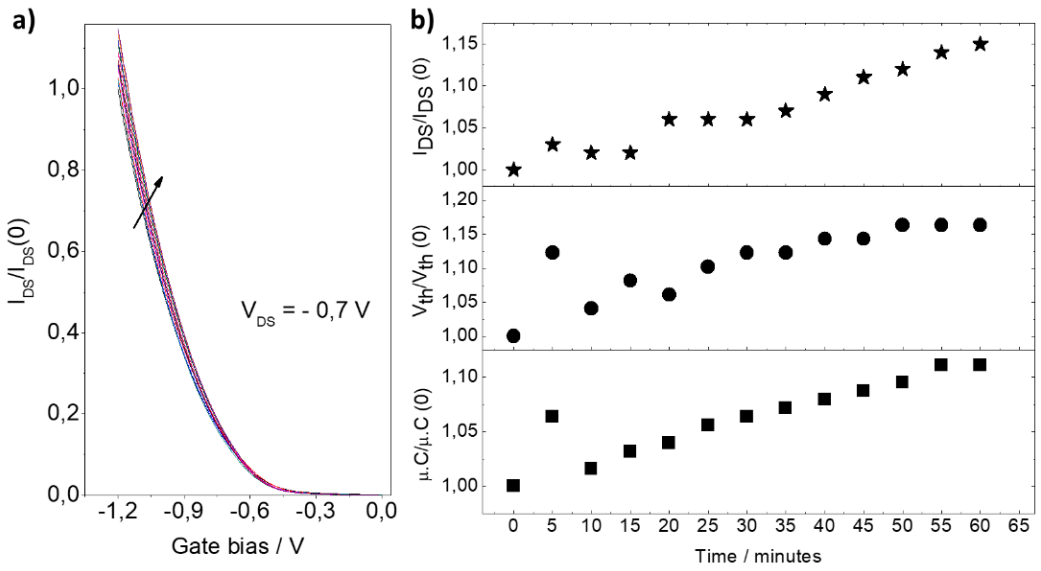

Figure 4-4: *Biosensing system with phosphate buffer saline solution at flow rate of 210 µL.min^{-1}: a) Normalized I_{DS} vs V_{GS} curves obtained every 5 minutes during bias stress measurement and b) evolution of I_{DS}/I_{DS} (0), V_{th}/V_{th} (0) and µ.C/µ.C (0) as a function of time. I_{DS} (0), V_{th} (0) and µ.C (0) are values extracted from the first I_{DS} vs V_{GS} measurement.*

The 4% drift of I_{DS} towards higher value seen in previous continuous current monitoring experiment (**Figure 4-3**) was equally present in the multiple I_{DS} vs V_{GS} sweep bias stress measurement (**Figure 4-4**). For the latter, the drift in I_{DS} at the maximum gate bias was about 15% (upper panel of **Figure 4-4.b**). In analysing the other figures of merit, it was found that V_{th} exhibited minor fluctuation while µ.C deflected by 10% to saturation (middle and bottom panel of **Figure 4-4.b**). A possible explain of these variations in the device figures of merit can be that gate bias can facilitate penetration of ions into the OS. These ions possibly change the distribution of charges in the OS leading to a variation of their mobility. However, the deflection of the figures of merit of the system were minor in the time scale of the experiment (**Figure 4-3** and **4-4**). The system is robust and reliable for 2 h continuous operation in flowing electrolyte condition.

4.3.2. Label-free detection of the hybridization of deoxyribonucleic acid (DNA)

4.3.2.1. *In operando* single parametric label-free detection of DNA hybridization

To demonstrate the utility of the developed system as point-of-care testing device, the detection of the hybridization of 100 nM of DNA was tested. A fully complementary target ssDNA (ssDNA-t) to the ssDNA-Cap immobilised on the device gate electrodes and a non-complementary ssDNA (ssDNA-nc) were selected as analytes to be added to the fluidic channel of the device. The ssDNA-t interacts specifically with the ssDNA-Cap by Watson and Crick base pairing events[36]. The ssDNA-nc was used as a negative control to evaluate the selectivity of the device for detection of DNA hybridization. The chemical

structure of ssDNA-Cap, ssDNA-t and ssDNA-nc can be found in **supporting information (Figure S4-1)**.

The sensing experiments were performed by using the characterisation set up depicted in **Figure 4-15** of **section 4.5.2**. The evolution of the drain current was measured as a function of time while changing from a flowing phosphate buffer saline solution (1x PBS) to a diluted ssDNA-t (100 nM) or ssDNA-nc (100 nM) in 1x PBS through the fluidic channel. For reference measurement, the commutation from 1x PBS to 1x PBS was also carried out. 1x PBS mimics the physiological fluids (pH of 7.4 for a salt concentration of 137 mM). The obtained currents were normalized (S_N) to the current obtained before change (I_{PBS}) using equation (4.2):

$$S_N = \frac{I_{ssDNA} - I_{PBS}}{I_{PBS}} \quad (4.2)$$

A clear difference in the S_N signal was observed, when the solution injected into the fluidic channel was switched from 1x PBS to 100 nM of ssDNA-t diluted in 1x PBS. S_N increased sharply, then gradually towards saturation (black curve in **Figure 4-5**). In comparison to the reference (blue curves) the change in S_N was 92% in about 25 seconds.

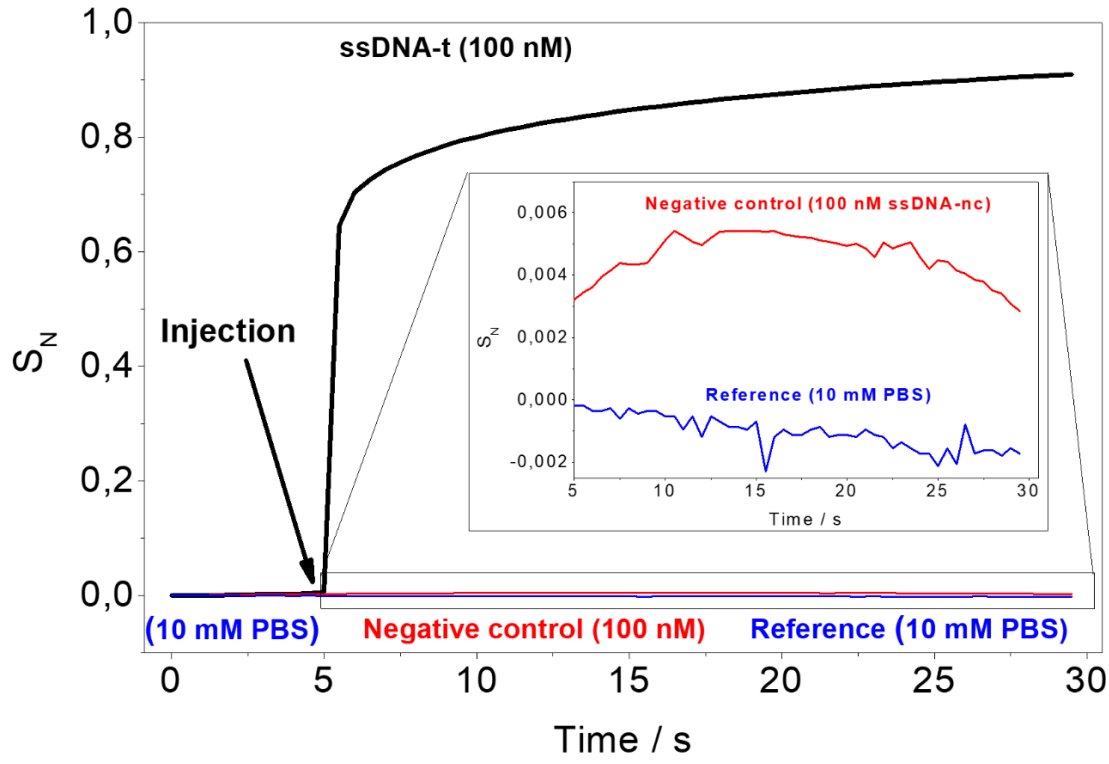

Figure 4-5: *In operando specific detection of the hybridization of ssDNA-t diluted in phosphate buffer saline solution (1x PBS) with ssDNA-Cap by the developed biosensing system. The flow rate of the analytes through the fluidic channels was 210 µL.min^{-1}. The arrow indicated the switching of the flow of 1x PBS to that of ssDNA-t, or ssDNA-nc or 1x PBS. The insert is the zoom in of the evolution of S_N when ssDNA-nc or 1x PBS was the analyte.*

It can be noticed that the flowing of ssDNA-nc, negative control, into the fluidic channel has a very small impact on S_N (red curve in **Figure 4-5**). The signal resembles a fluctuation of about 0.6% over time. Hence the system can specifically discriminate ssDNA-t from a non-complementary ssDNA.

As mentioned previously, the difference between ssDNA-nc and ssDNA-t is that the latter can interact with the ssDNA-Cap to form double helix DNA on the gate terminal of the device via Watson and Crick base pairing type. Such conformational change in the DNA structure on the gate can be the origin of the change of S_N on injection of ssDNA-t. The hybridization may induces an increase in the net negative charges (almost double) and a redistribution of dipoles orientation on the gate surface, which affects the devices figures of merit, namely the threshold voltage, capacitance and/or mobility to induce this decrease seen in the recorded drain current (**Figure 4-6**).

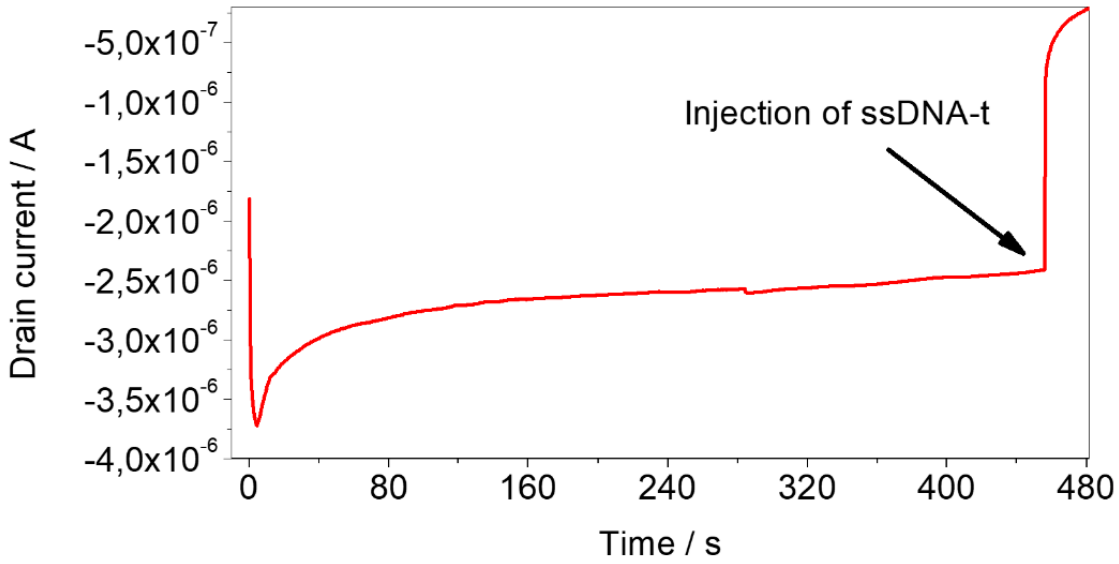

Figure 4-6: *In operando specific detection of the hybridization of ssDNA-t diluted in phosphate buffer saline solution (1x PBS) with ssDNA-Cap by the developed biosensing system. The flow rate of the analytes through the fluidic channels was 210 µL.min^{-1}. The arrow indicated the switching of the flow of 1x PBS to that of 100 nM ssDNA-t diluted in 1x PBS.*

4.3.2.2. Multiparametric label-free detection of DNA hybridization

To understand the changes in the drain current seen during *in operando* bio-detection, transfer characteristics were recorded before and after the experiment. This provided information on figures of merit that predominantly alter the S_N signal. Equally, it allows multiparametric sensing of bio interaction, which is one of the benefits of OFET based sensors[37]. **Figure 4-7** show typical transfer characteristics of 3 replicates from different devices before and after real-time sensing of the hybridization of 100 nM ssDNA-t with capturing probe on the gate terminal. Black curves, stand as reference, were recorded just

before the real-time experiments with 1x PBS flowing over the fluidic channel. The blue and red curves were measured straight after the saturation of the sensor response to the real-time detection of 100 nM ssDNA-t. The blue corresponds to the flowing of 100 nM ssDNA-t and the red is that of 1x PBS. Blue curves were measured 2 minutes prior to its corresponding red curves to check the effect of the presence ssDNA-t in the electrolyte on device performance after sensor saturation.

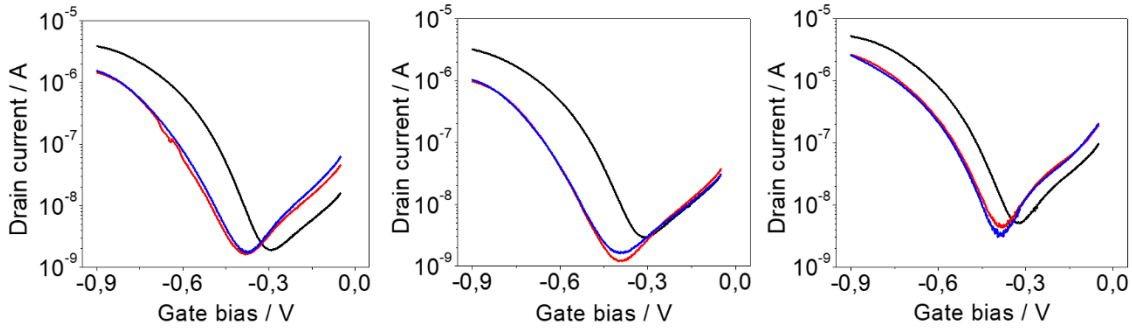

Figure 4-7: *Detection of the hybridization of 100 nM of ssDNA-t diluted in 1x PBS with ssDNA-Cap by the developed biosensing system: The flow rate of the analytes through the fluidic channels was 210 µL.min^{-1}. The curves are typical transfer curves from 3 different devices. The black curves were recorded just before real time detection of 100 nM ssDNA-t. The blue and red were measured straight after the saturation of the sensor response during real-time biodetection of ssDNA. The electrolyte for the black, blue and red curves were 1x PBS, 100 nM of ssDNA-t and 1x PBS, respectively.*

The on-state drain current of the blue curves, were reproducibly and significantly lower than that of the blank curves over 9 individual tested sensors in the array (3 EGOFETs/device). It drops from an initial value of 3.9 ± 0.8 µA to 1.5 ± 0.5 µA (**Table S4-3**). These results echo the drop in the current (increase of S_N signal) seen during *in operando* detection of DNA hybridization. A shift in V_{th} towards more negative gate bias, were equally noticed (from -0.433 ± 0.004 V to -0.505 ± 0.03 V). Note: The measured red curves (recorded drain currents after DNA hybridization with 1x PBS as electrolyte) were identical to the blue curves. This implied that the presence of up to 100 nM of ssDNA-t in the electrolyte, after hybridization of all available ssDNA-Cap on the gate, does not have any impact on the device response in flowing electrolyte condition. Equally, the bonding strength between the two DNA is strong enough to hold 2 minutes 1x PBS flowing through the fluidic channel.

It is clear that I_{DS} in concert with V_{th} are the predominant figures of merit that change while biorecognition happen in this device. This is predictable given the device structure. The gate terminals were considerably larger than the active layers (× 2). And it was coated with an mixture of self-assembled-monolayer of ssDNA-Cap plus MCH. This renders the gate terminal surface negative thanks to the SAMs. Logically, one could

expects the capacitance of the EDL at the gate to be considerably large. The bonding of ssDNA-t to the capturing ssDNA on the gate results in a conformational change of DNA on its surface. The impact of this is a negative shift of V_{th} as observed due to the increase of the energetic gap between the gate and the OS layer and a decrease of the drain current. Similar experience carried out with the negative control reinforces this explaination, as only a minor decrease of the drain current and a small shift of V_{th} toward positive gate bias were registered (**Figure 4-8**). Thus the system is selective as it discriminated the non-complementary DNA.

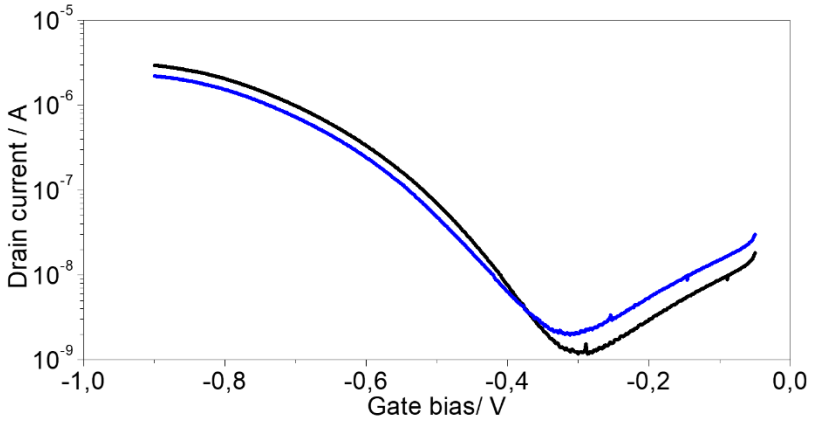

Figure 4-8: *A typical negative control response of the biosensor. The black curve is the reference (1x PBS) and the bleu is the negative control (100 nM of ssDNA-nc diluted in 1x PBS).*

For an EGOFET functionalised on the gate the shift in V_{th} observed on binding of the analyte reflects a change in the work function of the gate electrode and this is what dominates the sensing mechanism[15].

4.4. Conclusion

A label-free biosensor system consisting of an array of EGOFET integrated with a multichannel microfluidic platform was developed on a flexible substrate with a combination of facile techniques. The device achieved excellent electrical performance, and long-term operation stability under flowing 1x PBS electrolyte condition. The performances of the EGOFETs in the array were reproducible and repeatable on different substrates. The device utility in the field of biosensors and bioelectronics was demonstrated by reproducibly and reliably label-free detecting the hybridization of DNA in line under flowing electrolyte condition with good selectivity. The sensing relies on a shift on device threshold voltage due to the change in gate electrode work function up on DNA hybridization. The time for assay-to-results was about 30 seconds, and thus was fast in comparison to conventional techniques such as DNA Enzyme-linked Immunosorbent assay (ELISA) kits (~1 h). The errors in the measured figures of merit was, similar to

DNA ELISA kits, less than 15%. The design of the device will allow detection of multiple analytes if specific receptors to the molecules of interest are immobilised on individual gate electrodes in the array. Equally, the developed technology can be integrated with other systems for applications in healthcare, environment monitoring, homeland defence as an in-line high-throughput point-of-care testing tools.

4.5. Methods

4.5.1. Materials

Teijin DuPont film Co. Ltd. provided 125 μm thick poly(ethylene 2,6-naphthalate) (PEN) foils and platfix CS2325NA4 adhesive. Silicon wafers and Shipley 1805 photoresist were obtained from the Manchester Centre for Mesoscience & Nanotechnology (CMN). Diketopyrrolopyrrole-alt-5,5-(2,5-di(thien-2-yl)thieno[3,2-b]thiophene] (DPPDTT, Mw 399 066 and Mn ~68 100) was obtained from Dr D. Tate and directly used without further purification. Polymethylmethacrylate (PMMA) sheet (3 mm thick), double sided tape (280 μm thick) were purchased from 3M (number 7961MP), and stainless-steel tube from Tomlinson Tube & Instruments Ltd. Stopcock 3-way male lock was purchased from Cole-Parmer Instrument Company Ltd. Deoxyribonucleic acid (capture, target and probe), 1x PBS, DL-dithiothreitol (DTT), 1,2-dichlorobenzene, dimethyl sulfoxide, and all others solvents were purchased from Sigma-Aldrich.

4.5.2. Fabrication of the system

4.5.2.1. Defining source, drain and gate electrodes on PEN substrates

An array of Au (40 nm) interdigitated source and drain electrodes were patterned by a Shipley 1805 photoresist (S1805) direct laser lithography process on a polyethylene naphthalate substrate (PEN). The process is detailed in the experimental section of **Chapter 3**. The interfinger distance was 60 μm (channel length) and their perimeter was 16000 μm (channel width). The array consists of 16 interdigitated drains and sources. Each drain has its own contact path. The sources were connected four by four to a contact path.

The same procedure used to pattern the source drain electrodes was employed to define an array of gate electrodes onto another PEN substrate that was stuck on to a 3 mm thick PMMA sheet with a double-sided tape (280 μm). The array of gate electrode consists of 16 of 1 mm^2 Au connected four by four to a contact path. CO_2 laser (100 W, 10 $mm.s^{-1}$) was used to cut 8 holes of diameters of 1.4 mm at the edged on the gate electrode array

substrate. And stainless-steel tubes were inserted into these holes (Length of about 5 mm and a radius of 0.7 mm) to serves as analyte inlet and outlet. Note: the contact paths were designed to connect the device to external circuit via zero-insertion force connectors mounted onto printed circuit boards. Also, 5 nm chromium layer was used as an adhesion promoter of Au to the PEN (**Figure 4-9**).

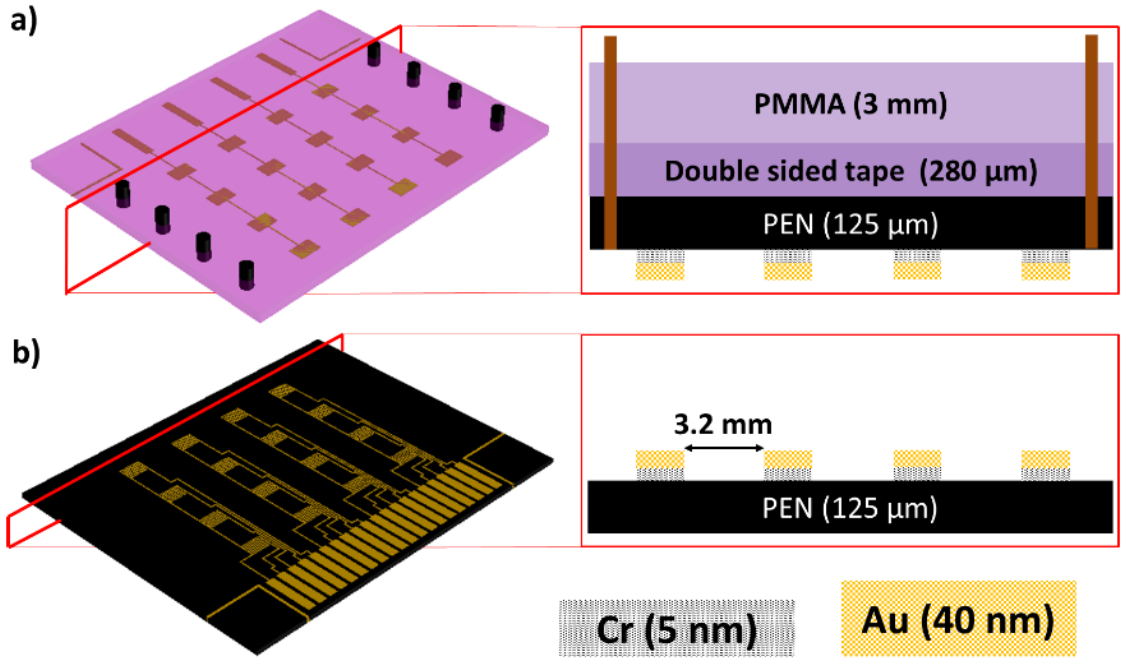

Figure 4-9: *3D AutoCAD model of the a) bottom and c) top cover of the system and a zoom (not in scale) of the corresponding cross section view (brown lines represent the stainless-steel tubing for inlet and outlet with diameter of 1.4 mm).*

4.5.2.2. Deposition of the active layer and generation of fluidic channels

The bottom cover, PEN substrate with patterned source drain electrode were sonicated in acetone and then isopropanol for 5 minutes in each. The substrate was then blown dry with a stream of nitrogen and exposed to UV/O_3 for 15 minutes to remove organic contaminant. At the same time a 8 mg.ml^{-1} solution of poly(diketopyrrolo-pyrrole-dithiophene-thienothiophene) (DPPDTT) was prepared. Note: the solution was heated at 130 °C for at least 1 h to obtain a polymer solution without visible aggregates. The freshly prepared DPPDTT solution was spin-coated at 1500 rpm for 2 minutes on the UV/O_3 treated substrate and annealed at 140 °C for 40 minutes to fully dry the film. Double-sided tape was laser cut (CO_2 laser) to define 4 fluidic channels. The length, width and thickness of the channel are respectively 25362 µm, 1600 µm and 280 µm (~11.4 µL). The double-sided tape was mounted onto the substrate under a binocular microscope with a tweezer. The edges of the substrate and that of the double-side tape were used to get the best possible alignment of the fluidic channels with the interdigitated electrodes. Note:

each fluidic channel contains 4 IDE source and drain electrodes covered with DPPDTT (**Figure 4-10**).

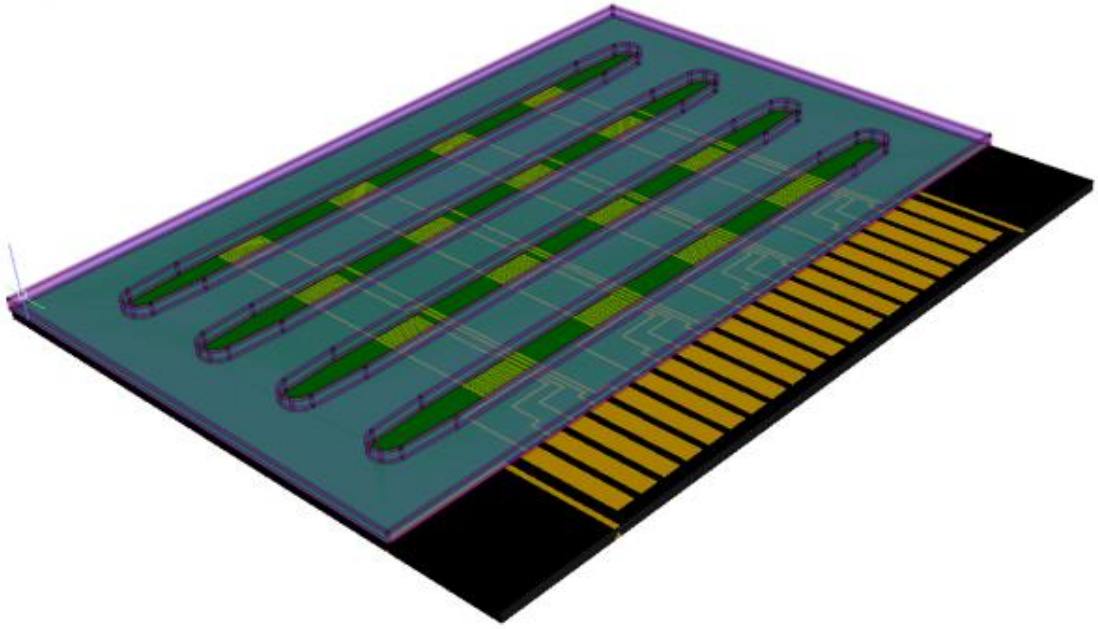

Figure 4-10: *3D AutoCAD model of the source/drain electrode array substrate covered with DPPDTT (green) including double sided tape with 4 fluidic channels.*

4.5.2.3. Bio-functionalisation of the gate electrodes with self-assembled monolayers and assembly of the system

The 16 gate electrodes on the top cover were functionalised with a self-assembled monolayer of thiol-terminated single stranded DNA and 6-mercaptohexanol (MCH). This was conducted by taking, a 100 μM solution of [ThiC6] TTA GTT CTC CAG CTA TCT T diluted in 1x PBS (0.01 M phosphate buffer, 0.0027 M potassium chloride and 0.137 M sodium chloride in deionized water, pH 7.4, at 25 °C) and mixing it with DL-dithiothreitol (15 $mg.ml^{-1}$). This solution was left to stand for 10 minutes at room temperature to form thiol-terminated single strand capturing DNAs (ssDNA-Cap) via the reduction of the disulphide bonds (**Figure 4-11**).

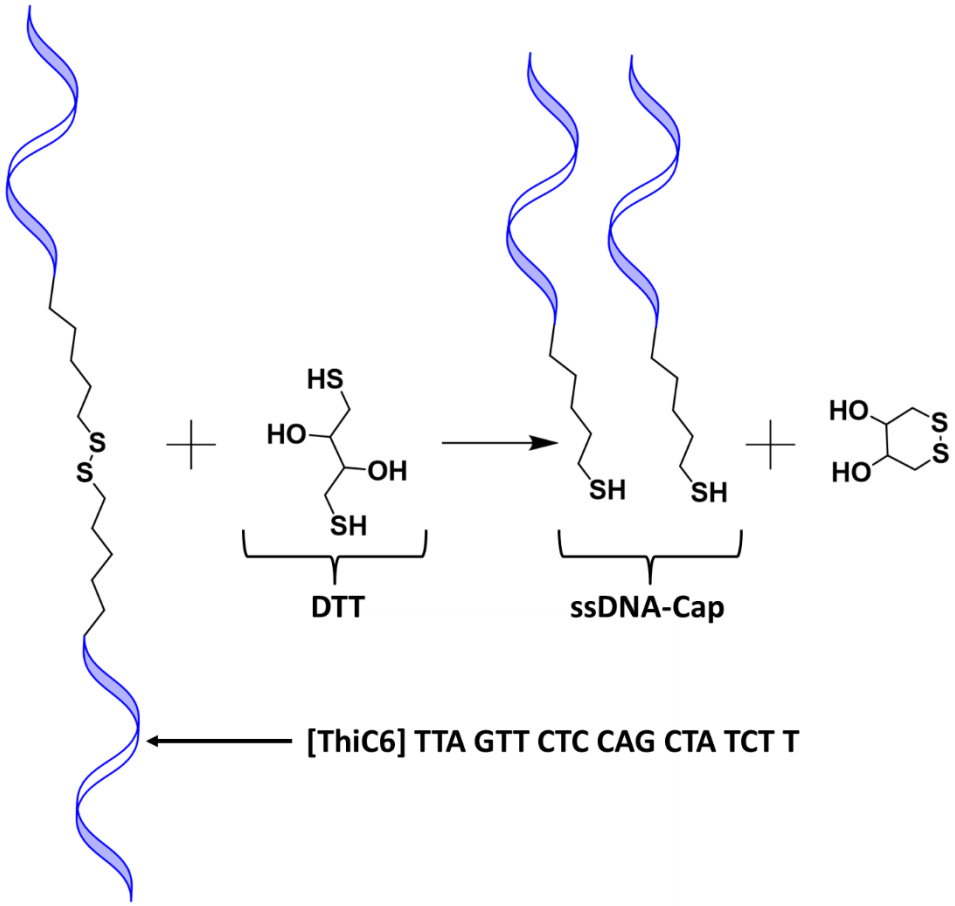

Figure 4-11: *Reduction of disulphide bond of [ThiC6] TTA GTT CTC CAG CTA TCT T by DL-dithiothreitol (DTT) to obtain capturing single stranded DNA (ssDNA-Cap)*

The obtained solution was desalted with an Illustra Microspin G25 column (following the supplier protocol: Sigma Aldrich) and diluted in 1x PBS to produce 1 µM ssDNA capturing solution. At the same time, a 1 mM solution of 6-mercaptohexanol in a mixture of dimethyl sulfoxide (DMSO) with 1x PBS (9:1 ratio) was prepared. The gate electrodes were covered with the prepared solution contained 1 µM of ssDNA-Cap for 1 h. The gate was then flushed three times with 1x PBS to remove non-bonded ssDNA-Cap and subsequently covered with the solution of 6-mercaptohexanol for 1 h. The gate electrode was further flushed (× 3) with 1x PBS and blown dry under a stream of nitrogen. Note: prior to the incubations, the gate electrode was subject to 10 minutes UV/O_3, technique that remove organic contaminants by converting them to volatile substance (e.g. carbon dioxide, nitrogen). The 6-mecaptohexanol was used to fill the void left by the ssDNA-Cap to minimise nonspecific binding of substance onto the gate (**Figure 4-12**).

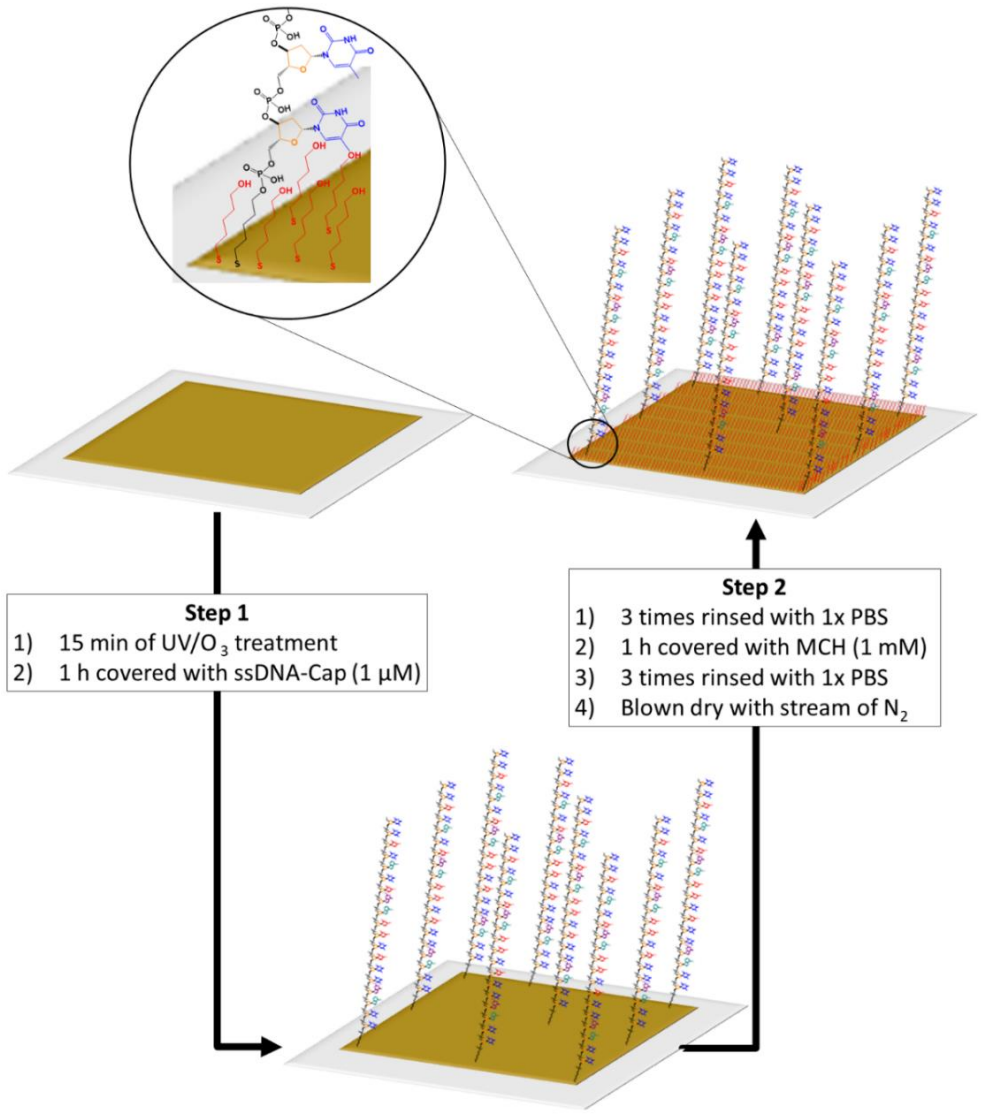

Figure 4-12: *Bio-functionalization of individual gate electrode (dark yellow) on PEN (dark white) with a mixture of self-assembled monolayer of ssDNA-Cap and MCH in two steps. After step 1, a SAM of ssDNA-Cap form on the gate electrode and after step 2 MCH fill the space left on the gate electrode. A zoom in showing the proportion between MCH (red) and ssDNA-Cap.*

The system was completed by sealing the bottom cover (**Figure 4-9**) with the top cover so that the area of bio-functionalized gate electrodes was inside the flow cells and in front of its corresponded contact IDE (**Figure 4-13**). Note assembly was carried out under a binocular microscope by hand.

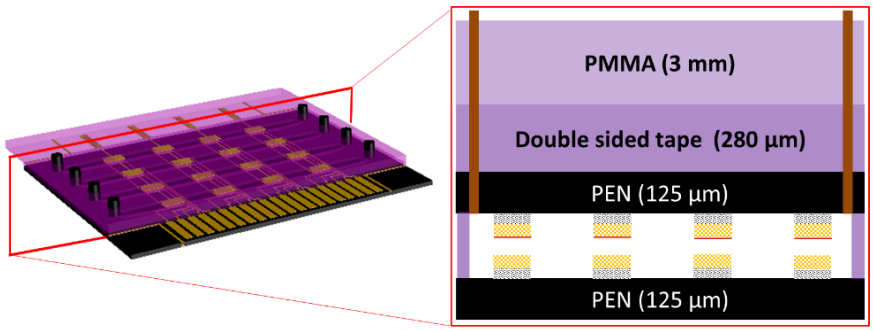

Figure 4-13: *3D AutoCAD model of the system and a zoom (not in scale) of its cross-section view (brown lines represent the hypodermic tubing for inlet and outlet).*

4.5.3. Characterisation of the system

4.5.3.1. Measurement of the device electrical performance.

The output and transfer characteristics of the EGOFETs were measured under continuous flow (210 µl.min^{-1}) of 1x PBS through the microfluidic cell using a semiconductor parameter analyzer (Agilent B1500A). For the transfer characteristic, the drain current (I_{DS}) was recorded as a function of the gate voltage (V_{GS}) (swept from - 0.05 V to - 0.9 V in steps of 0.001 V in forward and reverse direction) at a constant drain voltage (V_{DS} = - 0.7 V). For the output characteristic, I_{DS} was measured at constant V_{GS} while sweeping the V_{DS} from 0 V to - 0.7 V with an increment of 0.001 V. For the measurement of device stability, the drain current was recorded as a function of time at a constant V_{GS} (- 1.2 V) and V_{DS} (- 0.7 V) while 1x PBS was flowed through the flow cell at 210 µl.min^{-1}. The characterisation set up is illustrated in **Figure 4-14**.

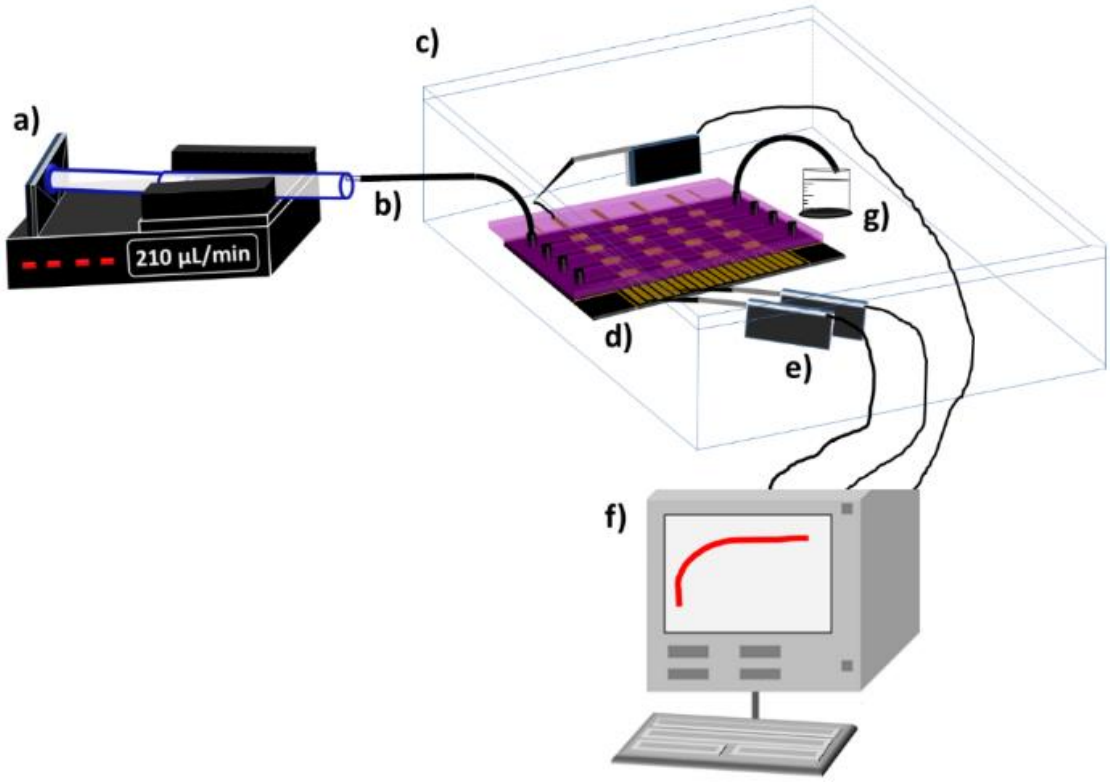

Figure 4-14: *Schematic illustration of the characterisation setup used to measure the electrical performance reproducibility, repeatability and stability of the system showing: a) syringe pump, b) tubing c) Faraday cage, d) the system, e) three probe station wired to f) an Agilent 1500B and g) a waste collector.*

4.5.3.2. Electrical measurement of the interaction between ssDNA.

Two syringe pumps (with adjustable speed) were equipped with two 12 ml syringes. One syringe was filled with 1x PBS and the other with a solution of either a target ssDNA-t ([Btn] AAG ATA GCT GGA GAA CTA A) or a non-complementary ssDNA-nc ([Btn] AGT CTT TCA GTA GGT TCA C)) diluted in 1x PBS or 1x PBS. The syringes were

coupled to a three-way stopcock. First 1x PBS was pumped into the flow cell at a rate of 210 µl.min^{-1} and the transfer curves were measured three-times in order to confirm that the current was stable. Then, the drain current was recorded over time at a constant V_{DS} (- 0.7 V) and V_{GS} (- 0.9 V) while 1x PBS was flowed through the channel. When the current was stable, the valve of the three-way stopcock was switched in order to inject the solution of the ssDNA (target or non-complementary strand) diluted in 1x PBS or 1x PBS into the flow cell and the current recorded. The transfer characteristic of the EGOFET was recorded after the transient measurement using the diluted ssDNA solution and 1x PBS after 2 minutes. The characterisation set up is illustrated in **Figure 4-15**.

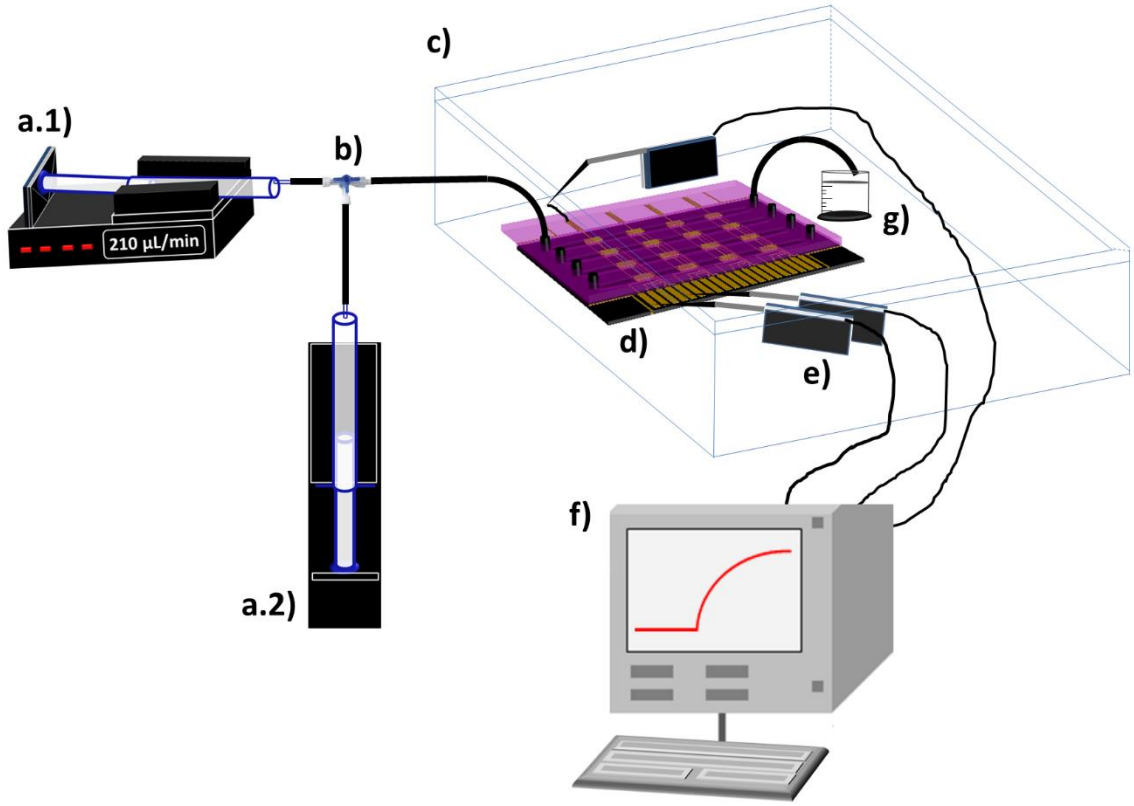

Figure 4-15: *Schematic illustration of the characterisation setup used to measure biomolecule interaction showing: (a.1 – a.2) syringe pumps (one filled with 1x PBS and the second with either 1x PBS, ssDNA-t or ssDNA-nc or 1x PBS, b) three way stopcock including tube to switch between the analyte c) Faraday cage, d) the system, e) three probe station wired to f) an Agilent 1500B and g) a waste collector.*

Acknowledgment

I would like to acknowledge CDT Ltd and EPSRC for generous financial support and Dr D. Tate for supplying DPPDTT.

References

1. Vashist, S. K., Luppa, P. B., Yeo, L. Y., Ozcan, A. & Luong, J. H. T. Emerging Technologies for Next-Generation Point-of-Care Testing. *Trends Biotechnol.* **33,** 692–705 (2015).

2. Rodriguez-Mozaz, S., Alda, M. J. L. De, Marco, M. P. & Barceló, D. Biosensors for environmental monitoring: A global perspective. *Talanta* **65,** 291–297 (2005).

3. Zhang, D. & Liu, Q. Biosensors and bioelectronics on smartphone for portable biochemical detection. *Biosens. Bioelectron.* **75,** 273–284 (2016).

4. Lee, Y. H., Jang, M., Lee, M. Y., Kweon, O. Y. & Oh, J. H. Flexible Field-Effect Transistor-Type Sensors Based on Conjugated Molecules. *Chem* **3,** 724–763 (2017).

5. Torsi, L., Magliulo, M., Manoli, K. & Palazzo, G. Organic field-effect transistor sensors: A tutorial review. *Chem. Soc. Rev.* **42,** 8612–8628 (2013).

6. Zang, Y., Huang, D., Chong-an, D. & Zhu, D. Device Engineered Organic Transistors for Flexible Sensing Applications. *Adv. Mater.* **28,** 4549–4555 (2016).

7. Di, C. A., Zhang, F. & Zhu, D. Multi-functional integration of organic field-effect transistors (OFETs): Advances and perspectives. *Adv. Mater.* **25,** 313–330 (2013).

8. Cramer, T., Campana, A., Leonardi, F., Casalini, S., Kyndiah, A., Murgiaa, M. & Biscarinia, F. Water-gated organic field effect transistors – opportunities for biochemical sensing and extracellular signal transduction. *J. Mater. Chem. B* **1,** 3728 (2013).

9. Kergoat, L., Piro, B., Berggren, M., Horowitz, G. & Pham, M. C. Advances in organic transistor-based biosensors: From organic electrochemical transistors to electrolyte-gated organic field-effect transistors. *Anal. Bioanal. Chem.* **402,** 1813–1826 (2012).

10. Wang, D., Noël, V. & Piro, B. Electrolytic Gated Organic Field-Effect Transistors for Application in Biosensors—A Review. *Electronics* **5,** 9 (2016).

11. Nguyen, T. T. K., Tran, H. V., Vu, T. T., Reisberg; S., Noël, V., Mattana, G., Pham; M. C. & Piro, B. Peptide-modified electrolyte-gated organic field effect transistor. Application to Cu^{2+} detection. *Biosens. Bioelectron.* **127,** 118–125 (2018).

12. Zhang, Q., Leonardi, F., Casalini, S. & Mas-Torrent, M. Mercury-Mediated Organic Semiconductor Surface Doping Monitored by Electrolyte-Gated Field-Effect Transistors. *Adv. Funct. Mater.* **27,** 1703899 (2017).

13. Schmoltner, K., Kofler, J., Klug, A., List-Kratochvil & J.W., E. Electrolyte-gated organic field-effect transistor for selective reversible ion detection. *Adv. Mater.* **25,** 6895–6899 (2013).

14. Diaccia, C., Berto, M., Di Lauro, M., Bianchini, E. & Pinti, M. Label-free detection of interleukin-6 using electrolyte gated organic field effect transistors. *Biointerphases* **12,** 05F401 (2017).

15. Macchia, L., Manoli, K., Holzer, B., Di Franco, C., Ghittorelli, M., Torricelli, F., Alberga, D., Mangiatordi, G., F., Palazzo, G., Scamarcio, G. & Torsi, L. Single-molecule detection with a millimetre-sized transistor. Nat. Commun. 9, 1–10 (2018).

16. Seshadri, P., Manoli, K., Schneiderhan-Marra, N., Anthes, U., Wierzchowiec, P., Bonrad, K., Di Franco, C. &Torsi, L. Low-picomolar, label-free procalcitonin analytical detection with an electrolyte-gated organic field-effect transistor based electronic immunosensor. Biosens. Bioelectron. 104, 113–119 (2018).

17. Kergoat, L., Piro, P., Berggren, M., Pham, M., Yassar, A. & Horowitz, G. DNA detection

with a water-gated organic field-effect transistor. Org. Electron. 13, 1–6 (2012).

18. Li, J., Zhao, Y., Tan, H. S., Guo, Y., Di, C-A., Yu, G., Liu, Y., Lin, M., Lim, S. H., Zhou, Y., Su, H. & Ong, B. S. A stable solution-processed polymer semiconductor with record high-mobility for printed transistors. *Sci. Rep.* **2,** 1–9 (2012).

19. Xinran Zhang, X., Richter, L. J., DeLongchamp, D. M., Kline, R. J., Hammond, M. R., McCulloch, I., Heeney, M., Ashraf, R. S., Smith, J. N., Anthopoulos, T. D., Schroeder, B., Geerts, Y. H., Fischer, D. A. & Toney, M. F. Molecular Packing of High-Mobility Diketo Pyrrolo-Pyrrole Polymer Semiconductors with Branched Alkyl Side Chains. *J. Am. Chem. Soc.* **133,** 15073–15084 (2011).

20. Magliulo, M., Mallardi, A., Mulla, M. Y., Cotrone, S., Pistillo, B. R., Favia, P., Vikholm-Lundin, I., Palazzo, G., Torsi, L. Electrolyte-gated organic field-effect transistor sensors based on supported biotinylated phospholipid bilayer. *Adv. Mater.* **25,** 2090–2094 (2013).

21. Gebala, M. & Schuhmann, W. Controlled orientation of DNA in a binary SAM as a key for the successful determination of DNA hybridization by means of electrochemical impedance spectroscopy. *ChemPhysChem* **11,** 2887–2895 (2010).

22. Herne, T. M. & Tarlov, M. J. Characterization of DNA probes immobilized on gold surfaces. *J. Am. Chem. Soc.* **119,** 8916–8920 (1997).

23. Levicky, R., Herne, T. M., Tarlov, M. J. & Satija, S. K. Using self-assembly to control the structure of DNA monolayers on gold: A neutron reflectivity study. *J. Am. Chem. Soc.* **120,** 9787–9792 (1998).

24. Strobel, M. & Lyons, C. S. An Essay on Contact Angle Measurements. *Plasma Process. Polym.* **8,** 8–13 (2011).

25. YuanT, Y. & Lee, R. *Contact Angle and Wetting Properties*. (Springer, Berlin, Heidelberg, 2013).

26. Peterlinz, K. A., Georgiadis, R. M., Herne, T. M. & Tarlov, M. J. Observation of Hybridization and Dehybridization of Thiol-Tethered DNA Using Two-Color Surface Plasmon Resonance Spectroscopy. *J. Am. Chem. Soc.* **119,** 3401–3402 (1997).

27. Urasinska-Wojcik, B., Cocherel, N., Wilson, R., Burroughes, J., Opoku, J., Turner, M. L. & Majewski, L. A. 1 Volt organic transistors with mixed self-assembled monolayer/Al2O3 gate dielectrics. *Org. Electron.* **26,** 20–24 (2015).

28. Ahmed, R., Sams, M., Simbrunner, C., Ullah, M., Rehman, K., Schwabegger, G., Sitter, H. & Ostermann, T. Reproducibility and stability of C60 based organic field effect transistor. *Synth. Met.* **161,** 2562–2565 (2012).

29. Horowitz, B. G. Organic Field-Effect Transistors. *Adv. Mater.* **10,** 365–377 (1998).

30. Casalini, S., Leonardi, F., Cramer, T. & Biscarini, F. Organic field-effect transistor for label-free dopamine sensing. *Org. Electron.* **14,** 156–163 (2013).

31. Lago, N., Buonomo , M., Imran, S., Bertani, R., Wrachien, N., Bortolozzi, M., Pedersen, M. G. & Cester, A. TIPS-Pentacene as Biocompatible Material for Solution Processed High-Performance Electronics Operating in Water. IEEE Electron Device Lett. 39, 1401–1404 (2018).

32. Porrazzo, R., Luzio, A., Bellani, S., Bonacchini, G. E., Noh, Y-Y., Kim, Y-H., Lanzani, G., Antognazza, M. R. & Caironi, M. Water-Gated n-Type Organic Field-Effect Transistors for Complementary Integrated Circuits Operating in an Aqueous Environment. *ACS Omega* **2,** 1–10 (2017).

33. Zhang, Q., Leonardi, F., Casalini, S., Temiño, I. & Mas-Torrent, M. High performing solution-coated electrolyte-gated organic field-effect transistors for aqueous media operation. *Sci. Rep.* **6,** 1–10 (2016).

34. Kim, S. H., Hong, K., Xie, W., Lee, K. H., Zhang, S., Lodge, T. P., Frisbie, C. D. Electrolyte-gated transistors for organic and printed electronics. *Adv. Mater.* **25,** 1822–1846 (2013).

35. Berto, M., Diacci, C., D'Agata, R., Pinti, M., Bianchini, E., Di Lauro, M., Casalini, S., Cossarizza, A., Berggren, M., Simon, D., Spoto, G., Biscarini, F. & Bortolotti, C., A. EGOFET Peptide Aptasensor for Label-Free Detection of Inflammatory Cytokines in Complex Fluids. Adv. Biosyst. 2, 1700072 (2017).

36. Donohue, J. & Trueblood, K. N. Base pairing in DNA. *J. Mol. Biol.* **2,** 363–371 (1960).

37. Das, A., Tyagi, A. K., Grell, M., Richardson, T. H. & Turner, M. L. Multiparameter OFET sensor at low power. in *Proceedings of the International Conference on Nanoscience, Engineering and Technology, ICONSET 2011* 500–504 (IEEE, 2011).

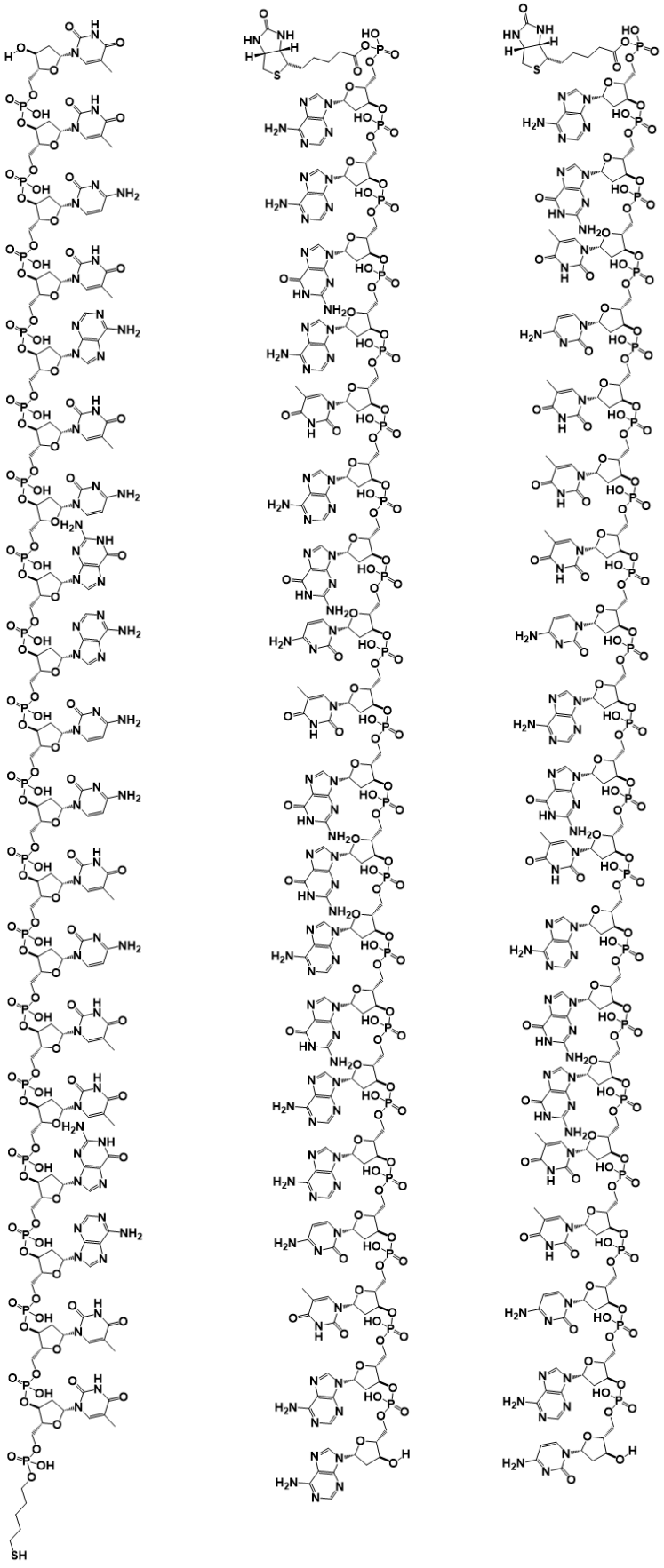

Figure S4-1: *Chemical structure from left to right of ssDNA-Cap, ssDNA-t and ssDNA-nc*

	Control	ssDNA
Water contact angle	49° ± 1°	39.1° ± 0.3°

Table S4-1: *Water contact angle of a clean gate (Au), after incubation in phosphate buffer saline solution (1x PBS) with 100 nM of ssDNA-Cap (ssDNA) or without (control). Standard deviations were obtained from 3 successive measurement.*

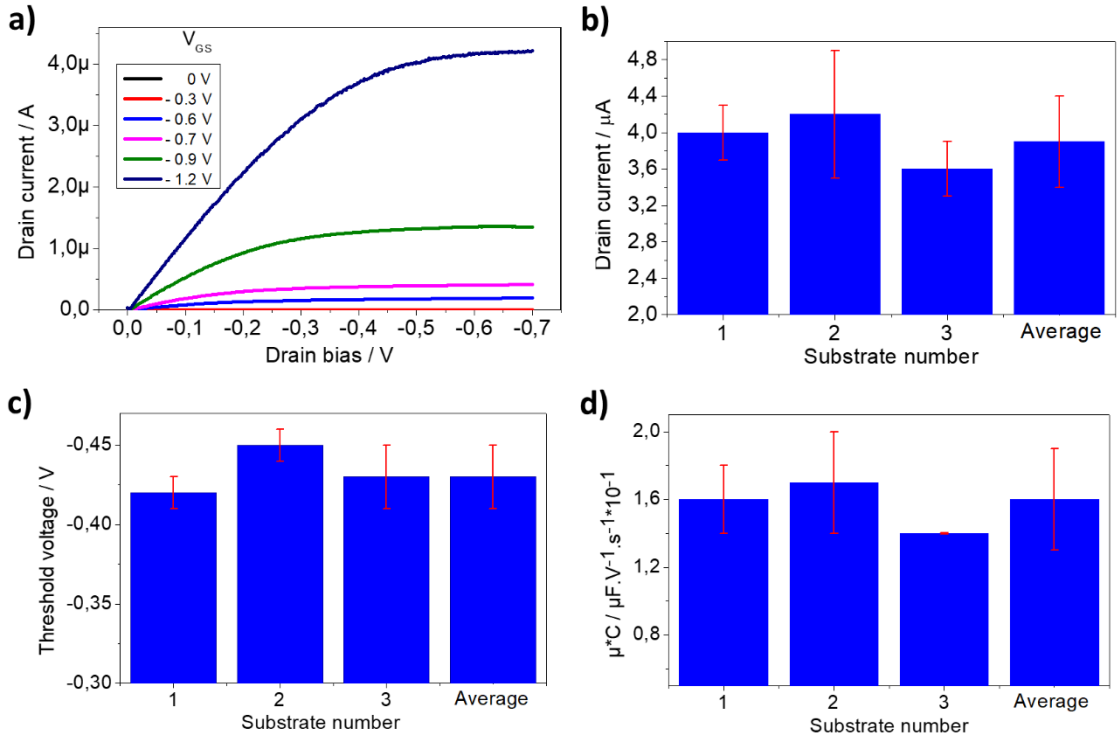

Figure S4-2: *a) Typical output curve of the system. Average device figures of merit (12 per substrate), namely in b) drain current at -0.9 V gate bias, b) V_{th} threshold voltage and c) normalized transconductance (µ.C).*

	Min	Average	Max
I_{DS} (V_{GS} =-0.9 V) / µA	2.9	3.9 ± 0.5	5.2
I_{on}/I_{off} × 10^3	0.6	1.5 ± 0.7	3
V_{th} / V	-0.39	-0.43 ± 0.02	-0.47
µ × C / µF.V^{-1}.s^{-1}	0.13	0.16 ± 0.03	0.23

Table S4-2: *Figures of merit obtained from 3 replicates of the biosensing systems with 1x PBS flowing through the fluidic channel at the rate of 210 µL.min^{-1}.*

	I_{DS} (V_{GS} =-0.9 V) / µA	V_{th} / V
1x PBS (before DNA hybridization)	3.9 ± 0.8	-0.433 ± 0.004
1x PBS (After DNA hybridization)	1.5 ± 0.5	-0.505 ± 0.030

Table S4-3: *Average drain current at maximum gate bias (-0.9 V) and threshold voltage obtained from the biosensing device with standard deviations over 9 replicates obtained before and after DNA hybridization on the gate electrode surface.*

Blank page

Chapter 5: Electrolyte-Gated Organic Field-Effect Transistor Array with Printed DPPDTT Semiconducting Polymer.

Contributors: ***A. Doumbia****, J. Tong and M. L. Turner.*

Authors contributions:

M. L. Turner and ***A. Doumbia*** *conceived the presented idea.* ***A. Doumbia*** *technically leads the project: designed, planned, carried out the experiments, and collected and analysed the data. J. Tong assisted* ***A. Doumbia*** *during AFM and optical microscope data recording. All authors discussed the results.* ***A. Doumbia*** *took the lead in writing the manuscripts (M. L. Turner provided critical feedback).*

5.1. Abstract

Electrolyte-Gated Organic Field-Effect Transistors (EGOFETs) are attracting a great deal of interest for application in bioelectronics. In this field the fabrication of stable arrays of EGOFETs produced *en masse* with minimal devices crosstalk exhibiting reproducible high performance is crucial for realistic applications. In this contribution a reliable EGOFET array with a patterned conducting channel is demonstrated by µ-dispensing poly[2,5-(2-octyldodecyl)-3,6-diketopyrrolopyrrole-alt-5,5-(2,5-di(thien-2-yl)thieno [3,2-b]thiophene)] (DPPDTT) into pre-fabricated wells at a speed of 3 mm.s^{-1} on a thin and flexible poly(ethylene 2,6-naphthalate) (PEN) (125 µm) support. Uniform device performance (µ ~0.13 $cm^2.V^{-1}.s^{-1}$, I_{on}/I_{off} ~10^2) was obtained with a tungsten needle acting as the gate. Replacement of tungsten with gold as the gate electrode resulted in a shift on the device threshold voltage by about 0.4 V and a three-fold increase in I_{on}/I_{off}. Integration of a microfluidic platform with the array of EGOFET, enabled devices to continuously operate for over 40 minutes in flowing electrolyte conditions. The degradation of figures of merit, namely on-state drain current, threshold voltage and normalized transconductance were respectively 8%, 18% and 11% after 40 minutes bias stress measurement under flowing electrolyte conditions. The reproducibility, stability and mobility were comparable to current state-of-art and showed that reliable high performance EGOFET arrays can be produced with a roll to roll compatible *en masse* solution deposition technique, namely µ-dispensing.

5.2. Introduction

Bioelectronics is a growing research area at the interface of physics, chemistry, materials science, biology, and electrical engineering. It offers new or improved technologies and methodologies that can improve the healthcare sector[1 and 2]. An important device for this burgeoning research area is the Electrolyte-Gated Organic Field-Effect Transistor (EGOFET)[3 and 4]. This is an organic transistor with a droplet of electrolyte acting as the gate insulator. Generally, an ion impermeable organic semiconductor is employed to allow the formation of electrostatic electrical double layers upon biasing the gate and drain terminals (source grounded). These EDLs, at interfaces of the conducting channel and the gate terminal with the electrolyte, produce an electrostatic interfacial capacitance, in the order of $\mu F/cm^2$, that permits a large current modulation below one volt[5]. Note: the bias applied at the terminal has to be within the electrochemical stability window of the semiconductor for pure field-effect carrier transport.

The attractiveness of the EGOFET device originates from the coupling of technical advantages of OFET (*e.g.* signal amplification, acting as an electronic switch, miniaturization, and integration with the other electronics systems, high interface sensitivity) with the use of aqueous media as the electrolyte. EGOFET has already been developed and used for biosensing[6], triggering drug administration[7] as well as biological phenomenon stimulation and recording[8 and 9].

To deliver the technology for the desired niche markets, *en masse* fabrication of uniform high-performance EGOFET arrays (for high-throughput) with minimal device crosstalk and stable, long-term operation is crucial. Device crosstalk is an issue observed in organic electronic systems including OFET[10]. When an OFET is in an array and the conducting channels are interconnected, the electrode of one transistor may act as the second source or gate of the nearest devices leading to an alteration of its electrical figures of merit. This interference between devices can be reduced via the patterning of the conducting channel[11 and 12]. Among a range of techniques that exists to effectively pattern functional materials, drop on demand (DoD) printing is very promising[13 and 14]. In addition to directly deposited patterns of materials from solution, it minimizes the processing time, cost and facilitates *en masse* device production.

Recently, poly(diketopyrrolo-pyrrole- dithiophene- thienothiophene) (DPPDTT) as a low bandgap donor-acceptor polymeric semiconductor has attracted a great degree of attention. This polymer utilised in an OFET has shown a mobility exceeding 1 $cm^2.V^{-1}.s^{-1}$ with high reproducibly and good air and bias stability[15]. It has been demonstrated that such a polymer can perform well in EGOFET with at least two hours of continuous operation stability[16].

Herein, a reliable EGOFET array with printed DPPDTT acting as the conducting channel is demonstrated. Initially, devices were fabricated in the droplet gate configuration to evaluate the electrical performance reproducibility with water acting as the gate insulator. Then, a microfluidic cell was integrated into the device and the long-term operation under a flowing electrolyte was assessed.

5.3. Results

A schematic representation of the cross-sectional view of the device can be seen in **Figure 5-1**. It consists of poly(ethylene 2,6-naphthalate) (PEN) foils (125 µm thick) substrate on which gold (40 nm) interdigitated source and drain electrodes were patterned via direct laser lithography (DLL). Note: a thin layer of chromium (5 nm) was inserted between the gold and the substrate to promote adhesion. Over the interdigitating area, a window in a spin-coated Shipley 1805 photoresist (~300 nm deep) film was generated via DLL (See experimental section for more details). Similar substrates were provided by Cambridge Display Technology Ltd. On these substrates the window over the interdigitating area of the source drain electrode was made of SU-8 (~500 nm deep) instead of S1805. The main idea of the window was to confine the conducting polymer over the interdigitated area in order to prevent film dewetting phenomena that may happen during post-film deposition treatment (evaporation of solvent due to thermal heating). No difference in film quality was noticed between devices with SU-8 and S1805 based windows. Therefore, the study reported here was carried out with devices that window was made of SU-8. A photograph of an example of an array of the substrate with µ-dispensed DPPDTT onto the rectangular window is shown in **Figure 5-1.b and c**. A zoom of the interdigitated electrode area reveals good channel coverage by a 130 nm film of DPPDTT (**Figure 5-1.c**). It resembles the concentric ring-like deposition observed in µ-dispensed films as drying results in printed films[17, 18 and 19] with an aggregate in the middle. Interestingly, higher magnification shows that the edges of the printed film present several well-structured millimetric long micron scale width aggregates directed towards the centre of the film (**Figure 5-1.d**). This

suggests that the aggregate deposit from the edges to the centre of the film. See **Figure S5-1** in **supporting information** to appreciate the view of the aggregates coming from the edges to the middle of the film.

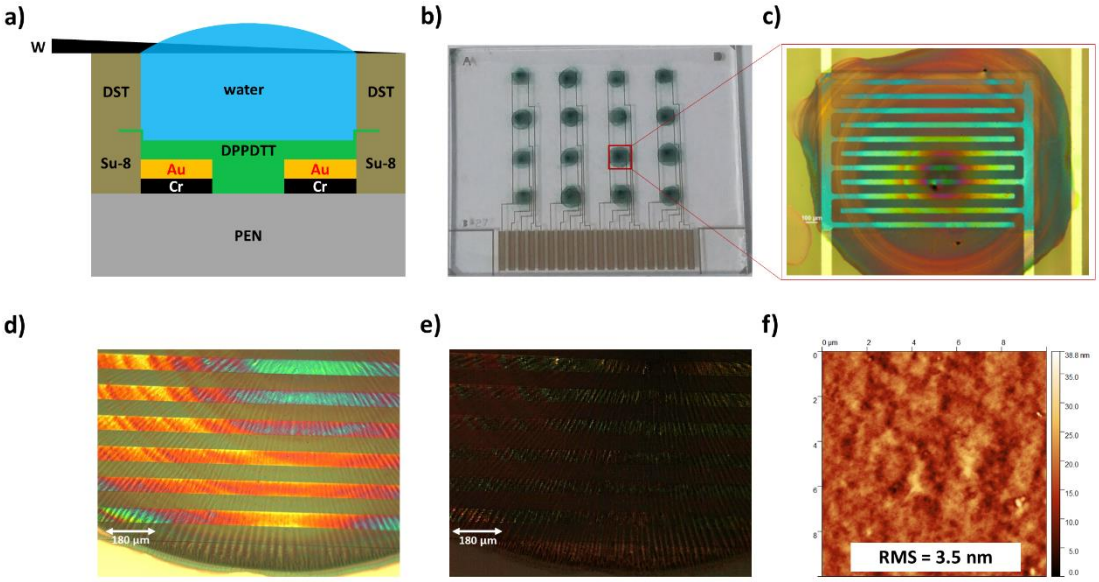

Figure 5-1: *EGOFET: a) Cross-section view of the device. PEN and DST (280 µm) stand for poly(ethylene 2,6-naphthalate) and double sided tape. b) A photograph of the substrate showing an array of sixteen interdigitated contact electrodes with a µ-dispensed DPPDTT film, c) Zoom of single transistor. Further optical microscope picture zoom at the edges of the film with polarization angle set to d) 0° and e) 90° and f) a typical atomic force micrograph of the edge of the film.*

Picture taking with incident polarisation of 90° shows disconnected microscale aggregate (**Figure 5-1.e**). This was also confirmed by 10 μm^2 field of view atomic force micrograph in tapping mode (**Figure 5-1.f**). Here the size of the aggregates was significantly larger (× 2) than that obtained with spincoated technique and comparable to that of PBTTT (**see Figure S5-2** in **supporting information**). Equally the surface was less smooth when compared to the spin-coated DPPDTT film (RMS of 3.5 nm against 2.6 nm). This difference in the size of the aggregates results from the fact that DPPDTT deposited via dispensing has longer time for self-assembly as solvent evaporation takes longer than spincoating. This was accentuated by annealing the dispensed DPPDTT at 50°C for 5 minutes to allow slow evaporation of the solvent (1,2-dichlorobenzene). This was followed by annealing at 140°C for 1 h to remove the residual solvent after film formation. In the spincoated film, this was carried out at 140° C for one hour. Note the concentration of the DPPDTT solution used in the spin-coating procedure was about two time higher than the µ-dispensing solution (4 mg/ml).

5.3.1. Electrical performance reproducibility of droplet gated EGOFET

The uniformity of electrical performance, an important characteristic array of the devices

as to fulfill[20] prior to its integration with other microsystems, was evaluated. Typical transfer characteristics along with statistic distribution of extracted figure(s) of merit are presented in **Figure 5-2**. Clear p-channel modulation of the drain current (I_{DS}) was achieved with 100% yield.

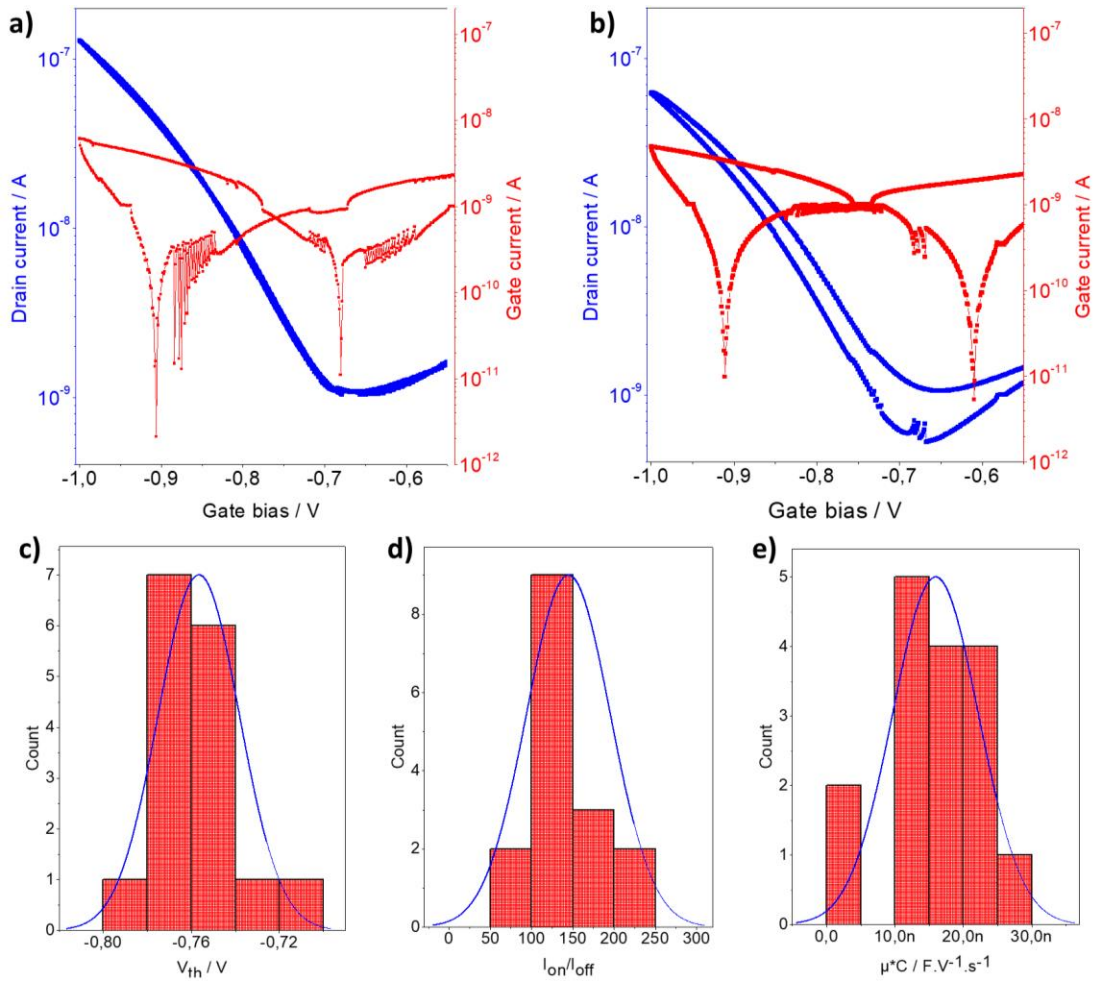

Figure 5-2: *Electrical response of water gated OFET array with tungsten acting as gate terminal: Typical transfer (blue) and gate current characteristics of EGOFET with printed DPPDTT for a) 81% and b) 19% of the fabricated devices. The V_{DS} was fixed to -0.7 V. Distribution of electrical figure of merit extracted from the transfer characteristic in saturation regime c) V_{th}, d) I_{on}/I_{off} and e) μ.C.*

Note: tap water (6 μL) purified with Milli-Q system (resistivity of 18 MΩ.cm) was employed as the electrolyte, and tungsten (W) needle served as the gate terminal. For 81% of the fabricated devices as in the typical I_{DS}-V_{GS} curve presented in **Figure 5-2.a**, shows no apparent hysteresis in the drain current between gate forward and backward bias sweep. The remaining 19% displays a higher backward I_{DS} as compared to the forward. For all the fabricated devices, poor drain to gate current ratio was found (~ 10^2). This is an order of magnitude lower than that of the spin-coated DPPDTT reported in **Chapter 3** (**Table 5-1**). However, the modulation of the drain current by the variation of gate bias does not follow the trends of I_{GS}. Hence, the drain current of these devices was not disturbed by the displacement current that flows towards the gate.

	V_{th} V	I_{on}/I_{off}	μ $cm^2.V^{-1}.s^{-1}$	μ.C $\mu F.V^{-1}.s^{-1}$
μ-dispensed DPPDTT	-0.76 ± 0.02	140 ± 50	0.13	0.016 ± 0.006
Spin-coated DPPDTT	-0.05 ± 0.03	$3 \pm 1 \times 10^3$	0.18	0.02 ± 0.01

Table 5-1: *Figures-of-merit of EGOFET developed in chapter 3 and here with spin-coated and μ-dispensed DPPDTT, respectively.*

To assess the electrical performance uniformity of the devices in the array, figures of merit were extracted using the model applied to OFET in saturation regime (see equation (4.1) in **Chapter 4**). A statistical distribution of the threshold voltage (V_{th}), on-to-off drain current ratio (I_{on}/I_{off}) and normalized transconductance are depicted in **Figure 5-2.c**, **d** and **e** respectively. Overall, the voltage required to induce significant mobile charges (hole) into the conducting channel (V_{th}) range from -0.79 V to about -0.72 V with value average around -0.76 ± 0.02 V. These values are higher than the EGOFET reported in **Chapter 3** based on the same polymer (**Table 5-1**) and most of the reported V_{th} for electrolyte-gate devices[16,21 and 22]. Such high V_{th} reflects the energetic mismatch between the gate terminal (W) and the conducting channel. Using a metal with work function closer to the HOMO of DPPDTT, such as gold may result in a reduction of these values and permit drain current saturation within the electrochemical stability windows of the electrolyte (water). The distribution of the I_{on}/I_{off} (140 ± 50) as well as that of the normalized transconductance (16 ± 6 $nF.V^{-1}.s^{-1}$) was also narrow (**Figure 5-2.e** and **d**). These results clearly show that the DPPDTT was uniformly printed as devices based on these films exhibit similar electrical properties (**Table S5-1**).

Using the capacitance obtained in **Chapter 3** for DPPDTT EGOFET gate with water (0.12 $\mu F.cm^{-2}$), a mobility of 0.13 $cm^2.V^{-1}.s^{-1}$ can be estimated. This mobility, value in the range of that of reported EGOFETs (see **Table 2-1** in **Chapter 2**), is slightly lower than that of the device with spin-coated DPPDTT reported in **Chapter 3**, which was about 0.18 $cm^2.V^{-1}.s^{-1}$. Both mobility was at less an order of magnitude inferior to that achieved in dielectric gated OFETs for DPPDTT[23 and 24]. At first this is counterintuitive as the capacitance of the EDLs (~$\mu F.cm^{-2}$) are superior to those of standard and high-k solid dielectrics[25 and 26]. Owing to such high gate capacitance, the electrical double layer induced a high charge density in the semiconductor[27]. With this reasoning, the mobility of EGOFET should be greater than that of OFET. However, higher gate capacitance come with more sensitivity of charge transport to interfacial properties, such as impurity, defect or surface roughness, due to compression of the charge carrier distribution closer to the electrolyte interface with the semiconductor. This may be pronounced in the developed

devices resulting in a lower mobility as compared to standard OFET based on DPPDTT. Note, this degradation of mobility in EGOFET as compared to OFET have been previously observed when the electrolyte was water[5].

For real application such as in-line and real-time biomolecule detection, in addition to being reproducible, the device in the array must operate consistently for the timescale of the measurement. The duration of the experiment depends on the target application. For point of care diagnosis, the response time could be within 30 minutes up to an hour. Another requirement for such an application is the portability, which can be facilitated via the integration of a microfluidic cell with the devices. Here the stability of the EGOFET with printed DPPDTT was tested by recording multiple transfer curves continuously for more than 30 minutes with water flowing through an integrated microfluidic cell on top of the channel (150 µl.min^{-1}). Details of the characterization procedure are available in the experimental section. Note tungsten was replaced by gold to acts as gate terminal in order to reduce the threshold voltage.

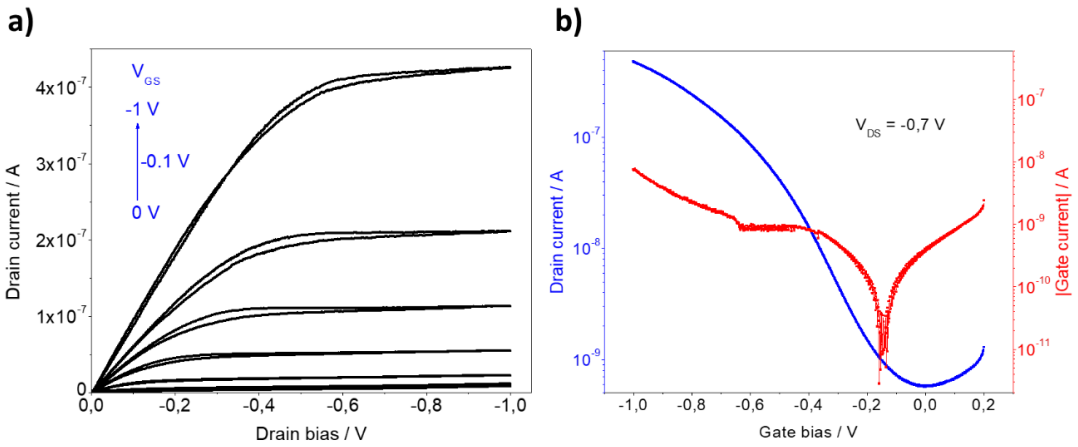

Figure 5-3: *a) Output, b) transfer (blue) and gate current (red) characteristics. The electrolyte employed was tap water purified with a Milli-Q system flowing through the fluidic channel at 150 µL.min^{-1}.*

5.3.2. Stability of DPPDTT EGOFET with the integrated microfluidic device.

Typical electrical characteristics of the device is reported in **Figure 5-3**. The device has same structure as the one used in **Chapter 4** except that no ssDNA was immobilized on the gate electrode and the semiconductor was µ-dispensed on the source-drain electrode (**Figure 5-1.c**). The device operated in ohmic contact, as no deviation from linearity is noticeable in the output curve at low drain bias (**Figure 5-3.a**). In addition, as for the EGOFET reported in **Chapter 4**, full I_{DS} saturation was achieved at all gate voltages. The performance of this device was improved as compared to droplet devices. For instance, the threshold voltage was found to be closer to zero gate bias (-0.3 V as compared to -

0.76 V), and the I_{on}/I_{off} was three times higher (800 vs 140). The superior performance is probably due to the nature of the gate terminal. The work function of tungsten is about -4.5 eV. That of thermally evaporated gold is between -4.9 eV and - 5.2 eV. The latter values are closer to the HOMO of DPPDTT, which is about -5.2 eV. Hence, less energetic difference exists between the gate and DPPDTT, about 0.3 eV, when gold is employed (left panel of **Figure 5-4**). This is half that between DPPDTT and tungsten (0.7 eV). This is likely the reason why less gate bias (~ -0.3 V) was required to turn the EGOFET device on with gold gate electrode as compared to the tungsten (~ -0.7 V) (right panel of **Figure 5-4**).

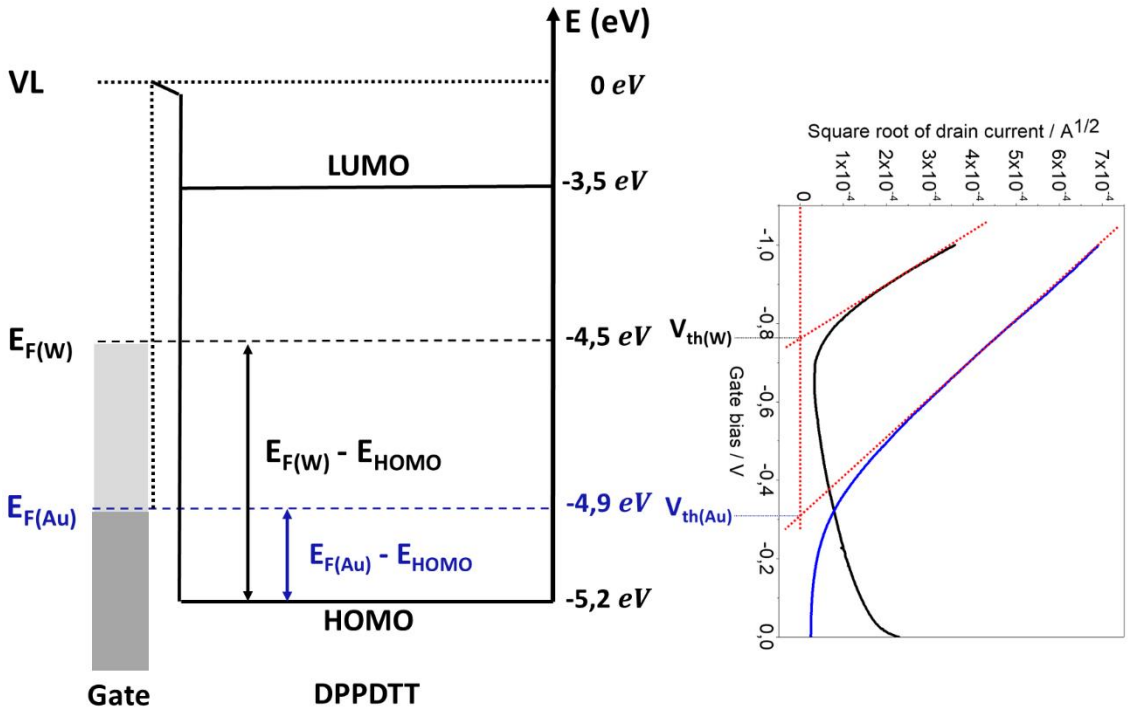

Figure 5-4: *Left panel: Energetic diagram (not in scale for clarity) of gate gold (Au) and tungsten (W) interface with DPPDTT. Right panel: square root of drain current as a function of gate bias with W and Au acting as gate terminal (V_{DS} = – 0.7 V). HOMO and LUMO are the highest occupied and lowest unoccupied molecular orbital of DPPDTT. VL, $E_{F(W)}$ and $E_{F(Au)}$ stand for the vacuum level, W and Au Fermi levels.*

Note: while the drain current was higher in microfluidic integrated device as compared to that of the droplet gate EGOFET, the gate current at maximum gate bias (-1 V) were identical.

The electrical performance stability of the device was evaluated under flowing electrolyte condition by continuously recording transfer curves. **Figure 5-5.a** illustrates the transfer characteristic obtained after every five records with the inset showing the corresponding gate current as a function of gate sweep number. The transfer curve changed in the low gate bias region (-0.6 V to 0.2 V) as indicated by the arrow in **Figure 5-5.a**.

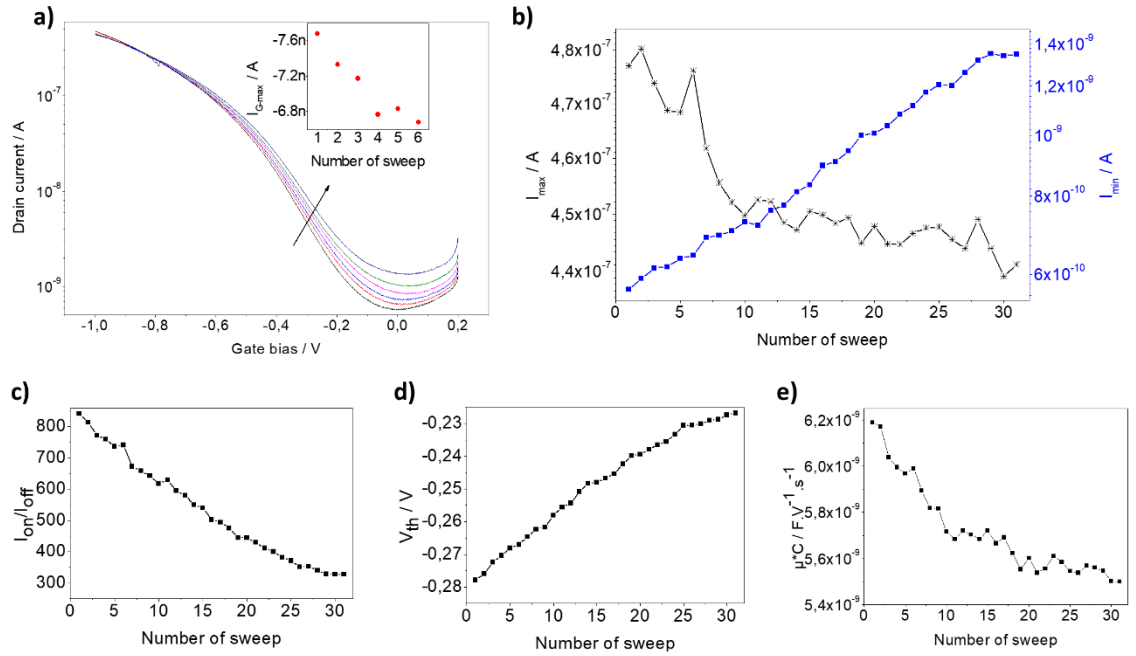

Figure 5-5: *Device electrical performance stability (V_{DS} = -0.7 V): a) Six transfer characteristics of the same device obtained after every five records (Inset shows the maximum gate current of the device). Extracted electrical characteristic, namely b) maximum and minimum drain currents (I_{max} and I_{min}), c) Current ratio (I_{on}/I_{off}), d) threshold voltage (V_{th}) and e) µ.C, as a function of the number of gate bias sweep.*

The saturation drain current (I_{max}) drop linearly by about 8% (**Figure 5-5.b**). In contrast to I_{max} the off-state current (I_{min}) increase from an initial value of 0.5 nA to 2 nA. This contrasted degradation between I_{max} and I_{min} results in a decreasing I_{on}/I_{off}, that seem to be more impacted by I_{max}. The threshold voltage and the normalized transconductance are also affected. Usually negative gate bias stress induces threshold voltage shift of OFET toward more negative values[28]. In this experiment the V_{th} shifts toward more positive voltage by moving from -0.28 V to -0.23 V in 40 minutes. This V_{th} shift phenomenon has also been observed in field-effect transistors[29 and 30]. However, in the EGOFET device reported here it is not reversible. As the performance variation (**Figure 5-5**) was more characterised by an increase in the off current, a possible explanation of V_{th} shift may be that the printed DPPDTT film get doped probably by water molecule. Alternatively, a shearing force water exerts on the surface of DPPDTT film during it flow process may induce permanent degradation of the top monolayer of the conducting channel. Equally, some air contaminant may deposit onto the surface of DPPDTT film prior to the electrical characterisation. These result into a change in DPPDTT film's surface potential and charges distribution. Thus, a drift in V_{th} and I_{DS} as the potential differences between DPPDTT and the gate partly dictates the value of V_{th}. These can be verified for instance by using spectroscopy techniques to analyse the morphological and compositional variation of the film before, during and after device operation.

5.4. Conclusion

The uniformity of the electrical performance and long-term operation of water gated OFET with printed DPPDTT was evaluated. Device-to-device reproducibility was satisfactory with small variation in the electrical parameters. The averages of the figures were an order of magnitude superior to the standard deviation. The use of gold instead of tungsten as the gate terminal improved the electrical figures of merit due to the lowering of the energetic difference between gate and semiconductor layer work functions. The results show measured field-effect mobility comparable to the state-of-the-art, as reported in **Chapter 2**, of about 0.13 $cm^2.V^{-1}.s^{-1}$, and a reasonable I_{on}/I_{off} (~800) can be achieved with EGOFET in which the organic semiconductor was deposit with an automated printer. The developed device was able to withstand 40 minutes operation with an electrolyte flowing through its fluidic channel. The degradation in the electrical figures of merit was 8%, 18% and 11% for the drain current (V_{GS} = -1 V and V_{DS} = -0.7 V), threshold voltage and normalized transconductance (**Table 5-2**).

I_{DS} (V_{GS} = -0.5 V) μA		**V_{th}** V		**$\mu.C \times 10^{-9}$** $F.V^{-1}s^{-1}$	
Initial	Final	Initial	Final	Initial	Final
0.48	0.44	-0.28 V	-0.23 V	6.2	5.5

Table 5-2: *Change in the figures of merit after bias stress measurement. Initial and final are the figures obtained prior and after the bias stress measurement, respectively.*

These results imply that the EGOFET technology may be compatible with roll to roll process. The microdroplet printing which was used to deposited DPPDTT is an additive technique, its can essentially be programmed to deposit functional materials from solution on demand, in a predefined position. It can be scaled up, via integration of multiple µ-dispensing print heads to deposit various functional materials on different substrate type, size, shape and composition at high speed (3 $mm.s^{-1}$) in one step and over a large area. Hence, the microdroplet robot can be integrated with other pre and post printing techniques such as surface functionalisation/treatment, film thermalization to deliver roll to roll fabrication of high performing and stable EGOFET devices integrated with a microfluidic platform.

5.5. Methods

5.5.1. Materials

Poly(ethylene 2,6-naphthalate) (PEN) foils (125 µm thick) and platfix CS2325NA4 adhesive were supplied by Teijin DuPont film Co. Ltd.. Diketopyrrolopyrrole-alt-5,5-(2,5-di(thien-2-yl)thieno[3,2-b]thiophene] (DPPDTT – Mw = 292 200 and Mn = 74900) was obtained from Ossila Ltd and used as received. Polymethylmethacrylate (PMMA) sheet (3 mm thick), double sided tape (280 µm thick number 7961MP) were purchased from 3M, and stopcock 3-way male lock from Cole-Parmer Instrument Company Ltd. 1,2-dichlorobenzene (DCB) was obtained from Sigma-Aldrich. Stainless-steel tube was purchased from Tomlinson Tube & Instruments Ltd. Silicon wafers, Shipley 1805 photoresist (S1805), polymethylglutarimide (PGMI) all other solvents were obtained from Manchester Centre for Mesoscience & Nanotechnology (CMN). The system used to deposit the organic semiconductor was a Fisnar F4200N.1 Dispensing robot equipped with a piezoelectric printhead available at the School of Chemical Engineering and Analytical Science (CEAS) of the University of Manchester.

5.5.2. Fabrication of the EGOFET with printed DPPDTT

5.5.2.1. Patterning of source drain and gate electrodes substrates

The geometry of the substrates, microfluidic cells, contact/gate electrodes, and the bank layer were drawn on AutoCAD. The PEN was cut down with an HPC CO_2 laser cutter (100 W, 10 mm.s^{-1}) to generate the pattern of the AutoCAD design, and then laminated on to Si substrates as explained in the experimental section of **Chapter 3**. Contact (source/drain electrodes) and gate electrodes arrays, 16 of each, were then designed on separate PEN foil (stuck on silicon carrier) via direct laser lithography following procedure outline in **Figure 5-6** (step 1 to 9).

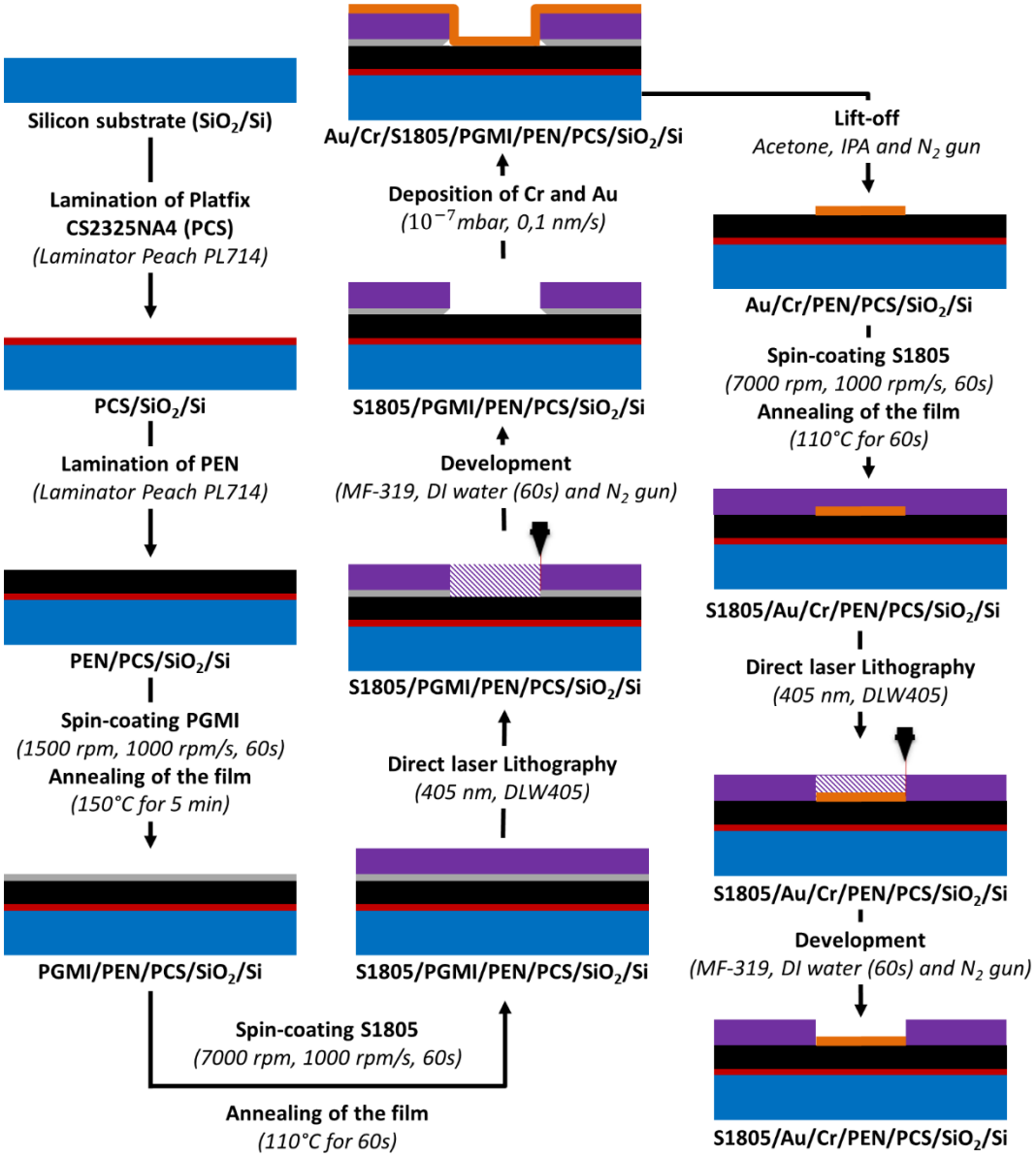

Figure 5-6: *Process flow chart for the patterning of poly(ethylene 2,6-naphthalate) (PEN) substrate with array of interdigitated source/drain and gate electrodes.*

Then S1805 was spincoated onto the patterned contact electrode substrate (Speed: 7000 rpm, acceleration: 1000 rpm.s^{-1}, time: 60s) and annealed at 110°C for a minute to remove residual solvent. This was followed by exposing the substrate to a 405 nm laser beam of a direct laser lithography machine (DLW405) to design the AutoCAD bank rectangular pattern on the contact electrodes substrates. The substrate was then immersed in an MF-319 solution, and in water for 60s each, rinsed with water and blown dry with a stream of nitrogen to generate rectangular wells over the interdigitated area of the contact electrodes with about 300 nm thick S1805. Note similar substrate were provided by Cambridge Display Technology Ltd., however the bank layer was made of 500 nm layer of Su8. The bank layer aims to electrically isolate the contact electrode from the electrolyte, and to guide the formation of the organic semiconductor during printing.

For the microfluidic integrated device another PEN substrate was patterned with array of 16 gold gate electrode (1 mm^2) using procedure detailed in experimental section of **Chapter 4**. This substrate was stuck on the PMMA sheet via a double-sided tape, and the CO_2 laser was used to cut 8 holes through both the PMMA and the PEN gate electrode substrate. Stainless-steel tubes were inserted into these holes to serve as the inlet/outlet of the microfluidic cell (see **Chapter 4** section **4.5.2.** for more details**)**.

5.5.2.2. Deposition of the DPPDTT films via an automated µ-dispenser

The DPPTTT was deposited into well generated over the interdigitated electrode by the bank layer. First, the ink was produced by dissolving 4 mg of DPPDTT in 1 ml of 1,2-dichlorobenzene (heated at 80 °C for about 30 minutes). At the same time, the patterned contact electrode substrate was sonicated in isopropanol for 5 minutes and blown dry with a stream of N_2. Four droplets (**Figure 5-6.c**) of the ink was injected into the well to fully cover the interdigitated contact electrodes with a thin film of DPPDTT. The resulting films were heated at 50ºC for 5 minutes then at 140ºC for an hour to fully dry the films (**Figure 5-6.a** and **b**). Note the distance between the substrate and nozzle of µ-dispenser was about 5 mm. The amplitude of the square wave was -250 V with a pulse width of 150 µs and the distance between droplets was fixed to 0.8 mm.

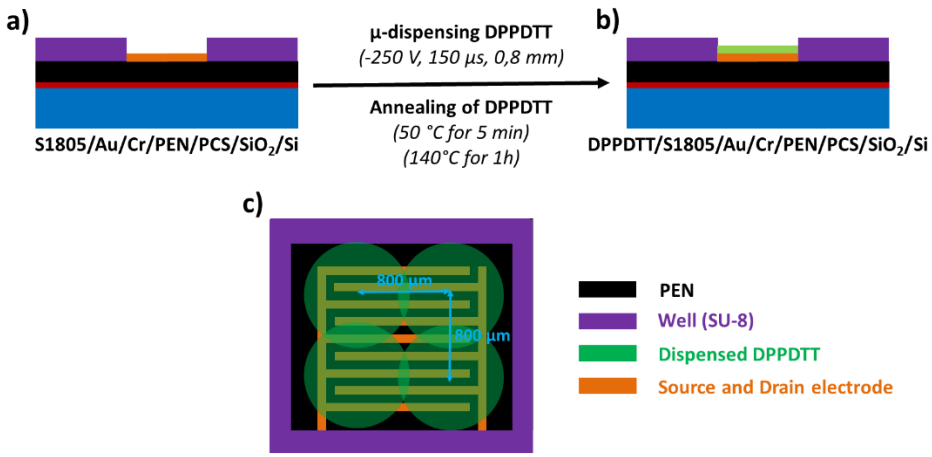

Figure 5-6: *(a,b) Process flow chart for the formation of a film of DPPDTT in the well over the electrode. c) Schematic representation of µ-dispensed DPPDTT showing the distance between droplet prior to film formation (not to scale)*

5.5.2.3. Film inspection

The organic semiconductor surface was inspected with an Olympus BX51 optical microscope equipped with two polarisers. Atomic Force Microscope in tapping mode was used to probe film surface.

5.5.2.4. Integration of electrolyte chamber or fluidic channels to the EGOFET

For the droplet gated configuration, EGOFETs with a droplet of water acting as the gate insulator, holes were laser cut into a double-sided tape and this was fixed over the interdigitated electrode as detailed in experimental section of **Chapter 3**. The device was then terminated by filling the holes with water from a Millipore Milli-Q system (resistivity of 18.2 MΩ.cm) (6 µl) and a tungsten needle inserted in it acted as the gate electrode.

In the case of the microfluidic platform integrated with the EGOFET, a top cover with an array of gate terminal and fluidic channels (four in total) was fabricated and assembled following procedure outlined in the experimental section of **Chapter 4**.

5.5.3. Device electrical testing

5.5.3.1. Electrical characterization

For the droplet gated EGOFET configuration, transfer, and gate current curves were measured in air at ambient condition with a semiconductor parameter analyser Agilent 1500B. The transfer and gate current curves consist of applying a constant voltage to the drain terminal (-0.7 V) while sweeping the bias applied to the gate terminal (forward and backward) from 0.2 V to -1 V, step of -1 mV while recording the current at the drain and gate terminal.

The microfluidic EGOFET configuration was electrically characterised similarly to measurement condition used to record the electrical characteristics of the droplet gate configuration in term of the manner in which the bias was applied to the terminals. However, the measurement was carried out with an electrolyte flowing through the microfluidic cell at a speed of 150 $\mu L.min^{-1}$ with a syringe pump (see experimental set up illustrated in **Figure 4.14** of **Chapter 4**). For the stability, multiple transfer curves were measured continuously with electrolyte flowing through the microfluidic chamber (150 $\mu L.min^{-1}$) for 40 minutes spaced by about 77s. The output curves are obtained by measuring the drain current when sweeping the drain voltage (from 0.05 V to -1 V, step of -1 mV) at different constant gate voltage (from 0 V to -1 V, step -0.1 V).

Acknowledgment

Many thanks to CDT Ltd. and EPSRC for generous financial support.

References

1. Wang, S., Oh, J. Y., Xu, J., Tran, H. & Bao, Z. Skin-Inspired Electronics: An Emerging Paradigm. *Acc. Chem. Res.* **51,** 1033–1045 (2018).

2. Simon, D. T., Gabrielsson, E. O., Tybrandt, K. & Berggren, M. Organic Bioelectronics: Bridging the Signaling Gap between Biology and Technology. *Chem. Rev.* **116,** 13009–13041 (2016).

3. Manoli, K., Magliulo, M., Mulla, M. Y., Singh, M., Sabbatini, L. Palazzo, G. & Torsi, T. Printable bioelectronics to investigate functional biological interfaces. *Angew. Chemie - Int. Ed.* **54,** 12562–12576 (2015).

4. Kergoat, L., Piro, B., Berggren, M., Horowitz, G. & Pham, M. C. Advances in organic transistor-based biosensors: From organic electrochemical transistors to electrolyte-gated organic field-effect transistors. *Anal. Bioanal. Chem.* **402,** 1813–1826 (2012).

5. Kergoat, L., Herlogsson, L., Braga, D., Piro, B., Pham, M-C., Crispin, X., Berggren, M. & Horowitz, G. A Water-Gate Organic Field-Effect Transistor. Adv. Mater. 22, 2565–2569 (2010).

6. Macchia, L., Manoli, K., Holzer, B., Di Franco, C., Ghittorelli, M., Torricelli, F., Alberga, D., Mangiatordi, G., F., Palazzo, G., Scamarcio, G. & Torsi, L. Single-molecule detection with a millimetre-sized transistor. Nat. Commun. 9, 1–10 (2018).

7. Foschi, G., Leonardi, F., Scala, A., Biscarini, F., Kovtun, A., Liscio, A. &Casalini, S. Electrical release of dopamine and levodopa mediated by amphiphilicamphiphilic β - cyclodextrins. Nanoscale. 7, 20025–20032 (2015).

8. Benfenati, V., Toffanin, T., Bonetti, S., Turatti, G., Pistone, A., Chiappalone, M., Sagnella, A., Stefani, A., Generali, G., Ruani, G., Saguatti, D., Zamboni, R. & Muccini, M. A transparent organic transistor structure for bidirectional stimulation and recording of primary neurons. Nat. Mater. 12, 672–680 (2013).

9. Desbief, S., Di Lauro, M., Casalini, S., David, G., Tortorella, S., Barbalinardo, M., Kyndiah, A., Murgia, M., Cramer, T., Biscarini, F. & Vuillaume D. Electrolyte-gated organic synapse transistor interfaced with neurons. Org. Electron. 38, 21–28 (2016).

10. Li, M., Tang, Q., Tong, Y., Zhao, X., Zhou, S. and Liu, Y. Effect of electrode design on crosstalk between neighboring organic field-effect transistors based on one single crystal. *Appl. Phys. Express* **11,** (2018).

11. Briseno, A. L., Stefan, C., Mannsfeld, B., Ling, M. M., Liu, S., Tseng, R. J., Reese, C., Roberts, M. E., Yang, Y., Wudl, F. & Bao, Z. Patterning organic single-crystal transistor arrays. *Nature* **444,** 913–917 (2006).

12. Kumatani, A., Liu, C., Li, Y., Darmawan, P., Takimiya, K., Takeo Minari, T. & Tsukagoshi, K. Solution-processed, self-organized organic single crystal arrays with controlled crystal orientation. *Sci. Rep.* **2,** 393 (2012).

13. Tekin, E., Smith, P. J. & Schubert, U. S. Inkjet printing as a deposition and patterning tool for polymers and inorganic particles. *Soft Matter* **4,** 703–713 (2008).

14. Shin, K. Y., Hong, J. Y. & Jang, J. Micropatterning of graphene sheets by inkjet printing and its wideband dipole-antenna application. *Adv. Mater.* **23,** 2113–2118 (2011).

15. Li, J., Zhao, Y., Tan, H. S., Guo, Y., Di, C-A., Yu, G., Liu, Y., Lin, M., Lim, S. H., Zhou, Y., Su,

H. & Ong, B. S. A stable solution-processed polymer semiconductor with record high-mobility for printed transistors. *Sci. Rep.* **2,** 1–9 (2012).

16. Doumbia, A., Webb, M., Turner, M. L., Behrendt, J. M. & Wilson, R. A printed electronic platform for the specific detection of biomolecules. Proc. SPIE 10364, Organic Sensors and Bioelectronics X, 103640N, 1–10 (2019).

17. Lim, G-H., Zhuo, J-M., Wong, L-Y., Chua, S-J., Chua, L-L. & Ho, P. K. H. A transition solvent strategy to print polymer:fullerene films using halogen-free solvents for solar cell applications. *Org. Electron. physics, Mater. Appl.* **15,** 449–460 (2014).

18. Zhan, Z., An, J., Wei, Y., Tran, V. T. & Du, H. Inkjet-printed optoelectronics. *Nanoscale* **9,** 965–993 (2017).

19. Oh, Y., Kim, J., Yoon, Y. J., Kim, H., Yoon, H. G., Lee, S-N., Kim, J. Inkjet printing of Al_2O_3 dots, lines, and films: From uniform dots to uniform films. *Curr. Appl. Phys.* **11,** 359–363 (2011).

20. Ahmeda, R., Sams, M., Simbrunner, C., Ullaha, M., Rehmana, K., Schwabegger G., Sitter, H. & Ostermann, T. Reproducibility and stability of C 60 based organic field effect transistor. *Synth. Met.* **161,** 2562–2565 (2012).

21. Yu Zhang, Y., Han, G., Qin, M., Shen, Y., Lu, X., Yi, Y.& Zhao, N. Spectroscopic Study of Charge Transport at Organic Solid-Water Interface. *Chem. Mater.* **30,** 5422–5428 (2018).

22. Nguyen, T. T. K., Anquetin, G., Reisberg, S., Noël, V., Mattana, G., Touzeau, J., Barbault, F., Pham, M-C. & Piro, B. Triggering the Electrolyte-Gated Organic Field-Effect Transistor output characteristics through gate functionalization using diazonium chemistry: Application to biodetection of 2,4-dichlorophenoxyacetic acid. *Biosens. Bioelectron.* **113,** 32–38 (2018).

23. Chen, Z., Lee, M. J., Ashraf, R. S., Gu, Y., Albert-Seifried, S., Nielsen, M. M., Schroeder, B., Anthopoulos, T. D., Heeney, M., McCulloch, I. & Sirringhaus, H. High-performance ambipolar diketopyrrolopyrrole-thieno[3,2-b]thiophene copolymer field-effect transistors with balanced hole and electron mobilities. *Adv. Mater.* **24,** 647–652 (2012).

24. Li, Y., Singh, S. P. & Sonar, P. A high mobility P-type DPP-thieno[3,2-b]thiophene copolymer for organic thin-film transistors. *Adv. Mater.* **22,** 4862–4866 (2010).

25. Faraji, S., Hashimoto, T., Turner, M. L. & Majewski, L. A. Solution-processed nanocomposite dielectrics for low voltage operated OFETs. *Org. Electron.* **17,** 178–183 (2015).

26. Kim, S. H., Yang, S. Y., Shin, K., Jeon, H., Lee, J. W., Hong, K. P. & Park, C. E. Low-operating-voltage pentacene field-effect transistor with a high-dielectric-constant polymeric gate dielectric. *Appl. Phys. Lett.* **89,** 1–4 (2006).

27. Panzer, M. J. & Frisbie, C. D. Polymer electrolyte-gated organic field-effect transistors: Low-voltage, high-current switches for organic electronics and testbeds for probing electrical transport at high charge carrier density. *J. Am. Chem. Soc.* **129,** 6599–6607 (2007).

28. Lee, W. H., Choi, H. H., Kim, D. H. & Cho, K. 25th anniversary article: Microstructure dependent bias stability of organic transistors. *Adv. Mater.* **26,** 1660–1680 (2014).

29. Han, S. Y., Park, K. T., Kim, C., Jeon, S., Yang, S-H. & Kong, H-S. Abnormal Behavior of

Threshold Voltage Shift in Bias-Stressed a-Si:H Thin Film Transistor under Extremely High Intensity Illumination. *ACS Appl. Mater. Interfaces* **7,** 15442–15446 (2015).

30. Szu-Han Ho, S-H., Chang, T-C., Lu, Y-H., Chen, C-E., Tsai, J-Y., Liu, K. J., Tseng, T-Y., Cheng, O., Huang, C-T. & Lu, C-S. Investigation of abnormal negative threshold voltage shift under positive bias stress in input/output n-channel metal-oxide-semiconductor field-effect transistors with TiN/HfO2 structure using fast I-V measurement. *Appl. Phys. Lett.* **104,** 113503 (2014).

Supporting information

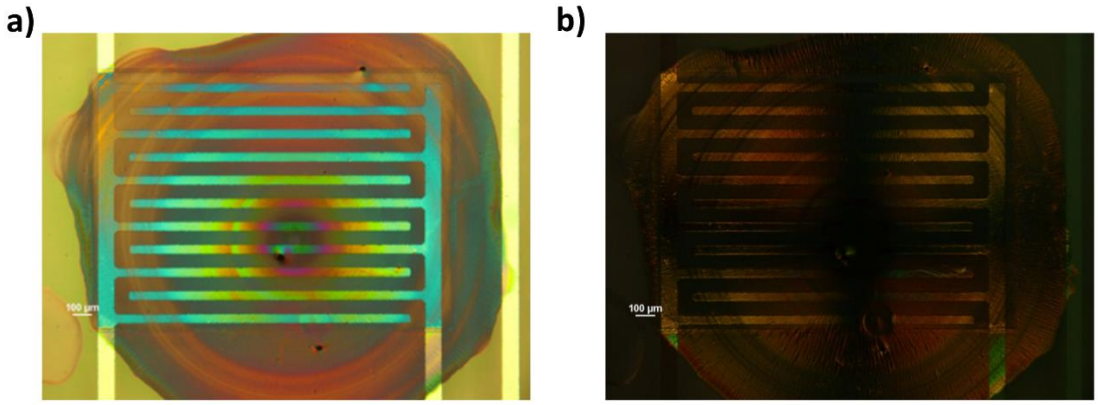

Figure S5-1: *Optical microscope picture of µ-dispensed DPPDTT at polarisation angle of a) 0° and b) about 80°.*

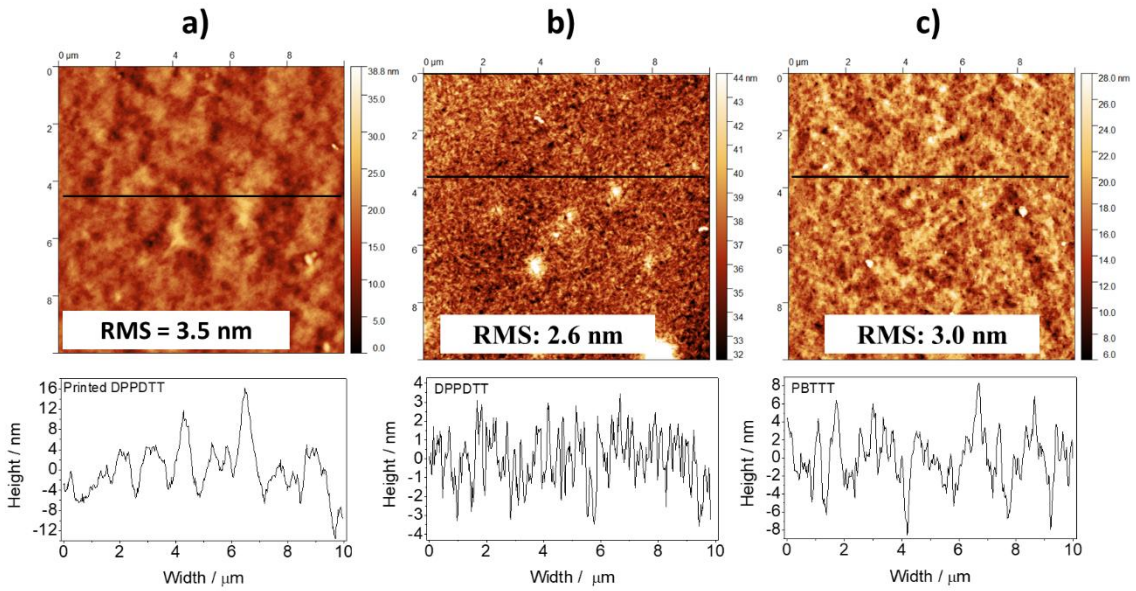

Figure S5-2: *Atomic force micrographs of thin film of DPPDTT obtained with a) µ-dispensing and b) spincoating procedure and that of c) spincoated PBTTT thin film together with the line scan profile.*

	Min	Average	Max
I_{on}/I_{off}	50	140 ± 50	250
V_{th} / V	-0.79	-0.76 ± 0.02	-0.72
$\mu \times C$ / $nF.V^{-1}.s^{-1}$	3.9	16 ± 6	25

Table S5-1: *Figures of merit obtained from 16 water-gated device with tungsten needle acting as the gate terminal.*

Blank page

Chapter 6: Conclusion and outlook

The work in this thesis has focused on the development of a reliable biosensing system based on an EGOFET for point of needs testing in area such as molecular diagnosis/prognosis, life sciences, environmental monitoring and homeland security. In particular it discusses:

- Widening the library of organic semiconducting polymers suitable for operation in water-gated field effect transistor configuration.
- The *in operando*, fast (~30s) and selective detection of the hybridization of ssDNA using an electrolyte-gated organic field-effect transistor integrated into a microfluidic device on flexible substrate under flowing analyte.
- Paved the way for *en masse* production of electrolyte-gated organic field effect transistor integrated into a microfluidic platform by showing that the semiconducting channel of the device can be printed with minor impact on electrical performance, reproducible device performance and continuous in-water operation.

In detail, the survey of the scientific progress (**Chapter 2**) suggested that for effective in electrolyte field effect operation the crystallinity and interdigitation of polymers side chain are fundamental. Prior to the presented work, field effect mobility of EGOFET device and on-off current ratio reported in the literature were as high as ~0.08 $cm^2.V^{-1}.s^{-1}$ and ~10^2 respectively. In **Chapter 3**, an average field effect mobility of 0.18 $cm^2.V^{-1}.s^{-1}$ and 0.15 $cm^2.V^{-1}.s^{-1}$ with on-off ratios of 10^3 and 10^4 were achieved with two unexplored organic donor-acceptor polymeric semiconductor (D-A) in EGOFET, namely in DPPDTT and IDT-BT. The electrical performance of these two polymers was compared against that of PBTTT, a well-established semiconducting polymer that has been previously reported in EGOFET. The electrical parameters of these polymers namely the field-effect mobility (μ), on-to-off current ratio (I_{on}/I_{off}), subthreshold swing (SS) and switch-on time (τ_{on}), were better (**Table 6-1**).

	$\mu \times C \times 10^{-8}$ F. $V^{-1}.s^{-1}$	**C** $\mu F.cm^{-2}$	**μ** $cm^2.V^{-1}.s^{-1}$	**SS** $mV.deca^{-1}$	**$I_{on}/I_{off} \times 10^3$**	**τ_{on}** s
PBTTT	5 ± 2	0.55	0.09	456	0.21 ± 0.07	2.8 ± 0.3
DPPDTT	2 ± 1	0.12	0.18	125	3 ± 1	1.2 ± 0.6
IDT-BT	1.3 ± 0.3	0.09	0.15	62	23 ± 1	0.18 ± 0.02

Table 6-1: *Summary of figures of merit obtained from EGOFET devices gated with purified water.*

This initial investigation demonstrated that these two polymers gave high performance EGOFET devices and suggests a direction for future work. The DPPDTT and IDT-BT produce less crystalline film than those of PBTTT, but these polymers have a more rigid and planar polymeric backbone[1]. DPPDTT films are more crystalline than films of IDT-BT[1]. Thus, the results obtained in **Chapter 3** suggest that crystallinity is crucial, and polymer backbone rigidity and planarity are important criteria to be considered for robust in-water operation. To appreciate the importance of backbone rigidity and planarity when compared to film crystallinity, one could focus on studying the electrical behaviours of EGOFET device with various morphology of DPPDTT films. Several film morphologies can be achieved by for example blending DPPDTT with low permittivity dielectric materials such as polystyrene at different ratio and deposited from mixture of a polar poor solvents with dichlorobenzene or chloroform. Attention needs to be focused on correlating the electrical performance to the properties of the films to clearly show how important each characteristic is to electrolyte operation of EGOFET device.

An interesting aspect of EGOFET technology is that the architecture allows the interfacing of low power electronic devices (operating voltage below 1 V) with fluids for biological or chemical interaction monitoring via change in interfacial properties. In prior art summarised in **Chapter 2**, EGOFET biosensor technologies have been developed to detect a bio-interaction selectively and sensitively. These platforms were dominated by EGOFET in the droplet gated configuration (droplet of the analyte serves as gate insulator of the device) that in single spot measurement detects the bio events but ex situ (interaction between analyte and receptor took place before sensing was carried out). Integrating a flow channel to EGOFET to confine and supply the analyte, as well as studying the bio-interaction in situ may facilitate multiplexed sensing which will be beneficial for applications of the device in sectors including life science and healthcare (e.g. in-line disease diagnosis/prognosis, real-time drug screening) for point of care testing as well as enable the transfer of the technology to the desired application. Thus, in **Chapter 4**, an array of electrolyte gate organic field-effect transistors, based on DPPDTT, were integrated into a microfluidic platform using a combination of polymer microfabrication and fast prototyping techniques. DPPDTT was selected as semiconducting channel because, among the three polymers investigated in **Chapter 3** it displays the highest mobility, a low threshold voltage (close to zero) and parasitic current, and an ideal field-effect characteristics (output curves show hard saturation and square root of drain current increases linearly with gate bias after the threshold voltage without any deflection). The devices were operated under continuous flow of physiological like

milieu. To study the potential of the technology for point of care application, a self-assembled-monolayer coupled to a thiol-terminated single strand of deoxyribonucleic acid was immobilised on to the array of gate terminals. Specific detection of DNA hybridization was demonstrated *in operando* with the analyte flowing through the fluidic channel at 210 $\mu L.min^{-1}$ (see **Figure 6-1** for the structure of the developed device together with the sensing results).

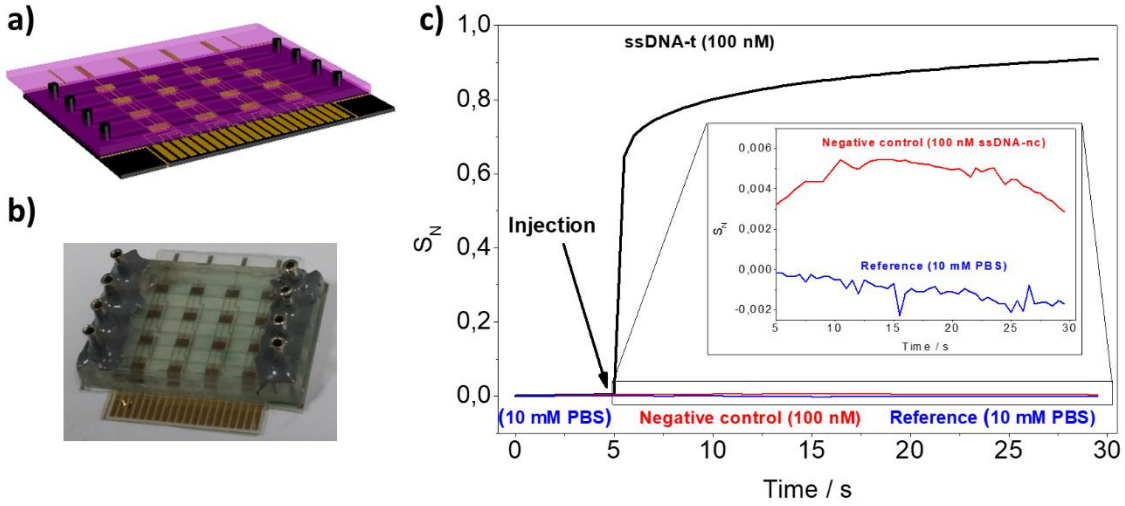

Figure 6-1: *a) AutoCAD 3D model and b) top view photograph of the biosensing system together with the sensing response. The arrow indicates when the analyte was injected into the fluidic channel.*

The sensing mechanism was dominated by a shift in device threshold voltage induced by gate work function change upon DNA-DNA interaction. The time for assay-to-result was about 30 s with a standard deviation measured to be less than 15%. The EGOFET based device was faster as compared to standard DNA ELISA Kits analysis technique (~1h). The developed system is versatile and can be converted into a sensor system to detect multiple analytes in parallel if a biorecognition element specific to the target molecules are immobilised onto the individual gate terminals in the array. This can be facilitated by immobilising thiolate molecule with tail group such as carboxylic, amine. And then covalently bind the biological molecules such as proteins, enzyme to the tail group of the self-assembled monolayer via NHS activation, amino, sulfo or carboxylic linking chemistry. Alternatively, the organic semiconductor can be the area to functionalise with the capturing molecules instead of the gate electrode using the same immobilization chemistry mentioned above providing the surface has compatible functional groups. As the developed device was designed so the electrode can be connected to an external source via zif connector as shown in **Figure 6-2**, The sixteen EGOFET in the array can be run simultaneously with a potentiometer (e.g. FETCP16 developed by JLM innovation). LabVIEW programmes are currently under development to simultaneously run the

sixteen transistors at the Organic Materials Innovation Centre of the School of Chemistry at the University of Manchester with the FETCP16.

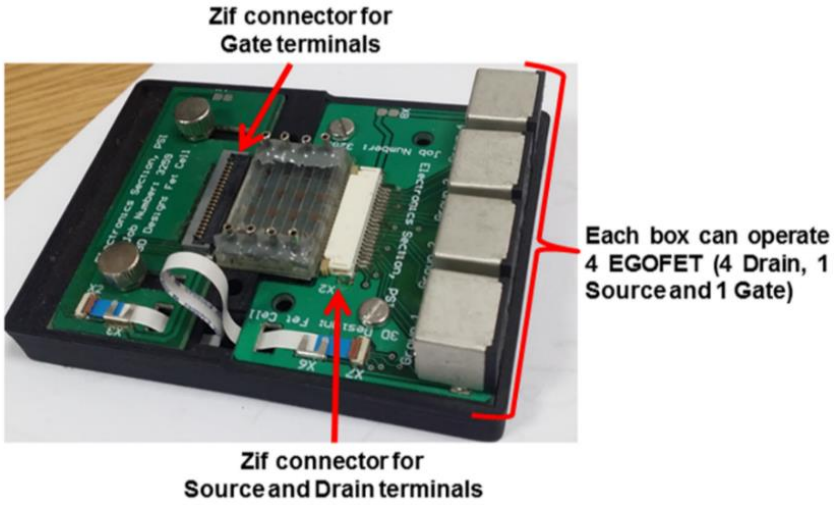

Figure 6-2: *Printed circuit board developed by the electronics section PSI of School of Chemistry of the University of Manchester with the developed EGOFET terminals connected to it via zero insertion force connector (zif).*

The thesis in **Chapter 5** concentrated on studying the impact of the deposition of the organic semiconductor (DPPDTT) with *en masse* compatible roll to roll printing technique on device performance and operational stability. Well-structured films of DPPDTT were obtained that performed uniformly and stably in EGOFET device with water acting as electrolyte. The printing process consisted of μ-dispensing DPPDTT into a 500 nm SU-8 pixel well over the interdigitated electrode area at a speed of 3 $mm.s^{-1}$ and thermal treating the film with two step annealing (50° C for 5 minutes and 140° C for one hour). The first thermal annealing step was used to slowly evaporate the solvent so that enough time was given to the DPPDTT molecules to self-organise. The second thermal cycle remove the residual solvent from the formed film. The electrical performance of the developed device was lower in mobility (0.13 $cm^2.V^{-1}.s^{-1}$ against 0.18 $cm^2.V^{-1}.s^{-}$) and on-to-off current ratio (10^2 against 10^3) when compared to the EGOFET fabricated with spin-coated DPPDTT. Replacing tungsten by gold as gate terminal induced a 0.4 V shift in the EGOFET threshold voltage and tripled the on-to-off current ratio. The shift in the threshold voltage was due to the potential difference between gold and DPPDTT being lower than that between DPPDTT and tungsten. The developed device operated stably with minor degradation on figures of merit under flowing electrolyte condition. The mobility, on-state drain current and threshold voltage changed by 11%, 8% and 18%, respectively. The results show promise that good performance EGOFET integrated into a microfluidic device can be produced *en masse* with solution printing technique such as μ-dispensing. Process using inkjet printing has already been demonstrated to deposit

patterns of the contacts on flexible and biocompatible substrates with ≤ 40 micrometres resolution[2 and 3]. Coupling these established techniques to the DPPDTT deposition process with μ-dispenser and microfluidic fabrication and integration established here could facilitate the development of a fully printed EGOFET integrated into a microfluidic device in which individual gate electrodes are functionalised with molecules specific to the target disease biomarkers. By this means, for instance low cost molecular diagnostic and prognostic tools that communicate wirelessly with computer at the Physician office for breast cancer, diabetes and stroke diseases can be realised. Work under investigation in line with this project include the monitoring of the presence of trinitrotoluene, Herceptin as well as the growth of organic piezoelectric crystal such as glycine in situ.

References

1. Noriega, R., Rivnay, J., Vandewal, K., Koch, F. P. V., Stingelin, N., Smith, P., Toney, M. F. & Salleo, A. A general relationship between disorder, aggregation and charge transport in conjugated polymers. *Nat. Mater.* **12,** 1038–1044 (2013).

2. Lim, J. A., Cho, J. H., Park, Y. D., Kim, D. H., Hwang, M. & Cho, K. Solvent effect of inkjet printed source / drain electrodes on electrical properties of polymer thin-film transistors. *Appl. Phys. Lett.* **88,** 082102 (2006).

3. Sele, C. W., Werne, T. Von, Friend, R. H. & Sirringhaus, H. Lithography-Free , Self-Aligned Inkjet Printing with Sub-Hundred-Nanometer Resolution **. *Adv. Mater.* **17,** 997–1001 (2005).